NASA Contractor Report 3936

NASA-CR-3936 19860006155

Heat Transfer Characteristics Within an Array of Impinging Jets

Effects of Crossflow Temperature Relative to Jet Temperature

L. W. Florschuetz and C. C. Su

GRANT NSG-3075
OCTOBER 1985

NASA Contractor Report 3936

Heat Transfer Characteristics Within an Array of Impinging Jets

Effects of Crossflow Temperature Relative to Jet Temperature

L. W. Florschuetz and C. C. Su
Arizona State University
Tempe, Arizona

Prepared for
Lewis Research Center
under Grant NSG-3075

National Aeronautics
and Space Administration

Scientific and Technical Information Branch

1985

CONTENTS

NOMENCLATURE

Symbols

a,b	coefficients in heat flux, Eq. (2.55), defined by Eqs. (3.24) and (3.26); in Fig. 1.1 and Table 4.1, b is thickness of jet plate
A_o^*	ratio of jet hole area to opposing impingement surface area (open area ratio), $\pi/[4(x_n/d)(y_n/d)]$
c_p	specific heat at constant pressure
C_D	jet hole discharge coefficient
$\overline{C}_D$	mean value of C_D over jet plate
d	jet hole diameter
G_c	crossflow mass flux averaged over channel cross-sectional area at entrance to individual spanwise row domain
G_{co}	value of G_c at entrance to overall array (x=0); i.e., average mass flux of initial crossflow
G_j	jet mass flux at individual hole or individual spanwise row based on jet hole area
$\overline{G}_j$	mean jet mass flux over entire array
G_j^*	superficial jet mass flux based on jet plate or impingement area
h	regional average heat transfer coefficient defined in terms of overall array parameters, Eqs. (2.1) and (3.33)
$\overline{h}$	mean value of h over entire array impingement region
h_r	regional average heat transfer coefficient defined in terms of individual spanwise row parameters, Eqs. (2.5) and (3.37)
k	thermal conductivity of fluid
L	streamwise length of jet plate and impingment surface (Figs. 1.1, 2.1, 2.2, 3.1, 3.2 and Table 4.1)
L_c	streamwise length of crossflow plenum (Fig. 3.2)
L_e	initial crossflow development length upstream of impingement region (Fig. 3.2, Table 4.1)

m_c	initial crossflow rate
m_j	total jet flow rate
M	initial crossflow-to-total jet flow ratio, m_c/m_j
N	number of spanwise rows of holes in streamwise direction for array of arbitrary length, L/x_n
N_c	number of spanwise rows of holes in streamwise direction for standard array, here equal to ten
N_s	number of jet holes across span of heat transfer test surface
N'_s	number of jet holes across span of channel
Nu	Nusselt number, hd/k
$\overline{Nu}$	mean value of Nu over entire array impingement region
Nu_r	Nusselt number, $h_r d/k$
$p(\bar{p})$	channel pressure (time-averaged value)
$\tilde{p}$	nondimensional channel pressure, $p/[\rho(\bar{G}_j/\rho)^2]$
Pr	Prandtl number, ν/α
Pr_{eff}	effective Prandtl number, $(\nu + \varepsilon_M)/(\alpha + \varepsilon_H)$
Pr_t	turbulent Prandtl number, $\varepsilon_M/\varepsilon_H$
$\bar{q}$	regional average impingement surface heat flux defined by Eq. (3.24)
r	regional average recovery factor defined in terms of overall array parameters, Eq. (2.2)
r_r	regional average recovery factor defined in terms of individual spanwise row parameters, Eq. (2.6)
Re_j	individual spanwise row jet Reynolds number, $G_j d/\mu$
$\overline{Re}_j$	mean jet Reynolds number over entire array, $\bar{G}_j d/\mu$
$\overline{St}^*$	special Stanton number defined by Eq. (7.1)
$t(\bar{t})$	static temperature (time-averaged value)

t_j	static temperature at jet exit plane
t'	static temperature fluctuation
$\overline{t'w'}$	time-averaged t'w'
$T(\bar{T})$	total temperature (time-averaged value)
T_o	mixed-mean total temperature at entrance of array (x=0), $T_{m,1}$
T_a	$\bar{T}$ of crossflow approaching spanwise row (i.e., at entrance to regional domain, Fig. 3.2)
T_c	characteristic temperature of crossflow (Section 3.4)
T_{cp}	crossflow plenum temperature
T_e	$\bar{T}$ at array entrance (Fig. 3.2)
T_j	jet plenum temperature (assumed same as mixed-mean total temperature at jet exit plane)
$T_{m,n}$	mixed-mean total temperature over channel cross-section at one-half streamwise hole spacing upstream of row n
T_s	impingement surface temperature
T_{rec}	recovery temperature considering overall array domain defined as impingement surface temperature for $\bar{q} = 0$ and $T_o = T_j$
$T_{rec,r}$	recovery temperature considering individual row domain defined as impingement surface temperature for $\bar{q} = 0$ and $T_{m,n} = T_j$
T_{ref}	fluid reference temperature considering overall array domain defined as fluid temperature at impingement surface (i.e., surface temperature) for $\bar{q} = 0$ and specified T_o and T_j
$T_{ref,r}$	fluid reference temperature considering individual row domain defined as fluid temperature at impingement surface (i.e., surface temperature) for $\bar{q} = 0$ and specified $T_{m,n}$ and T_j
$u,w(\bar{u},\bar{w})$	velocity components in x and z directions (Figs. 3.1 and 3.2) (time-averaged values)
u',w'	fluctuations of u and w
$\tilde{u},\tilde{w}$	$\bar{u}$ and $\bar{w}$ normalized by mean jet velocity, $\bar{u}/(\bar{G}_j/\rho)$ and $\bar{w}/(\bar{G}_j/\rho)$

u_a, w_a — $\bar{u}$ and $\bar{w}$ approaching spanwise row (i.e., at entrance to regional domain, Figs. 3.1 and 3.2)

u_e, w_e — $\bar{u}$ and $\bar{w}$ at array entrance (Figs. 3.1 and 3.2)

$\overline{u'w'}$ — time-averaged u'w'

W — width (span) of impingement heat transfer surface

x — streamwise coordinate (Figs. 1.1, 2.1, 2.2, 3.1, and 3.2)

$\tilde{x}$ — nondimensional x, x/L for overall array domain or x/x_n for regional domain

x_a — location of upstream edge of regional domain (used only in Section 3 to distinguish from x, Figs. 3.1 and 3.2)

x_n — streamwise jet hole spacing

y_n — spanwise jet hole spacing

z — coordinate normal to impingement surface (Figs. 3.1 and 3.2)

$\tilde{z}$ — nondimensional z, z/L for overall array domain or x/x_n for regional domain

z_n — channel height (jet exit plane-to-impingement surface spacing)

Greek Letters

α — molecular thermal diffusivity

β — defined following Eqs. (3.20)

ε — regional average heat flux, $\bar{q}$, for $T_s = T_j = T_o$, see Eq. (2.1)

ε_H — turbulent diffusivity for heat transfer

ε_M — turbulent diffusivity for momentum transfer

ε_r — regional average heat flux, $\bar{q}$, for $T_s = T_j = T_{m,n}$, see Eq. (2.5)

η — regional average fluid temperature difference influence factor defined in terms of overall array parameters, Eq. (2.1)

η_r — regional average fluid temperature difference influence factor defined in terms of individual spanwise row parameters, Eq. (2.5), see also Eqs. (2.9) and (2.11)

μ dynamic viscosity of fluid

ν kinematic viscosity of fluid

ρ density of fluid

θ $\bar{T} - T_s$

$\theta_1, \theta_2, \theta_3$ defined by subproblems following Eq. (3.13)

$\tilde{\theta}_1$ $\theta_1/(T_j - T_s)$

$\tilde{\theta}_2$ $\theta_2/(T_c - T_s)$

$\tilde{\theta}_3$ $\theta_3/[\bar{G}_j/\rho)^2/2c_p]$

Special Subscripts

,n value associated with individual spanwise jet row n within an array

,N value associated with first N upstream spanwise jet rows of an array

SUMMARY

Spanwise average heat fluxes, resolved in the streamwise direction to one streamwise hole spacing, referred to as regional average fluxes, were measured for two-dimensional arrays of circular air jets impinging on a heat transfer surface parallel to the jet orifice plate. The jet flow, after impingement, was constrained to exit in a single direction along the channel formed by the jet orifice plate and heat transfer surface. In addition to the crossflow that originated from the jets following impingement, an initial crossflow was present that approached the array through an upstream extension of the channel. Because of heat addition upstream of a given spanwise row within an array, the mixed-mean temperature of the crossflow approaching the row may be larger than the jet temperature. In the experimental model the mixed-mean initial crossflow temperature, and therefore the mixed-mean crossflow temperature approaching individual spanwise jet rows within the array, could be controlled independently of the jet temperature.

The regional average heat fluxes are considered as a function of parameters associated with corresponding individual spanwise rows within the array (the individual row domain). A linear superposition model was employed to formulate appropriate governing parameters for the individual row domain. The dependent parameters are a Nusselt number, a parameter characterizing the degree of influence on the regional average heat flux of the crossflow temperature within the array relative to the jet temperature (fluid temperature difference influence factor), and a recovery factor. Independent parameters are the individual row jet Reynolds number and crossflow-to-jet mass flux ratio, and the geometric parameters (streamwise jet hole spacing, spanwise hole spacing, and channel height each normalized by hole diameter). The effect of flow history upstream of an individual row domain (i.e., the normalized velocity and temperature distributions at the entrance to an individual row domain) is also considered.

It was found that the fluid temperature difference influence factors are relatively insensitive to jet Reynolds number. They approach zero (jet temperature dominates) as the crossflow-to-jet mass flux ratio approaches zero, and appear to approach unity (crossflow temperature dominates) at

crossflow-to-jet mass flux ratios ranging from about 0.5 to 2 as the channel height ranges from 3 to 1 hole diameters. These fluid temperature difference influence factors, as well as the Nusselt numbers and recovery factors, when compared for a fixed set of values of the independent parameters, were found to be independent of the streamwise position of the row within the array for rows downstream of the second row; however, because of flow history effects values at the first row were found to differ significantly from those for downstream rows. Therefore, test results for a single jet or a single line of jets in a crossflow, if applied to downstream rows within a two-dimensional array, could cause significant errors even if the effects of mixed-mean crossflow temperature and mean crossflow mass flux are accounted for. However, results for the last row of a three-row array, if properly formulated, can be applied to downstream rows of a larger array. For the test model conditions utilized it was found that accounting for recovery effects was not very significant in evaluating Nusselt numbers, but became quite significant for some cases in evaluating fluid temperature difference influence factors. In addition to the results formulated in terms of individual spanwise row parameters, the report contains a complete corresponding set of streamwise resolved (regional average) heat transfer characteristics formulated in terms of flow and geometric parameters characterizing the overall arrays.

1. INTRODUCTION AND BACKGROUND

When impinging jets are utilized for internal cooling of gas turbine components the overall cooling scheme configuration may be such that the jets are subject to a crossflow. Even if the cooling air is supplied to the component at a single temperature, the crossflow air approaching a jet may be at a higher temperature than the jet air because of upstream heat addition to the air comprising the crossflow. In addition to the effect of the crossflow on the flow field of the impinging jet, which may in turn affect the heat rate at the impingement surface, there will also be the effect of the crossflow temperature relative to the jet temperature on the impingement surface heat rate.

Most prior studies of heat transfer to single impinging jets or single spanwise rows of impinging jets subject to a crossflow were performed with the crossflow temperature essentially identical to the jet temperature; see, e.g., Metzger and Korstad (1972), Sparrow et al. (1975), and Goldstein and Behbahani (1982). Bouchez and Goldstein (1975), however, did study the effect on impingement heat transfer of crossflow temperature relative to jet temperature for a single circular jet.

Holdeman and Walker (1977), Srinivasan et al. (1982), and Wittig et al. (1983) studied the temperature profile development downstream of a row of jets mixing with a confined crossflow which approached the jets at a temperature different from the jet temperature. Since these studies were motivated by interest in dilution zone mixing in gas turbine combustion chambers, surface heat transfer characteristics in those cases where impingement did occur were not of interest and were approximately adiabatic during these tests. Therefore, heat fluxes were not determined.

Two-dimensional arrays of circular jets impinging on a heat transfer surface opposite the jet orifice plate produce conditions in which individual jets or rows of jets in the array are subject to a crossflow the source of which is other jets within the array itself. In gas turbine applications the flow from the jets is often constrained to exit essentially in a single direction along the channel formed by the jet orifice plate and the impingement surface.

Experimental studies of impingement surface heat transfer for such configurations motivated by gas turbine applications were reported, e.g., by Kercher and Tabakoff (1970), Florschuetz et al. (1980a, 1980b, 1981a, 1981b), Saad et al. (1980), and Behbahani and Goldstein (1983). In these studies the effect of the temperature of the crossflow approaching a spanwise jet row within the array relative to the jet temperature was not explicitly determined. In fact, such a determination cannot be made from these types of tests, i.e., when (1) the jet air source is from a single plenum, (2) the only crossflow arises from upstream jets within the array, and (3) the form of the thermal boundary condition at the impingement surface (e.g., uniform temperature or uniform flux) is fixed. Under such conditions the crossflow temperature approaching a given spanwise row within the array cannot be independently varied.

Saad et al. (1980) also reported spanwise average, streamwise resolved Nusselt numbers for one array geometry at a single jet flow rate for three different initial crossflow rates approaching the array from an upstream extension of the channel formed by the jet orifice plate and the impingement surface. The magnitude of the initial crossflow temperature relative to the jet temperature was not indicated. Presumably the temperature of the air in the initial crossflow plenum was the same as that for the air in the main jet array plenum.

Florschuetz et al. (1982, 1984) reported experimental results for two-dimensional arrays of circular jets with an initial crossflow approaching the array (Fig. 1.1). The initial crossflow originated from a separate plenum so that its flow rate and temperature could be independently controlled relative to the jet flow rate and temperature. Spanwise average, streamwise resolved (regional average) Nusselt numbers and values of a parameter, η, representing the influence of initial crossflow temperature relative to jet temperature were determined as a function of overall array flow parameters for a range of geometric parameter values.

Subsequently, the data was further analyzed in an attempt to determine regional average Nusselt numbers and η values defined solely in terms of parameters associated with the individual spanwise row opposite the given

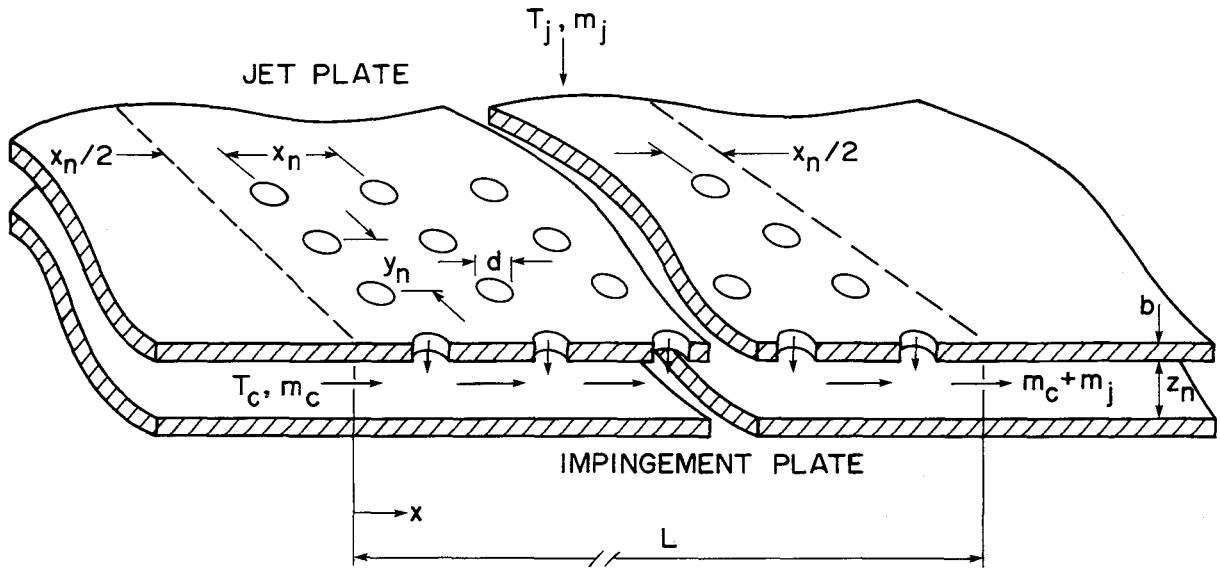

Fig. 1.1 Array of circular jets with an initial crossflow.

impingement region. The objective was to determine if the application of the results in this form could be generalized to apply to individual rows of a larger class of arrays or sub-arrays having similar geometries but an arbitrary number of spanwise rows in the overall array or in each sub-array. A sub-array would be one or more contiguous spanwise rows of jet holes having a uniform hole diameter, hole spacing, and hole pattern which are part of a larger overall array; see, e.g., Florschuetz et al. (1982) or Florschuetz and Tseng (1985).

It had been concluded that for the test conditions utilized recovery effects were not significant in influencing the Nusselt numbers and the η values defined in terms of overall array parameters. Based on this prior conclusion, the early analysis of the data in terms of individual row parameters also did not separately consider recovery effects. Apparently anomalous behavior of the reduced data (particularly the η parameter) for several geometric parameter sets led to the realization that although the influence of the recovery effect was normally small when considered relative

to overall array parameters, the same was not always true when considered in terms of individual row parameters.

A reformulation of the data reduction scheme so as to account for recovery effects (combined with the use of some additional test results) eliminated the anomalous behavior, and also permitted the evaluation of recovery factors. This report presents extensive results for regional average Nusselt numbers and η-type parameters (i.e., fluid temperature difference influence factors) for impingement surface regions associated with individual spanwise rows within a two-dimensional array of circular jets. Results are first presented for these quantities defined in terms of characteristic flow and geometric parameters associated with individual spanwise rows within the array, and then for the analogous quantities defined in terms of characteristic flow and geometric parameters for the overall array.

The Nusselt numbers and fluid temperature difference influence factors are considered to be the primary results required for relating heat fluxes to characteristic fluid temperatures in application to gas turbine components. Recovery effects in that application are normally expected to be negligible because of the large temperature differences involved. However, the significance of recovery effects as they affect regional average heat transfer characteristics at the impingement surface within a two-dimensional array are also examined in this report because of their possible importance in some instances when model tests are conducted with small temperature differences. Results for recovery factors are also presented.

This report is the last in a series of four reports covering the results of an extended series of research investigations on the cooling of surfaces with two-dimensional arrays of circular air jets. The configurations studied were of the general type depicted in Fig. 1.1. The first report [Florschuetz et al. (1980a)] presented experimental results for regional average Nusselt numbers for noninitial crossflow configurations. These were like the configurations of Fig. 1.1, except there was an upstream endwall to the channel located at $x = 0$. Thus, unlike the cases with initial crossflow, the only crossflow present was that originating from upstream jets within the array itself. Results were presented for nine different rectangular inline jet arrays - $(x_n/d, y_n/d)$ of (5,4), (5,6), (5,8), (10,4), (10,6), (10,8),

(15,4), (15,6), and (15,8) - each having ten spanwise rows of holes and each for jet plate-to-impingement surface spacings (channel heights) z_n/d of 1,2, and 3, and two arrays also for z_n/d of 6. Corresponding results were obtained in a number of cases for matching staggered hole pattern arrays in which alternate spanwise rows were offset one-half a spanwise hole spacing. Higher resolution regional average Nusselt numbers (resolved to one-third the streamwise hole spacing) which showed a "damped periodic" streamwise variation were also obtained for a number of configurations. All of these Nusselt number results were presented as a function of the mean jet Reynolds number for the array.

In the second report [Florschuetz et al. (1981a)] measured row-by-row flow distributions for the noninitial crossflow array configurations were presented and used to validate a theoretical model which provided a representation for the flow distributions in terms of a simple closed form expression. The regional average Nusselt numbers were then correlated in terms of the individual spanwise row jet Reynolds numbers, crossflow-to-jet mass flux ratios, and geometric parameters.

The third report [Florschuetz et al. (1982)] dealt with the effects of an initial crossflow approaching the array (Part I) and with the effects of nonuniform array geometries (Part II). In Part II the flow distribution model developed in the second report was extended to nonuniform array geometries and was validated by flow distribution measurements for several such geometries. Experimental results for regional Nusselt numbers for thirteen different nonuniform array configurations were presented. Utilizing the flow distribution models, the nonuniform array Nusselt number results were compared with the prior uniform array results [Florschuetz et al. (1980a)] and with the correlation based on the uniform array results [Florschuetz et al. (1981a)].

In Part I of the third report, the original flow distribution model was extended to cover configurations in which an initial crossflow was present. Measurements made to validate this extended model were also presented. In completing the model validation it was found necessary in some cases to account for the effect of the crossflow on the jet orifice discharge coefficients. Results of separate measurements performed to quantify the significance of this effect were also presented. Experimentally determined

regional average Nusselt numbers and η values defined in terms of overall array parameters were presented for eleven inline hole pattern configurations and one staggered pattern configuration, each for four different initial crossflow-to-jet flow rate ratios ranging from zero to unity. As already noted, some of the raw test data which served as the basis for results presented in the third report, combined with some more recently acquired additional test data, served as the basis for the results developed and documented in the present report.

2. OVERVIEW OF PROBLEM FORMULATION

This section presents an overview of the problem formulation. The reader or user interested primarily in understanding the manner in which the results are formulated in order to examine the results and/or utilize them, but who is not concerned with details of analysis, measurements, and data reduction, should read this section before turning to the results presented and discussed in Sections 6, 7, 8, and 9. This section should also be helpful as an overview to the reader who is interested in the various details as well as the primary formulation of parameters and the results.

The basic test model geometry and nomenclature are shown schematically in Fig. 1.1. Most of the jet arrays tested in the presence of an initial crossflow had uniform inline hole patterns as illustrated in Fig. 1.1. However, two jet arrays were also tested for corresponding staggered patterns in which alternate spanwise rows were offset by one-half a spanwise hole spacing.

For steady-state conditions, heat rates could be measured for regional areas centered opposite spanwise hole rows, covering the span of the impingement heat transfer surface, with a streamwise length of one streamwise hole spacing. Thus, the regional average heat flux, $\bar{q}$, associated with any given spanwise row of the array (Figs. 2.1 and 2.2) could be determined. It was desired to obtain the basic set of heat transfer characteristics for the case of constant fluid properties. Hence, the tests were conducted at relatively small temperature differences; e.g., the maximum surface-to-jet temperature difference utilized was about 35 K.

2.1 Overall Array Domain

First consider the regional average heat fluxes ($\bar{q}$) as a function of parameters associated with the overall array (Fig. 2.1). The total jet flow rate (m_j) and the initial crossflow rate (m_c) are specified. The mixed-mean total temperature of the jet flow at the jet exit plane (T_j) and the mixed mean total temperature of the initial crossflow (T_o) at the entrance to the array (x=0) are also specified since these mixed-mean total temperatures will

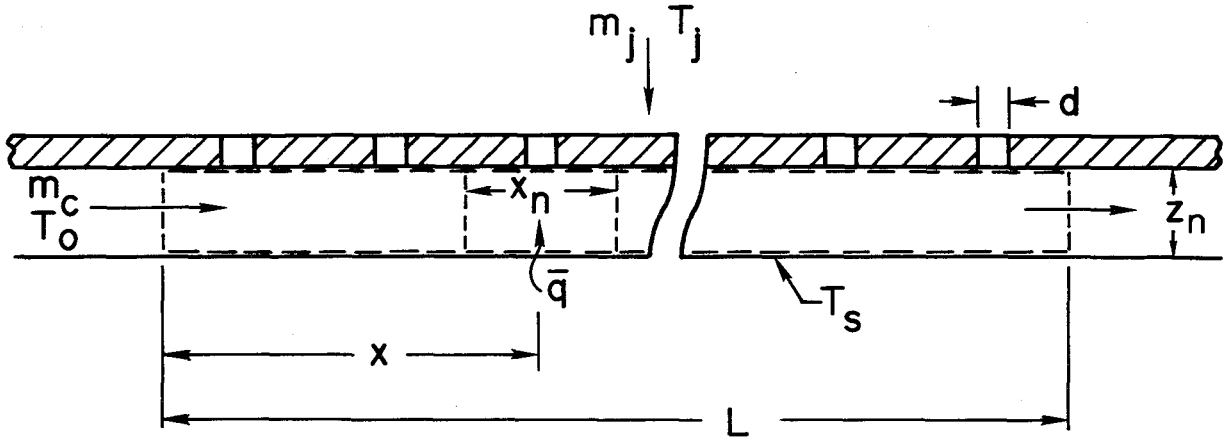

Fig. 2.1 Definition of overall array domain and associated parameters.

normally be available based on energy balances carried out upstream of these boundaries. Since in the present case the objective is to cool the surface by designing impinging jets into the system, the jet flow (always present) is considered to be the primary flow, while the initial crossflow (which, in general, may or may not be present) is considered the secondary flow. Thus, it is convenient to consider $(T_s - T_j)$ as the primary temperature potential and consider the condition T_o different from T_j as a secondary effect. Working from the differential energy equation and boundary conditions written in terms of total temperature for the overall array domain indicated in Fig. 2.1, retaining the dissipation term, but assuming constant fluid properties and a uniform specified impingement surface temperature (T_s), it is shown in Section 3 using linear superposition arguments that the regional average heat flux can be expressed in the form

$$\bar{q} = (k/d)Nu[(T_s-T_j) - \eta(T_o-T_j)] + \varepsilon \qquad (2.1)$$

In this equation ε represents the heat flux which would occur if all three temperatures were equal. $Nu = hd/k$ may be regarded as the Nusselt number and h as the heat transfer coefficient for the special case when $T_o = T_j$ and recovery effects are absent; and η may be regarded as a fluid temperature

difference influence factor reflecting the strength of the influence on the heat flux when T_o differs from T_j. The jet hole diameter is d and the fluid thermal conductivity is k.

It is customary in the heat transfer literature when considering recovery effects to define a recovery temperature and a corresponding normalized form, the recovery factor. The recovery temperature is normally defined as the steady-state surface temperature corresponding to a zero surface heat flux. However, in the present problem, the zero heat flux surface temperature for a given jet temperature will be influenced not only by recovery effects but also by the level of the crossflow temperature relative to the jet temperature. It is also noted that we are considering a uniform impingement surface temperature boundary condition and are concerned with regional average heat fluxes. Therefore, the recovery temperature, T_{rec}, is defined as the surface temperature for a zero mean heat flux, $\bar{q} = 0$, under the condition that T_o is the same as T_j. In the present problem the recovery factor could be defined in terms of either characteristic crossflow or characteristic jet flow conditions. It is here defined in terms of jet flow conditions because the jet flow is considered the primary flow:

$$r = (T_{rec} - t_j)/[(G_j/\rho)^2/2c_p] \tag{2.2}$$

where t_j is the static temperature and ρ is the density at the jet exit plane. Considering Eq. 2.1 with the above definitions of T_{rec} and r, r may be expressed in terms of ε as

$$r = 1 - (\varepsilon/h)/[(G_j/\rho)^2/2c_p] \tag{2.3}$$

Eq. (2.1) may now be recast in the form

$$\bar{q} = (k/d)Nu[(T_s-T_j) - \eta(T_o-T_j) + (1-r)(G_j/\rho)^2/2c_p] \tag{2.4}$$

By dimensional analysis based on the governing differential equations and boundary conditions for the velocity and temperature fields it is shown in Section 3 that the three dimensionless parameters, Nu, η, and r, for computing

regional average heat fluxes based on Eq. (2.4) may be considered to depend at least on the following parameters associated with the overall array:

Geometric parameters (x/L, x_n/d, y_n/d, z_n/d, L/x_n)

Flow and fluid parameters ($\overline{Re}_j$, m_c/m_j, Pr)

Here $\overline{Re}_j = \overline{G}_j d/\mu$ is the array mean jet Reynolds number, where $\overline{G}_j$ is the mean jet mass flux over the array, and Pr is Prandtl number. In addition there is a dependence on the normalized velocity and temperature profiles of the initial crossflow at the entrance to the array, but this effect turns out to be insignificant except in some cases when the initial crossflow is dominant. In general, there may also be a dependence on hole pattern; i.e. inline vs. staggered.

Experimentally determined values of Nu and η as a function of the overall array flow and geometric parameters summarized above are presented in graphical form in Section 7 and in tabular form in Appendix B. Values of r are not presented because they were found to be essentially identical to values of r_r which is a recovery factor defined in the following subsection solely in terms of individual spanwise row parameters. As noted in the next subsection results for r_r are presented graphically in Section 8.2.

For the gas turbine application of Eq. (2.4), temperature differences ($T_s - T_j$) are normally large enough such that the last term in square brackets on the right side of this equation may be safely neglected, especially since the values of r turn out to be close to unity. However, the second term on the right may sometimes be quite significant, so that knowledge of η is required.

It also turns out, as shown in Section 8.1, that for the model tests conducted at nominally ambient pressures and temperatures on which the results presented in this report are based, neglect of the third term associated with recovery effects has negligible effect on the determination of Nu, and in those few cases where the effect on η is noticeable it is of minor significance.

2.2 Individual Spanwise Row Domain

Now consider $\bar{q}$ as a function of parameters associated with the domain of an individual spanwise row n as specified in Fig. 2.2. The mass flux at the jet exit plane (G_j) and the mean mass flux for the crossflow approaching row n (G_c) are specified. As in the case of the overall array domain the mixed-mean total temperature at the jet exit plane (T_j) is specified as the characteristic jet temperature. The characteristic crossflow temperature is specified as the mixed-mean total temperature ($T_{m,n}$) at the channel cross-section located at the upstream edge of the impingement surface region immediately opposite row n; i.e., one-half a streamwise hole spacing upstream of row n. In terms of these parameters, the regional average heat flux opposite row n may be expressed as (see Section 3 for details)

$$\bar{q} = (k/d)Nu_r[(T_s-T_j) - \eta_r(T_{m,n}-T_j)] + \varepsilon_r \tag{2.5}$$

The subscript r is used to distinguish quantities defined solely in terms of row parameters from the corresponding unsubscripted quantities considered in terms of overall array parameters. The interpretation of the parameters ε_r, Nu_r, and η_r is analagous to that given for ε, Nu, and η following Eq. (2.1).

A recovery temperature $T_{rec,r}$ and recovery factor r_r may also be defined in analogous fashion to T_{rec} and r. That is, let $T_{rec,r}$ be defined as the surface temperature for $\bar{q} = 0$, under the condition that $T_{m,n} = T_j$. Then define the recovery factor as

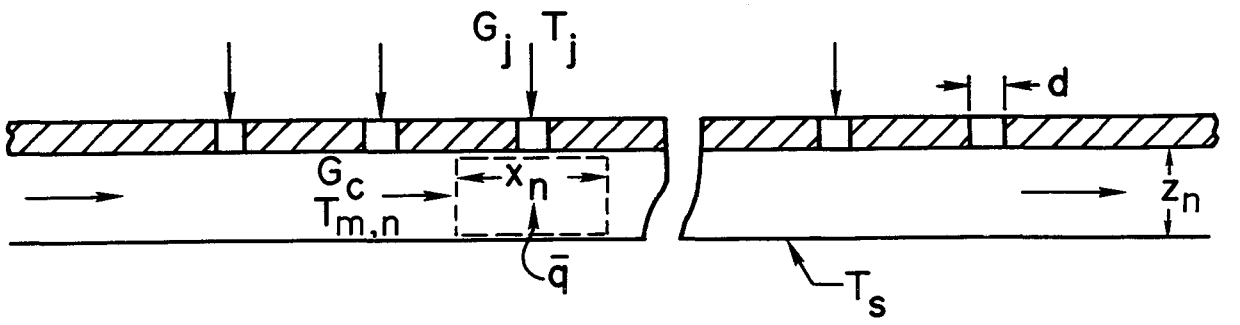

Fig. 2.2 Definition of individual spanwise row domain and associated parameters.

$$r_r = (T_{rec,r} - t_j)/[(G_j/\rho)^2/2c_p] \tag{2.6}$$

With these definitions and Eq. (2.5), r_r may be expressed in terms of ε_r as

$$r_r = 1 - (\varepsilon_r/h_r)/[(G_j/\rho)^2/2c_p)] \tag{2.7}$$

Eq. (2.5) may be recast in the form

$$\bar{q} = (k/d)Nu_r[(T_s-T_j) - \eta_r(T_{m,n}-T_j) + (1-r_r)(G_j/\rho)^2/2c_p] \tag{2.8}$$

Following arguments discussed in Section 3 of this report the parameters Nu_r, η_r, and r_r may be considered as functions of the following individual row parameters:

Geometric parameters (x_n/d, y_n/d, z_n/d)

Flow and fluid parameters (Re_j, G_c/G_j, Pr)

where $Re_j = G_j d/\mu$. Here also there will, in general, be a dependence on the normalized velocity and temperature profiles of the crossflow at the entrance to the individual row domain. These normalized profiles will also, in general, vary depending on the position of the row within the array.

Experimentally determined values of Nu_r and η_r as a function of the geometric and flow parameters summarized above are presented in graphical form in Section 6 and in tabular form in Appendix A. Values of r_r are presented in graphical form in Section 8.2.

Similar to the regional heat flux Eq. (2.4) formulated in terms of overall array parameters, in the application of Eq. (2.8) to gas turbine component cooling temperature differences ($T_s - T_j$) will normally be large enough such that the last term in the square brackets on the right side of this equation can be safely neglected, especially since the values of r_r turn out to be close to unity (Section 8.2). However, the second term on the right may sometimes be quite significant, so that knowledge of η_r is required.

Based on experimental results it is shown in Section 8.1 that for model tests conducted at nominally ambient pressure and temperature levels, recovery effects as represented by the third term on the right side of Eq. (2.8) may in certain cases be quite significant in affecting the determination of η_r while at the same time having only a minor effect on the determination of Nu_r.

2.3 Alternate Formulation and Interpretation of Fluid Temperature Difference Influence Factor

An alternate formulation of the regional average heat flux equation and an alternate interpretation of the fluid temperature difference influence factors (η or η_r) can be obtained by defining a fluid reference temperature, T_{ref}, as equivalent to the surface temperature for a zero regional average heat flux, $\bar{q}$. (T_{ref} should not to be confused with the recovery temperature, T_{rec}.) Consider Eq. (2.8) for $\bar{q}$ in terms of individual spanwise row parameters. Setting $T_s = T_{ref,r}$ and $\bar{q} = 0$ one obtains, with the aid of Eq. (2.6),

$$\eta_r = (T_{ref,r} - T_{rec,r})/(T_{m,n} - T_j) \tag{2.9}$$

Substituting this back into (2.8) one obtains, again with the aid of (2.6),

$$\bar{q} = (k/d)Nu_r(T_s - T_{ref,r}) = h_r(T_s - T_{ref,r}) \tag{2.10}$$

Eqs. (2.6), (2.9), and (2.10) together are equivalent to Eq. (2.8).

In general, for problems like the one under consideration here with two characteristic fluid temperatures, a reference temperature defined as equivalent to the surface temperature at zero surface heat flux will depend on both recovery effects and the magnitude of one fluid temperature relative to the other (here $T_{m,n}$ relative to T_j). However, note that for $r_r = 1$, the recovery temperature is equal to the jet total temperature, $T_{rec,r} = T_j$, so that for this important special case

$$\eta_r = (T_{ref,r} - T_j)/(T_{m,n} - T_j) \tag{2.11}$$

and $T_{ref,r}$ is influenced only by $T_{m,n}$ and T_j.

A similar set of equations applies when considering the regional average heat flux in terms of overall array parameters. These may be obtained by dropping the subscript r in the above set of equations and replacing $T_{m,n}$ by T_o.

The η_r and η parameters defined and utilized in the present work are similar to 'effectiveness' parameters often utilized in connection with film cooling problems. However, in film cooling problems the injected (or jet) flow is normally considered as the secondary flow, whereas in the present jet impingement problem we consider the jet flow as the primary flow as explained in Section 2.1. It may also be noted here that we choose not to use the term adiabatic wall temperature in referring to the fluid reference temperature, $T_{ref,r}$, defined above. This term is misleading unless one is dealing with a uniform heat flux heat transfer surface. In the present study the impingement heat transfer surface was isothermal. Furthermore, the reference temperature is defined as the surface temperature for a zero regional average heat flux. For an isothermal surface (or isothermal region on a surface) to have a zero heat rate (or zero average heat flux), the local heat flux need not be zero everywhere over the surface (or region), and therefore the surface (or region) need not be adiabatic.

The η_r and η parameters defined in the present work are similar, but not identical, to the η -parameter defined by Bouchez and Goldstein (1975) in their study of a single impinging jet in a crossflow. Differences are, first, as in film cooling studies, they considered the crossflow as the primary flow; and second, their η -parameter was appropriately defined in terms of a local adiabatic wall temperature as a reference temperature, since their results were obtained for an adiabatic wall rather than an isothermal surface.

3. SUPERPOSITION MODEL AND DIMENSIONAL ANALYSIS

The primary objective of the investigation is to experimentally determine heat transfer characteristics at the impingement surface for two-dimensional arrays of circular jets including the effect of an initial crossflow approaching the array at a temperature different from the jet temperature, and to formulate the results in a manner which is not only accessible to the designer but also does not unduly restrict the range of applicability of the results. The method of formulation of the results must therefore be a balance between simplicity and generality. In order to approach this objective, the techniques of modeling by linear superposition and dimensional analysis are both employed.

In this section the problem is formulated in detail. The differential equation and boundary conditions governing the fluid temperature field are assumed to be linear, so that in formulating the impingement surface heat flux a decomposition of the problem using superposition techniques is utilized. Relying on the governing equations the essential variables and parameters are identified in dimensionless forms.

Consider a midchord cooling arrangement of a turbine airfoil which utilizes jet array impingement in the presence of an initial crossflow; e.g., where leading edge jet cooling air, after impingement, flows toward the trailing edge becoming an initial crossflow to the midchord jet array. In some designs, the total temperature of leading edge injection air (denoted by T_{cp}) might have the same value as that of the midchord jet array injection (denoted by T_j) while in other possible designs one might have $T_{cp} \neq T_j$. In either case, the mixed-mean total temperature of the initial crossflow approaching the first upstream row (row 1) of the midchord jet array, $T_{m,1}$ (later also denoted by the special symbol T_o), will in general differ from T_j. Similarly, the mixed-mean total temperature approaching any given spanwise row n within the array, $T_{m,n}$, will in general differ from T_j. It is highly desireable for the designer to have available results for heat transfer characteristics in the midchord jet array portion of the channel which are at least nominally independent of the detailed configuration and conditions associated with the source of the initial crossflow approaching the array

entrance. This would permit him to analyze alternative array designs as a part of various overall design concepts. The designer is provided with even more flexibility if he has available heat transfer characteristics applicable to arbitrary individual spanwise rows of a two-dimensional array which are nominally independent of the detailed geometric and other design conditions associated with the overall array.

Hence, in the following analyses two separate but related flow field domains associated with the flow field in the midchord array region of the crossflow channel are considered. First, there is the overall jet array domain physically bounded by the jet plate and the impingement (or heat transfer) surface, and considered to extend from the entrance (x=0) to the exit (x=L) of the jet array portion of the channel (Figs. 1.1 and 2.1). Second, there is the regional domain associated with any given individual spanwise row of the array, also physically bounded by the jet plate and the impingement surface, but considered to extend over a length of the channel equivalent to one streamwise hole spacing centered at the given spanwise row (Fig. 2.2).

In the following analyses, the main objective is to formulate and examine a regional average value of the impingement surface heat flux, $\bar{q}$. The value considered is averaged across the span of the impingement surface, but in the streamwise direction is averaged over increments of length x_n centered directly opposite the centerlines of the spanwise rows of holes in the array (Figs. 2.1 and 2.2).

The analyses presented in this section lead to a formulation of this regional average heat flux, first as a function of parameters associated with the overall jet array domain, and second as a function of parameters associated with the individual spanwise row (regional) domain for which the regional average is defined. The resulting formulations were presented in Section 2 in summary form. A detailed development of the formulations is presented in the following sections.

3.1 Velocity Field

In order to consider the velocity field for the overall array domain (Fig. 2.1), the boundary condition at the jet exit plane must be established.

The pressure at the upstream side (the plenum side) of the jet orifice plate is assumed to be uniform while the pressure on the channel side will, in general, decrease in the downstream direction along the channel. A model for the resulting jet flow distribution was previously developed by assuming the discrete hole array to be replaced by a surface over which the injection is continuously distributed [Florschuetz et al. (1981a, 1981b, 1982) and Florschuetz and Isoda (1983)]. Solutions for the jet flow distribution, $G_j/\bar{G}_j$, the crossflow-to-jet mass flux ratio, G_c/G_j, and the channel pressure, $p(x)$, each based on the model, were found to give very good agreement with measured values for the discrete arrays considered in this study. For later reference in completing the dimensional analysis, the functional dependence for the jet flow distribution and for the channel pressure gradient are required. Based on the results of the previously developed model these are, in dimensionless form,

$$(G_j/\bar{G}_j)A_o^* = G_j^*/\bar{G}_j = fcn[\tilde{x},\ (x_n/d)(y_n/d),\ z_n/L,\ \overline{Re}_j(L/d),\ M] \tag{3.1}$$

$$d\tilde{p}/d\tilde{x} = fcn[\tilde{x},\ (x_n/d)(y_n/d),\ z_n/L,\ \overline{Re}_j(L/d),\ M] \tag{3.2}$$

where the open area ratio is $A_o^* = \pi/[4(x_n/d)(y_n/d)]$, $\tilde{p} = \bar{p}/[\rho(\bar{G}_j/\rho)^2]$, and $\tilde{x} = x/L$.

As already explained, heat fluxes at the impingement surface were to be measured as values averaged across the span of the surface, but spatially resolved in the streamwise direction. Therefore, for simplicity, the formulation of parameters for the velocity field is presented using a steady two-dimensional turbulent flow model with continuously distributed injection as shown in Fig. 3.1. Thus, for the present purpose, velocity variations in the spanwise coordinate are not considered.

In reality, the velocity field for a two-dimensional array of impinging jets with confined crossflow involves complex recirculating flows, especially when the crossflow is weak. However, the minimum streamwise increment to be considered for average heat transfer characteristics is one streamwise hole spacing, x_n. It is assumed at the outset that the velocity and temperature

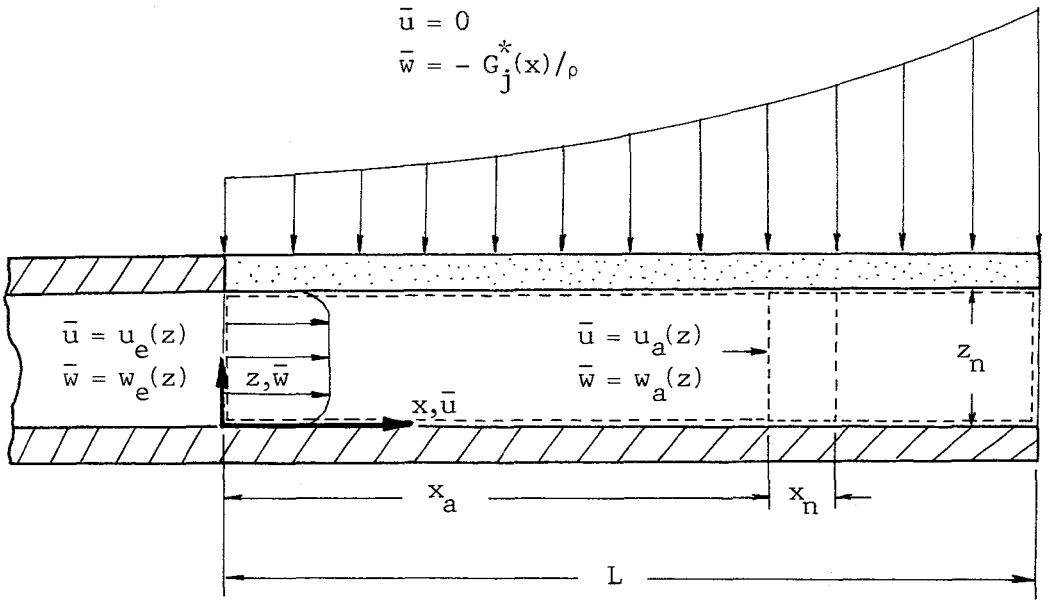

Fig. 3.1 Velocity field boundary conditions for continuous injection model with initial crossflow.

fields downstream of a given streamwise location have negligible influence on the surface heat flux averaged over a streamwise increment, x_n, situated immediately upstream of the location. Hence, for the present purpose, the streamwise coordinate x is assumed to be a one-way coordinate, and the governing equations are written in boundary layer form.

For constant fluid properties and negligible body forces, the time-averaged momentum equation is [Kays and Crawford (1980)]

$$\bar{u}\frac{\partial \bar{u}}{\partial x} + \bar{w}\frac{\partial \bar{u}}{\partial z} + \frac{1}{\rho}\frac{d\bar{p}}{dx} = \frac{\partial}{\partial z}\left(\nu\frac{\partial \bar{u}}{\partial z} - \overline{u'w'}\right)$$

where ν is the kinematic viscosity, an overbar denotes a time-averaged value, and the prime indicates the fluctuation quantities. Since the gradient transport model works well for boundary layer flow, we define the turbulent diffusivity for momentum transfer, ε_M, by

$$- \overline{u'w'} = \varepsilon_M \frac{\partial \bar{u}}{\partial z}$$

The time-averaged momentum equation becomes

$$\bar{u} \frac{\partial \bar{u}}{\partial x} + \bar{w} \frac{\partial \bar{u}}{\partial z} + \frac{1}{\rho} \frac{d\bar{p}}{dx} = \frac{\partial}{\partial z}\left[(\nu + \varepsilon_M)\frac{\partial \bar{u}}{\partial z}\right] \tag{3.3}$$

The continuity equation is

$$\frac{\partial \bar{u}}{\partial x} + \frac{\partial \bar{w}}{\partial z} = 0 \tag{3.4}$$

Considering the domain of the overall array shown in Fig. 3.1, we have the following boundary conditions

$$\bar{u} = u_e(z), \ \bar{w} = w_e(z) \quad ; \text{ at } x = 0, \ 0 < z < z_n \tag{3.5a}$$

$$\bar{u} = 0 \quad , \ \bar{w} = 0 \quad ; \text{ at } 0 \leq x \leq L, \ z = 0 \tag{3.5b}$$

$$\bar{u} = 0 \quad , \ \bar{w} = -G_j^*(x)/\rho \ ; \text{ at } 0 \leq x \leq L, \ z = z_n \tag{3.5c}$$

Note that the velocity components at the array entrance, u_e and w_e, are specified as functions of z.

Define the following dimensionless variables

$$\tilde{x} = x/L$$

$$\tilde{z} = z/L$$

$$\tilde{u} = \bar{u}/(\bar{G}_j/\rho)$$

$$\tilde{w} = \bar{w}/(\bar{G}_j/\rho)$$

$$\tilde{p} = \bar{p}/[\rho(\bar{G}_j/\rho)^2]$$

In dimensionless form the problem specified by Eqs. (3.3), (3.4), and (3.5) becomes

$$\tilde{u}\frac{\partial\tilde{u}}{\partial\tilde{x}} + \tilde{w}\frac{\partial\tilde{u}}{\partial\tilde{z}} + \frac{d\tilde{p}}{d\tilde{x}} = \frac{\partial}{\partial\tilde{z}}\left[\left(\frac{1+\varepsilon_M/\nu}{\overline{Re}_j}\right)\frac{1}{(L/d)}\frac{\partial\tilde{u}}{\partial\tilde{z}}\right] \tag{3.6a}$$

$$\frac{\partial\tilde{u}}{\partial\tilde{x}} + \frac{\partial\tilde{w}}{\partial\tilde{z}} = 0 \tag{3.6b}$$

$$\tilde{u} = \frac{u_e(\tilde{z})}{\bar{G}_j/\rho}\ ,\quad \tilde{w} = \frac{w_e(\tilde{z})}{\bar{G}_j/\rho}\ ;\quad \text{at } \tilde{x} = 0,\ 0 < \tilde{z} < z_n/L \tag{3.7a}$$

$$\tilde{u} = 0\ ,\quad \tilde{w} = 0\ ;\quad \text{at } 0 \le \tilde{x} \le 1,\ \tilde{z} = 0 \tag{3.7b}$$

$$\tilde{u} = 0\ ,\quad \tilde{w} = -G_j^*/\bar{G}_j\ ;\quad \text{at } 0 \le \tilde{x} \le 1,\ \tilde{z} = z_n/L \tag{3.7c}$$

It is now assumed that ε_M/ν is a function only of the normalized time-averaged velocity field and/or space coordinates, i.e.,

$$\varepsilon_M/\nu = \text{fcn}(\tilde{u},\ \tilde{w};\ \tilde{x},\ \tilde{z}) \tag{3.8}$$

Based on Eqs. (3.6) and (3.7), with the aid of (3.1), (3.2) and (3.8), the functional dependence of the dimensionless time-averaged velocities, $\tilde{u}$ and $\tilde{w}$, in the domain of the overall array is

$$\tilde{u} = \text{fcn}\left[\tilde{x},\ \tilde{z},\ (x_n/d)(y_n/d),\ z_n/L,\ \overline{Re}_j(L/d),\ M,\ \frac{u_e(\tilde{z})}{\bar{G}_j/\rho},\ \frac{w_e(\tilde{z})}{\bar{G}_j/\rho}\right] \tag{3.9a}$$

$$\tilde{w} = \text{fcn}\left[\tilde{x},\ \tilde{z},\ (x_n/d)(y_n/d),\ z_n/L,\ \overline{Re}_j(L/d),\ M,\ \frac{u_e(\tilde{z})}{\overline{G}_j/\rho},\ \frac{w_e(\tilde{z})}{\overline{G}_j/\rho}\right] \tag{3.9b}$$

By analogous arguments, considering a regional domain over an impingement surface increment x_n (located at $x = x_a$ in Fig. 3.1) one can arrive at

$$\tilde{u} = \text{fcn}\left[\tilde{x},\ \tilde{z},\ (x_n/d)(y_n/d),\ z_n/x_n,\ Re_j(x_n/d),\ G_c/G_j,\ \frac{u_a(\tilde{z})}{G_j/\rho},\ \frac{w_a(\tilde{z})}{G_j/\rho}\right]$$

and (3.10a)

$$\tilde{w} = \text{fcn}\left[\tilde{x},\ \tilde{z},\ (x_n/d)(y_n/d),\ z_n/x_n,\ Re_j(x_n/d),\ G_c/G_j,\ \frac{u_a(\tilde{z})}{G_j/\rho},\ \frac{w_a(\tilde{z})}{G_j/\rho}\right]$$

(3.10b)

where here $\tilde{x} = x/x_n$ and $\tilde{z} = z/x_n$. $u_a(z)$ and $w_a(z)$ represent the velocity profile of the crossflow at the upstream control surface (entrance) of the regional domain. In application to the discrete hole array Re_j is the jet Reynolds number for the particular spanwise row associated with the regional domain, defined by $Re_j = G_j d/\mu$, where G_j is the jet mass flux at the particular row. G_c is the mean mass flux of the crossflow at the entrance to the regional domain (i.e., approaching the spanwise row).

3.2 Temperature Field

Consider the physical model depicted in Fig. 3.2, where the discrete jet array injection over $0 < x < L$ has again been represented for simplicity as continuously distributed injection at a temperature T_j. The source of the initial crossflow approaching the array is represented as entering the initial crossflow channel $[-(L_e + L_c) < x < 0]$ at a single temperature T_{cp}. If one considers the domain $-(L_e + L_c) < x < L$ and $0 < z < z_n$, heat fluxes can be considered as functions of two specified fluid temperatures, T_j and T_{cp}, and the uniform surface temperature T_s. However, the heat flux of interest here at the impingement surface opposite the array injection area would then also be an explicit function of conditions upstream of $x = 0$. Here, since we are

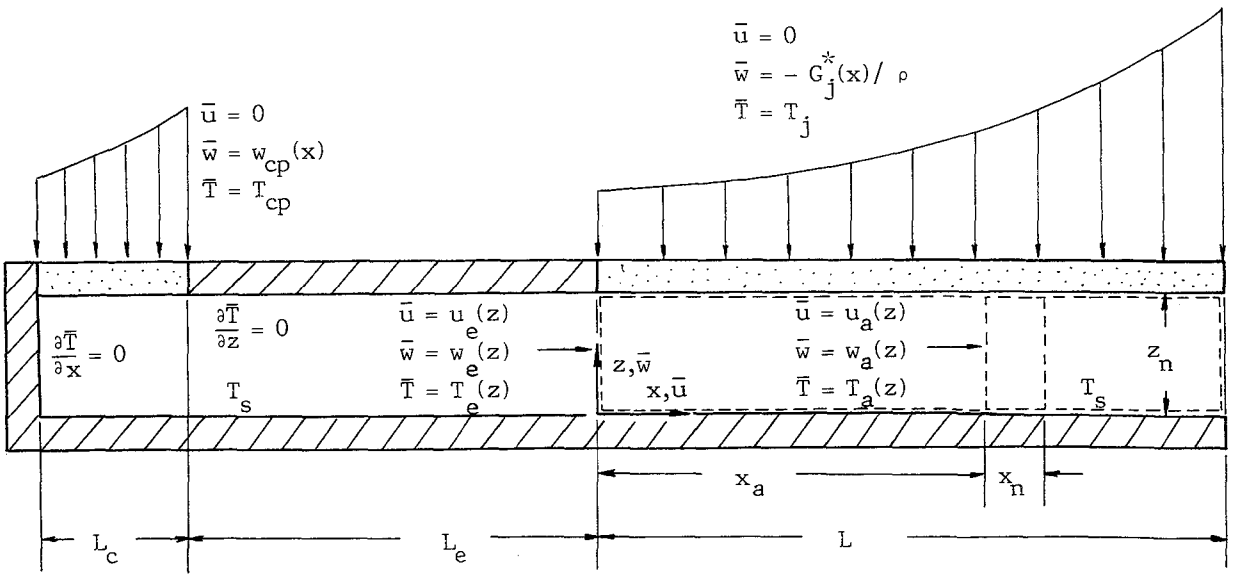

Fig. 3.2 Temperature field boundary conditions for continuous injection model with initial crossflow.

considering instead either the array domain or the individual row (regional) domain the heat flux of interest is a function of the temperature distribution at the upstream control surface (or entrance) of either the array domain or the row domain, as well as a function of T_j and T_s. In Fig. 3.2 the entrance temperature distributions are represented as $T_e(z)$ at $x = 0$ for the array domain and $T_a(z)$ at $x = x_a$ for the row domain. In either domain, for a steady turbulent boundary layer type flow with constant fluid properties and negligible body forces, the time-averaged energy equation may be expressed in terms of the time-averaged total temperature, $\bar{T}$, as [Kays and Crawford (1980)]

$$\bar{u}\,\frac{\partial \theta}{\partial x} + \bar{w}\,\frac{\partial \theta}{\partial z} - \frac{\partial}{\partial z}\left[(\alpha+\varepsilon_H)\,\frac{\partial \theta}{\partial z}\right] = \frac{\partial}{\partial z}\left[\left(1 - \frac{1}{Pr_{eff}}\right)(\nu+\varepsilon_M)\,\frac{\partial}{\partial z}\left(\frac{\bar{u}^2}{c_p}\right)\right] \tag{3.11}$$

where here we have set $\theta = \bar{T} - T_s$, so that the boundary condition written for the impingement heat transfer surface will be homogenous in θ. The turbulent diffusivity for heat, ε_H, is defined by

$$-\overline{t'w'} = \varepsilon_H \frac{\partial \bar{t}}{\partial z}$$

where t is the static temperature. The effective Prandtl number, defined as $(\nu+\varepsilon_M)/(\alpha+\varepsilon_H)$ may be expressed in terms of the turbulent Prandtl number, $Pr_t = \varepsilon_M/\varepsilon_H$, as

$$Pr_{eff} = (1 + \varepsilon_M/\nu)/[(\varepsilon_M/\nu)(1/Pr_t) + 1/Pr]$$

Consider now the array domain. The relevant boundary conditions are

$$\theta = T_j - T_s \qquad \text{at } 0 \leq x \leq L,\ z = z_n \tag{3.12a}$$

$$\theta = T_e(z) - T_s \qquad \text{at } x = 0,\ 0 < z < z_n \tag{3.12b}$$

$$\theta = 0 \qquad \text{at } 0 \leq x \leq L,\ z = 0 \tag{3.12c}$$

The differential equation (3.11) and boundary conditions (3.12) are linear in the dependent variable θ. The problem contains three nonhomogeneous conditions, one each in Eqs. (3.11), (3.12a), and (3.12b). Therefore, we may decompose it into three subproblems, each with one nonhomogeneous condition. Let

$$\theta = \theta_1 + \theta_2 + \theta_3 \tag{3.13}$$

where the three subproblems are:

Subproblem 1:

$$\bar{u}\ \frac{\partial \theta_1}{\partial x} + \bar{w}\ \frac{\partial \theta_1}{\partial z} - \frac{\partial}{\partial z}\left[(\alpha+\varepsilon_H)\ \frac{\partial \theta_1}{\partial z}\right] = 0$$

$$\theta_1 = T_j - T_s \qquad \text{at } 0 \leq x \leq L,\ z = z_n$$

$$\theta_1 = 0 \qquad \text{at } x = 0,\ 0 < z < z_n$$

$$\theta_1 = 0 \qquad \text{at } 0 \leq x \leq L,\ z = 0$$

Subproblem 2:

$$\bar{u}\ \frac{\partial \theta_2}{\partial x} + \bar{w}\ \frac{\partial \theta_2}{\partial z} - \frac{\partial}{\partial z}\left[(\alpha+\varepsilon_H)\ \frac{\partial \theta_2}{\partial z}\right] = 0$$

$$\theta_2 = 0 \qquad \text{at } 0 \leq x \leq L,\ z = z_n$$

$$\theta_2 = T_e(z) - T_s \qquad \text{at } x = 0,\ 0 < z < z_n$$

$$\theta_2 = 0 \qquad \text{at } 0 \leq x \leq L,\ z = 0$$

Subproblem 3:

$$\bar{u}\ \frac{\partial \theta_3}{\partial x} + \bar{w}\ \frac{\partial \theta_3}{\partial z} - \frac{\partial}{\partial z}\left[(\alpha+\varepsilon_H)\ \frac{\partial \theta_3}{\partial z}\right] = \frac{\partial}{\partial z}\left[\left(1 - \frac{1}{Pr_{eff}}\right)(\nu+\varepsilon_M)\ \frac{\partial}{\partial z}\left(\frac{\bar{u}^2}{2c_p}\right)\right]$$

$$\theta_3 = 0 \qquad \text{at } 0 \leq x \leq L,\ z = z_n$$

$$\theta_3 = 0 \qquad \text{at } x = 0,\ 0 < z < z_n$$

$$\theta_3 = 0 \qquad \text{at } 0 \leq x \leq L,\ z = 0$$

Now each of the subproblems may be normalized. Clearly for Subproblem 1 it is appropriate to let

$$\tilde{\theta}_1 = \theta_1/(T_j - T_s)$$

For subproblem 2, the nonhomogeneous boundary condition is not, in general, a constant but represents a crossflow temperature distribution. Therefore, let

$$\tilde{\theta}_2 = \theta_2/(T_c - T_s)$$

where T_c represents a characteristic crossflow temperature at the entrance to the domain which is yet to be specified. Subproblem 3 has no immediately obvious characteristic temperature difference, but based on inspection of the nonhomogeneous term in the differential equation we select a dynamic temperature, basing it on the array mean jet velocity. Let

$$\tilde{\theta}_3 = \theta_3/[(\bar{G}_j/\rho)^2/2c_p]$$

With these definitions the original equation defining the superposition, Eq. (3.13), becomes

$$\theta = \tilde{\theta}_1(T_j - T_s) + \tilde{\theta}_2(T_c - T_s) + \tilde{\theta}_3\,[(\bar{G}_j/\rho)^2/2c_p] \tag{3.14}$$

Normalizing the variables x, z, u and w as before, the three subproblems may be written in the following forms:

Subproblem 1:

$$\tilde{u}\frac{\partial\tilde{\theta}_1}{\partial\tilde{x}} + \tilde{w}\frac{\partial\tilde{\theta}_1}{\partial\tilde{z}} - \frac{\partial}{\partial\tilde{z}}\left(\beta\frac{\partial\tilde{\theta}_1}{\partial\tilde{z}}\right) = 0 \tag{3.15}$$

$$\tilde{\theta}_1 = 1 \qquad \text{at } 0 \leq \tilde{x} \leq 1,\ \tilde{z} = z_n/L \tag{3.16a}$$

$$\tilde{\theta}_1 = 0 \qquad \text{at } \tilde{x} = 0,\ 0 < \tilde{z} < z_n/L \tag{3.16b}$$

$$\tilde{\theta}_1 = 0 \qquad \text{at } 0 \leq \tilde{x} \leq 1,\ \tilde{z} = 0 \tag{3.16c}$$

Subproblem 2:

$$\tilde{u}\frac{\partial\tilde{\theta}_2}{\partial\tilde{x}} + \tilde{w}\frac{\partial\tilde{\theta}_2}{\partial\tilde{z}} - \frac{\partial}{\partial\tilde{z}}\left(\beta\frac{\partial\tilde{\theta}_2}{\partial\tilde{z}}\right) = 0 \tag{3.17}$$

$$\tilde{\theta}_2 = 0 \qquad \text{at } 0 \leq \tilde{x} \leq 1,\ \tilde{z} = z_n/L \tag{3.18a}$$

$$\tilde{\theta}_2 = \frac{T_e(\tilde{z}) - T_s}{T_c - T_s} \qquad \text{at } \tilde{x} = 0,\ 0 < \tilde{z} < z_n/L \tag{3.18b}$$

$$\tilde{\theta}_2 = 0 \qquad \text{at } 0 \leq \tilde{x} \leq 1,\ \tilde{z} = 0 \tag{3.18c}$$

Subproblem 3:

$$\tilde{u}\frac{\partial\tilde{\theta}_3}{\partial\tilde{x}} + \tilde{w}\frac{\partial\tilde{\theta}_3}{\partial\tilde{z}} - \frac{\partial}{\partial\tilde{z}}\left(\beta\frac{\partial\tilde{\theta}_3}{\partial\tilde{z}}\right) = \frac{\partial}{\partial\tilde{z}}\left[(Pr_{eff} - 1)\beta\frac{\partial\tilde{u}^2}{\partial\tilde{z}}\right] \tag{3.19}$$

$$\tilde{\theta}_3 = 0 \qquad \text{at } 0 \leq \tilde{x} \leq 1,\ \tilde{z} = z_n/L \tag{3.20a}$$

$$\tilde{\theta}_3 = 0 \qquad \text{at } \tilde{x} = 0,\ 0 < \tilde{z} < z_n/L \tag{3.20b}$$

$$\tilde{\theta}_3 = 0 \qquad \text{at } 0 \leq \tilde{x} \leq 1,\ \tilde{z} = 0 \tag{3.20c}$$

where

$$\beta = \left[\frac{1}{\overline{Re}_j(L/d)}\left(\frac{1}{Pr} + \frac{1}{Pr_t}\frac{\varepsilon_M}{\nu}\right)\right]$$

If we now assume that the turbulent Prandtl number is a function only of the normalized time-averaged velocity field and/or space coordinates, and the molecular Prandtl number, i.e.,

$$Pr_t = fcn(\tilde{u}, \tilde{w}, \tilde{x}, \tilde{z}, Pr)$$

and recall Eq. (3.8), we can conclude by inspecting Eqs. (3.15) and (3.16) for Subproblem 1 that

$$\tilde{\theta}_1 = fcn(\tilde{u}, \tilde{w}, \tilde{x}, \tilde{z}, z_n/L, \overline{Re}_j(L/d), Pr) \tag{3.21}$$

where the functional dependence of $\tilde{u}$ and $\tilde{w}$ is given by Eqs. (3.9). Similarly, from Eqs. (3.17) and (3.18) for Subproblem 2

$$\tilde{\theta}_2 = \text{fcn}(\tilde{u}, \tilde{w}, \tilde{x}, \tilde{z}, z_n/L, \overline{Re}_j(L/d), \frac{T_e(\tilde{z}) - T_s}{T_c - T_s}, Pr) \tag{3.22}$$

where the additional parameter $\frac{T_e(\tilde{z}) - T_s}{T_c - T_s}$ indicates the normalized temperature distribution of the initial crossflow at the array entrance. Finally, from Eqs. (3.19) and (3.20) for Subproblem 3

$$\tilde{\theta}_3 = \text{fcn}(\tilde{u}, \tilde{w}, \tilde{x}, \tilde{z}, z_n/L, \overline{Re}_j(L/d), Pr) \tag{3.23}$$

3.3 Regional Average Heat Flux

The regional average heat flux, $\bar{q}$, is defined by (see Fig. 3.2 for coordinates, see also Figs. 2.1 and 2.2)

$$\bar{q} = -\frac{1}{x_n}\int_{x_a}^{x_a+x_n} k(\partial\bar{T}/\partial z)_{z=0}dx = -\frac{k}{x_n}\int_{x_a/L}^{x_a/L+x_n/L} (\partial\theta/\partial\tilde{z})_{\tilde{z}=0}\, d\tilde{x} \tag{3.24}$$

Substituting Eq. (3.14) into Eq. (3.24) yields

$$\bar{q} = a(T_s - T_j) + b(T_s - T_c) + \varepsilon \tag{3.25}$$

where

$$a = \frac{k}{x_n}\int_{x_a/L}^{x_a/L+x_n/L} (\partial\tilde{\theta}_1/\partial\tilde{z})_{\tilde{z}=0}\, d\tilde{x} \tag{3.26}$$

$$b = \frac{k}{x_n} \int_{x_a/L}^{x_a/L+x_n/L} (\partial\tilde{\theta}_2/\partial\tilde{z})_{\tilde{z}=0}\, d\tilde{x} \tag{3.27}$$

$$\varepsilon = -\frac{k}{x_n} \frac{(\bar{G}_j/\rho)^2}{2c_p} \int_{x_a/L}^{x_a/L+x_n/L} (\partial\tilde{\theta}_3/\partial\tilde{z})_{\tilde{z}=0}\, d\tilde{x} \tag{3.28}$$

Examining Eqs. (3.26), (3.21), and (3.9), we may write

$$\frac{ax_n}{k} = \text{fcn}\left[x_a/L,\ x_n/d,\ y_n/d,\ z_n/d,\ L/x_n,\ \overline{Re}_j,\ M,\ \frac{u_e(\tilde{z})}{G_{co}/\rho},\ \frac{w_e(\tilde{z})}{G_{co}/\rho},\ Pr\right] \tag{3.29}$$

Similarly, inspecting Eqs. (3.27), (3.22), and (3.9) we conclude that

$$\frac{bx_n}{k} = \text{fcn}\left[x_a/L,\ x_n/d,\ y_n/d,\ z_n/d,\ L/x_n,\ \overline{Re}_j,\ M,\ \frac{u_e(\tilde{z})}{G_{co}/\rho},\ \frac{w_e(\tilde{z})}{G_{co}/\rho},\ \frac{T_e(\tilde{z})-T_s}{T_c-T_s},\ Pr\right] \tag{3.30}$$

and finally from Eqs. (3.28), (3.23), and (3.9) we observe that

$$\frac{\varepsilon x_n/k}{(\bar{G}_j/\rho)^2/(2c_p)} = \text{fcn}\left[x_a/L,\ x_n/d,\ y_n/d,\ z_n/d,\ L/x_n,\ \overline{Re}_j,\ M,\ \frac{u_e(\tilde{z})}{G_{co}/\rho},\ \frac{w_e(\tilde{z})}{G_{co}/\rho},\ Pr\right] \tag{3.31}$$

For simplicity in writing governing equations and especially boundary conditions, the above formulations were developed assuming two-dimensional velocity and temperature fields with continuous injection. Therefore, x_n, y_n and d did not initially enter the problem explicitly except through the open area ratio A_o^* arising in the flow distribution model used to specify the

velocity boundary condition at the injection surface (jet exit plane) [see Eq. (3.1)]. In the real three-dimensional, discrete array injecton problem x_n, y_n, and d would each appear separately through boundary conditions, and x_n and y_n would each appear also in defining a regional average heat flux. In the context of the normalization following Eqs. (3.5) these would have appeared all normalized by L; i.e., x_n/L, y_n/L, and d/L. In writing the functional dependences expressed above by Eqs. (3.29), (3.30), and (3.31), we have chosen to re-normalize the geometric parameters so that x_n, y_n, and z_n are always normalized by d, and the parameter L by x_n. Note that L/x_n is equivalent to the number of spanwise rows in an array of length L with streamwise hole spacing x_n. Also u_e and w_e have been re-normalized using G_{co}, the mean initial crossflow velocity, in place of $\bar{G}_j$. These two velocities are directly related through M and the geometric parameters.

For the present problem, the jet flow is considered the main flow, and the crossflow is considered the secondary flow. Therefore, it is convenient to consider (T_s-T_j) as the primary temperature potential and the condition to $T_c \neq T_j$ as a secondary effect. Also, the recovery effects associated with the term ε in Eq. (3.25) will often be small or negligible. In this spirit, consider the special case $T_c = T_j$ and $\varepsilon = 0$ as a reference condition. Then Eq. (3.25) reduces to

$$\bar{q} = (a + b)(T_s - T_j) = h(T_s - T_j)$$

where

$$h = a + b \tag{3.32}$$

Thus h = a + b may be interpreted as a heat transfer coefficient in the traditional sense for a two-temperature problem with negligible recovery effects.

Now rewrite Eq. (3.25) eliminating a in favor of h using (3.32),

$$\bar{q} = h(T_s - T_j) - b(T_c - T_j) + \varepsilon$$

The first two terms on the right hand side include contributions to the heat flux because of temperature differences, while the third term, ε, is a contribution associated solely with recovery effects. Factoring h out of the first two terms gives

$$\bar{q} = h[(T_s - T_j) - b/h(T_c - T_j)] + \varepsilon$$

Let

$$\eta = b/h = b/(a + b)$$

Then

$$\bar{q} = h[(T_s - T_j) - \eta(T_c - T_j)] + \varepsilon \tag{3.33}$$

where η may be interpreted as a fluid temperature difference influence factor.

Define an array Nusselt number, Nu, as

$$Nu = \frac{hd}{k}$$

Then

$$Nu = \frac{ax_n}{k}\frac{d}{x_n} + \frac{bx_n}{k}\frac{d}{x_n}$$

From Eqs. (3.29) and (3.30), we have

$$Nu = fcn[x_a/L,\ x_n/d,\ y_n/d,\ z_n/d,\ L/x_n,\ \overline{Re}_j,\ M,\ \frac{u_e(\tilde{z})}{G_{co}/\rho},\ \frac{w_e(\tilde{z})}{G_{co}/\rho},\ \frac{T_e(\tilde{z})-T_s}{T_c-T_s},\ Pr] \tag{3.34}$$

In a similar manner, η may be written as

$$\eta = \frac{bx_n/k}{ax_n/k + bx_n/k}$$

From Eqs. (3.29) and (3.30), it is concluded that

$$\eta = \text{fcn}\left[x_a/L,\ x_n/d,\ y_n/d,\ z_n/d,\ L/x_n,\ \overline{Re}_j,\ M,\ \frac{u_e(\tilde{z})}{G_{co}/\rho},\ \frac{w_e(\tilde{z})}{G_{co}/\rho},\ \frac{T_e(\tilde{z})-T_s}{T_c-T_s},\ Pr\right] \tag{3.35}$$

Now, define a recovery temperature, T_{rec}, as the surface temperature for $\bar{q} = 0$ and $T_c = T_j$, and a corresponding recovery factor, r, as

$$r = \frac{T_{rec} - t_j}{G_j^2/(2c_p\rho^2)}$$

where G_j is the jet mass flux opposite the region ($x = x_a$), for which $\bar{q}$ is set to zero. With the aid of Eq. (3.33) and the definition of Nu this may be written in the following alternate forms

$$r = 1 - \frac{\varepsilon/h}{G_j^2/(2c_p\rho^2)} = 1 - \frac{\varepsilon x_n/k}{(\bar{G}_j/\rho)^2/(2c_p)}\,\frac{d}{x_n}\,\frac{1}{Nu}\,\frac{1}{(G_j/\bar{G}_j)^2} \tag{3.36}$$

Examining Eqs. (3.36), (3.34), (3.31) and (3.1), it may be concluded that

$$r = \text{fcn}\left[x_a/L,\ x_n/d,\ y_n/d,\ z_n/d,\ L/x_n,\ \overline{Re}_j,\ M,\ \frac{u_e(\tilde{z})}{G_{co}/\rho},\ \frac{w_e(\tilde{z})}{G_{co}/\rho},\ \frac{T_e(\tilde{z})-T_s}{T_c-T_s},\ Pr\right]$$

Now consider the regional domain over the impingement surface increment x_n (located at $x = x_a$, Fig. 3.2). Following parallel arguments to those presented in Sections 3.1, 3.2, and 3.3 for the array domain, the following results are obtained:

$$\bar{q} = h_r[(T_s-T_j) - \eta_r(T_c-T_j)] + \varepsilon_r \tag{3.37}$$

with

$$Nu_r = \text{fcn}\left[x_n/d,\ y_n/d,\ z_n/d,\ Re_j,\ G_c/G_j,\ \frac{u_a(\tilde{z})}{G_c/\rho},\ \frac{w_a(\tilde{z})}{G_c/\rho},\ \frac{T_a(\tilde{z})-T_s}{T_c-T_s},\ Pr\right] \quad (3.38)$$

$$\eta_r = \text{fcn}\left[x_n/d,\ y_n/d,\ z_n/d,\ Re_j,\ G_c/G_j,\ \frac{u_a(\tilde{z})}{G_c/\rho},\ \frac{w_a(\tilde{z})}{G_c/\rho},\ \frac{T_a(\tilde{z})-T_s}{T_c-T_s},\ Pr\right] \quad (3.39)$$

$$r_r = \text{fcn}\left[x_n/d,\ y_n/d,\ z_n/d,\ Re_j, G_c/G_j,\ \frac{u_a(\tilde{z})}{G_c/\rho},\ \frac{w_a(\tilde{z})}{G_c/\rho},\ \frac{T_a(\tilde{z})-T_s}{T_c-T_s},\ Pr\right] \quad (3.40)$$

where

$$Nu_r = h_r d/k$$

$$r_r = \frac{T_{rec,r} - t_j}{G_j^2/(2c_p\rho^2)} = 1 - \frac{\varepsilon_r/h_r}{G_j^2/(2_{cp}\rho^2)}$$

and (u_a, w_a), T_a, and T_c are, respectively, the velocity distribution, the temperature distribution, and the yet to be specified characteristic temperature of the crossflow at the entrance to the regional domain (Fig. 3.2). Note that the subscript r is employed to distinguish the heat transfer parameters for the regional domain [i.e., the domain of an individual spanwise row (Fig. 2.2)] from those for the overall jet array domain.

It is important to recognize that the set of independent variables on which Nu_r, η_r, and r_r depend does not include the position coordinate x_a/L or L/x_n (number of rows in array) which are included in the set on which Nu, η, and r depend. However, Nu_r, η_r, and r_r do, in general, depend on the normalized velocity and temperature profiles at the entrance to the individual row domain. The sensitivity of this dependence will be examined in Section 6.3 relying on the experimental results.

3.4 Characteristic Crossflow Temperature

To this point the characteristic temperature of the crossflow, T_c, has not been specified either for the initial crossflow at the array entrance or

for the crossflow at the entrance of an individual row domain. In both applications and experimental modeling it is not possible to independently control the detailed temperature profile approaching an array or approaching an individual row within an array. However, in experimental modeling it is possible to independently control the initial crossflow plenum air temperature, T_{cp}; and in design applications the temperature of the source of the initial crossflow air must either be controlled or otherwise specified. From the view point of both analyzing an overall airfoil cooling scheme and experimental modeling, the mixed-mean total temperature would appear to be a good choice for the characteristic crossflow temperature since its value at any channel cross-section can be calculated through an overall energy balance over the channel upstream of the cross-section considered. Therefore, in reduction of experimental data the following are employed:

$$T_c = T_{m,1} = T_o \text{ for the domain of the overall array}$$

and

$$T_c = T_{m,n} \text{ for the domain of individual spanwise row n}$$

$T_{m,1}$ denotes the mixed-mean total temperature of the crossflow approaching the first row (row 1) of the array. Since this is also the mixed-mean total temperature at the array entrance (i.e., at x = 0) it is assigned a special symbol, T_o. $T_{m,n}$ is the mixed-mean total temperature at one-half streamwise hole spacing upstream of spanwise row n.

In summary, the dependent <u>array</u> parameters are Nu, η, and r. They are considered, in general, to be a function of the independent <u>array</u> parameters:

$(x_a/L,\ x_n/d,\ y_n/d,\ z_n/d,\ L/x_n,\ \overline{Re}_j,$ M, normalized velocity and temperature distributions at array entrance, Pr)

The dependent <u>row</u> parameters are Nu_r, η_r, and r_r. They are considered, in general, to be a function of the independent <u>row</u> parameters:

(x_n/d, y_n/d, z_n/d, Re_j, G_c/G_j, normalized velocity and temperature distributions approaching spanwise row, Pr)

Examination of Eq. (3.33) with $T_c = T_o$ indicates that three linearly independent data sets ($\bar{q}$, T_s-T_j, T_o-T_j) are required to determine the three parameters h, η, and ε, from which the corresponding dimensionless parameters Nu, η, and r may be found. A similar observation applies for Eq. (3.37) with $T_c = T_{m,n}$ from which Nu_r, η_r, and r_r may be determined. In principle, each of the three separate steady-state tests required to obtain the three data sets must be conducted while holding constant the applicable set of independent parameters summarized in the preceding paragraph.

4. EXPERIMENTAL FACILITY

The basic experimental facility was that originally used for a comprehensive series of noninitial crossflow tests [Metzger et al. (1979), Florschuetz et al. (1980a, 1981a)], but for the present study set up in a modified form suitable for conducting tests with initial crossflow. The original facility was designed for conducting heat transfer tests but was also utilized for measurement of jet flow distributions. A complete description of the original facility was given by Florschuetz et al. (1980a) and a description of the initial crossflow configuration by Florschuetz et al. (1982). For the convenience of the reader, a description of the facility in the initial crossflow configuration will be given below and certain basic features, previously described in detail [Florschuetz (1980a)], will also be reviewed.

A cross-sectional view of the arrangement is shown in Fig. 4.1. There are two plenum chambers, each with two sections of porous plenum packing supported by screens, supplied individually with dried and filtered laboratory compressed air, one for introducing air to the main jet plate, and one for introducing the initial crossflow air to the channel. An electric resistance heater (not shown) in the line immediately upstream of the initial crossflow plenum permits independent control of the initial crossflow air temperature at levels above the jet plenum air temperatures. The initial crossflow was introduced to the channel through two spanwise rows of jet holes. The main jet plates, each with ten spanwise rows of holes, are interchangeable. The plenum/jet plate assembly was mounted over the test plate unit (impingement plate) through interchangeable spacers which fixed the channel height (i.e., the jet exit plane-to-impingement surface spacing). The spacers also formed the upstream end-surface and side walls of the channel, thus constraining the initial crossflow and the jet flow to discharge in a single direction to the laboratory environment at atmospheric pressure. The test plate unit consists of a segmented copper heat transfer test plate with individual segment heaters, the necessary thermal insulation, and the test plate support

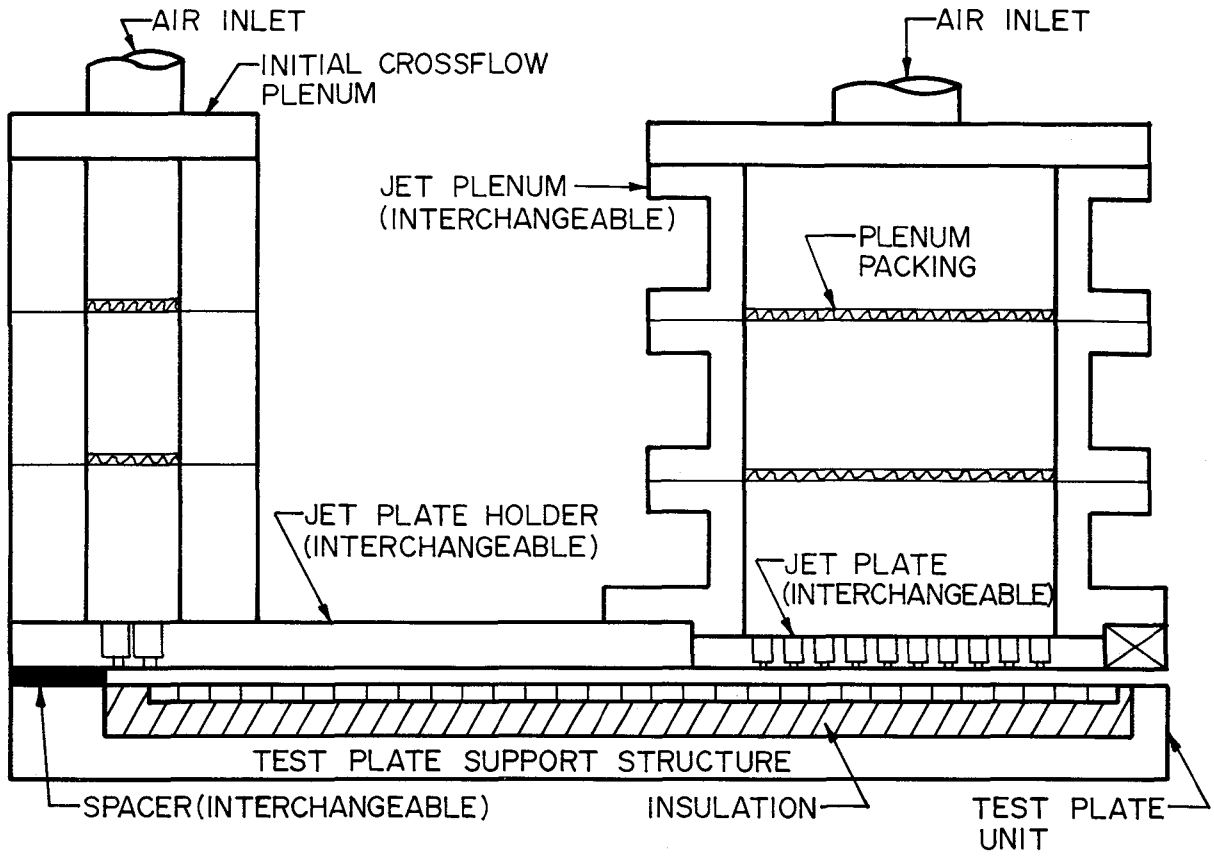

Fig. 4.1 Initial crossflow test facility schematic.

structure. The segmented design provides for control of the streamwise thermal boundary condition at the heat transfer surface, as well as for determination of spatially resolved heat transfer coefficients in the streamwise direction. Note that in the configuration shown the spanwise rows of jet holes are centered over the test plate segments, one row per segment. This results in a streamwise resolution of measured heat transfer coefficients equivalent to one streamwise jet hole spacing. There are a total of 31 segments in the test plate, 19 upstream of the jet array, 10 immediately opposite the array, and two downstream of the array.

Significant geometric characteristics of the configurations tested are summarized in Table 4.1. Arrays of length L = 12.7 cm with matching jet plenum (see Fig. 1.1 for precise definition of L) were designated as size B. The jet plates are identified by the notation $B(x_n/d,y_n/d)I$ where the I designates an inline hole pattern, replaced by S to designate a staggered pattern. A staggered pattern was identical to its inline counterpart, except that alternating spanwise rows of holes were offset by one-half the spanwise spacing. Note that the overall channel width (Fig. 4.1) exceeded the width of the heat transfer test plate and that the number of holes across the channel (N'_s) exceeded the number across the test plate (N_s). Jet holes were always symmetrically aligned with both the edges of the channel and the edges of the heat transfer test plate. Reckoned from the centerline of the second (i.e., downstream) spanwise jet row of the initial crossflow plenum, the channel length available for flow development upstream of the jet array (initial crossflow development length, 24.1 cm) ranged from 16 to 95 hydraulic diameters, depending on the channel height. It may also be noted that this length was 19 times the streamwise hole spacing in the main jet array (x_n = 1.27 cm.). Average jet plate discharge coefficients are also included in Table 4.1 [Florschuetz et al. (1981a)].

The standard jet plates and spacers were machined from aluminum. The jet plate thickness, b, at each hole location was equal to the jet hole diameter. This was achieved by appropriately counterboring jet plates of a larger overall thickness, 1.1 cm (Fig. 4.1). This design feature was dictated

Table 4.1. Geometric Parameters and Mean Discharge Coefficients for Jet Plates Tested.

Jet Plate $B(x_n/d, y_n/d)I$	A_o^*	d and b	N_s	N'_s	$\bar{C}_D$
B(5,4)I(& S)	0.0393	0.254	12	18	0.85
B(5,8)I	0.0196		6	9	0.80
B(10,4)I	0.0196	0.127	24	36	0.76
B(10,8)I(& S)	0.0098		12	18	0.76(0.74)

Channel heights, (z/d) = 1, 2, and 3

Fixed Parameters:

Channel width (span), w = 18.3 cm

Heat transfer test plate width, 12.2 cm

Heat transfer test plate length, 39.4 cm

Overall channel length, 43.2 cm

Initial crossflow channel length, 26.0 cm

B-size jet array and plenum length, L = 12.7 cm

Downstream exit length, 4.5 cm

Initial crossflow development length, 24.1 cm

Standard number of spanwise rows of jet holds, $N_c = L/x_n = 10$

I = Inline, S = staggered hole pattern

primarily by the desire to insure accurate channel heights during test runs, a particularly critical requirement for the narrowest channel heights. The counterbore was three jet hole diameters, except for the narrowest hole spacings were a two-diameter counterbore was used. The B(10,8)I jet plate was originally machined with a 2d counterbore and utilized in that form for both noninitial crossflow heat transfer tests and discharge coefficient tests. The counterbored holes were subsequently bored out to 3d, with both the heat transfer tests (at z/d = 1) and discharge coefficient tests repeated over a range of jet Reynolds numbers. The results were identical to within experimental uncertainty.

The jet plate holder was machined from an acrylic resin to minimize thermal coupling between the initial crossflow and jet plenums. One jet plate, B(5,4)I, was also machined from an acrylic resin in addition to the standard aluminum plate. Impingement surface heat transfer test results obtained with the aluminum and acrylic resin plates under otherwise identical conditions were compared to assess possible effects of heat leak through the jet plate and lateral conduction within the plate. These effects were found to be insignificant.

The copper test plate segments were 0.635 cm thick and 1.19 cm wide with 0.079 cm balsa wood insulation bonded between adjacent segments to minimize heat leak. The individual heaters were foil-type bonded to the underside of each segment, each with power input controlled by a separate variac. The ends and undersides of the segment/heater assemblies were bonded to basswood, selected for the combination of structural and insulating qualities it provided. Those insulation surfaces which would have formed part of the channel and been exposed to the air flow were surfaced with 0.079 cm Lexan plastic to provide a smooth aerodynamic surface and prevent possible erosion of the wood insulation materials. The primary temperature instrumentation in the test plate consisted of copper-constantan thermocouples mounted in the center of each copper segment, with a redundant thermocouple in each segment offset 1.52 cm in the spanwise direction. Several segments at intervals along the plate had additional thermocouples mounted out to the edge to verify that the spanwise temperature distributions during testing were essentially

uniform. A thermocouple was also positioned at the center of the cross-section of each of the two plenums to measure the temperatures of the initial crossflow air and the jet air just before it entered the jet orifices.

5. EXPERIMENTAL APPROACH AND DATA REDUCTION

The basic experimental approach and the data reduction methods as they relate to the problem formulation summarized in Section 2 are outlined below followed by a discussion of the experimental uncertainties associated with the reduced data to be presented in Sections 6, 7, and 8. Details such as those relating to flow measurement techniques, determination of heat rates at individual segments of the heat transfer test plate, temperature and pressure measurements, and evaluation of fluid properties were the same as previously reported by Florschuetz et al. (1980a) and, therefore, are not repeated here.

5.1 Procedures and Test Conditions

For a given test run, a basic jet orifice plate geometry and channel height was selected. These are specified in the following form: $B(x_n/d,y_n/d,z_n/d)I$ where B designates the particular jet plate length (L = 12.7 cm) and I designates the inline hole pattern for which most of the initial crossflow tests were conducted (S is used to designate a staggered hole pattern). Geometric details of the jet orifice plates and the test model were summarized in Table 4.1. Once the geometry was fixed, setting the total jet flow rate and the initial crossflow rate resulted in a set of fixed values for all of the independent dimensionless parameter sets summarized in Sections 2.1 and 2.2. The measured distributions of the jet and crossflow mass fluxes (G_j and G_c) over the spanwise rows, needed for representing heat transfer characteristics in term of individual row parameters, were reported by Florschuetz and Isoda (1983). The exhaust pressure at the exit of the jet array channel was one atmosphere.

Referring to Eq. (2.1) it is clear that for the fixed conditions described in the preceding paragraph, measurement of three independent data sets ($\bar{q}$,T_s-T_j,T_o-T_j) would permit determination of Nu, η, and ε. Originally these data sets were obtained as follows. The value of T_j was fixed nominally at ambient temperature level. Then a uniform maximum T_s was set such that $T_s-T_j \simeq 35K$ by individually adjusting $\bar{q}$ at each copper segment of the heat transfer test plate, including those in the initial crossflow channel. The segment surface areas of length x_n in the streamwise direction were the areas

over which the regional average heat fluxes could be controlled and measured. The initial crossflow plenum temperature (T_{cp}) was fixed roughly midway between T_j and the maximum T_s. This condition gave one data set. Keeping T_j and the initial crossflow plenum temperature fixed, a second set was obtained by adjusting each $\bar{q}$ to roughly half the prior values, and a third set by cutting $\bar{q}$ essentially to zero. T_o was determined for each data set by an energy balance over the initial crossflow channel utilizing the measured heat inputs and initial crossflow plenum temperature. In the original data reduction an equation similar in form to (2.1) was utilized, but with ε neglected. The redundancy associated with three data sets and two unknowns was used to provide a check on the calculated results for Nu and η. The typically good consistency resulting from these checks was taken as an indication that there was no need to account for recovery effects when evaluating Nu and η.

This data was later reanalyzed to obtain heat transfer characteristics in terms of individual row parameters based on Eq. (2.5) with $T_{m,n}$ evaluated via an energy balance. The energy balance was over a control volume encompassing the height of the channel and extending from the initial crossflow plenum to a cross-section of the channel located one-half a streamwise hole spacing upstream of row n. This energy balance required as input information: (i) the measured heat rates from each segment of the test plate up to but not including the segment opposite row n, (ii) the initial crossflow plenum temperature and the initial crossflow rate, and (iii) the jet plenum temperature (equivalent to the mixed-mean total temperature at the jet exit plane) and the jet mass flux at each spanwise row of the array preceding row n. In this analysis ε_r was neglected just as ε had been. Results for Nu_r and η_r again typically showed good consistency when checked in terms of the redundancy associated with having three data sets available. However, anomalous behavior of these results for some cases (detailed in Section 8.1) observed when they were plotted against the flow parameters for the individual rows, led to the realization that something was awry in spite of the apparent consistency of the redundant data sets. At this point the data was reanalyzed using Eq. (2.5) but with ε_r included. The availability of three data sets ($\bar{q}$, T_s-T_j, $T_{m,n}-T_j$) for each geometry and flow rate condition permitted the

calculation of Nu_r, η_r, and ε_r, but in some cases the results then showed highly random scatter with some completely unrealistic magnitudes. It was concluded that the three originally obtained data sets were ill-conditioned in these cases. Hence, one of the three data sets for each case had to be replaced. The third data set for each case obtained with $\bar{q}$ essentially at zero was rerun, but this time the initial crossflow plenum temperature was maintained at a value approximately the same as the jet temperature. The first and second sets were retained for use in conjunction with the newly obtained third set. This combination was not ill-conditioned, and led to well behaved results for Nu_r and η_r, as well as values for ε_r. The revised combination of data sets was then also reduced using Eq. (2.1) to obtain values of Nu, η, and ε in terms of overall array parameters. There was only a negligible influence on the results for Nu and η compared to the values from the prior combination of data sets.

With ε_r and Nu_r determined, r_r was calculated from Eq. (2.7) using values of ρ based on one-dimensional adiabatic flow through the jet holes. Similarly values of r could be determined from Eq. (2.3). It was found that values of r and r_r were essentially identical. Note that the method of determination of Nusselt numbers and η (or η_r) values using Eq. (2.1) or (2.5) is independent of ρ. Only the recovery factors depend on the determination of ρ. The adiabatic assumption was justified by the fact that test run results with an acrylic resin jet plate when compared with those for an aluminum jet plate under otherwise identical conditions showed no significant effect.

In addition to the tests with initial crossflow present, tests were conducted with the test facility in the initial crossflow configuration shown in Fig. 4.1 but for the special case of zero initial crossflow. For each fixed geometry and jet flow rate condition tested, three data sets $(\bar{q}, T_s-T_j)$ were again obtained. In this case values of Nu were calculated utilizing Eq. (2.1) with η=0, since T_o-T_j is not a relevant parameter when there is no initial crossflow present. In this case there were only two unknowns (Nu and ε), so that the system of equations was overspecified. The three data sets, however, consistently fell on a straight line as should be expected.

For these zero initial crossflow cases with an isothermal impingement surface boundary condition, the mixed-mean total temperature $(T_{m,n})$

approaching spanwise row n within the array will differ from T_j, because of heat addition opposite rows upstream of row n, but $T_{m,n}$ cannot be controlled independently of both T_s and T_j. Therefore, the zero initial crossflow data sets cannot be used to determine Nu_r, η_r, and ε_r based on Eq. (2.5) because the resulting set of three equations in three unknowns is linearly dependent. Thus, for the zero initial crossflow tests only values of Nu are reported (note again that for these cases η is identically zero). This underscores the fact that in order to obtain results defined in terms of individual row parameters, it is necessary to conduct tests in such a way that $T_{m,n}$ can be controlled independently. Utilizing tests with an initial crossflow present is one method of accomplishing this.

5.2 Experimental Uncertainties

Composite experimental uncertainties for the primary heat transfer parameters presented in this report, Nu, η, Nu_r, and η_r, as well as for the recovery factors (r and r_r) were determined by the method of Kline and McClintock (1953). The composite uncertainty (ω_R) for a calculated parameter (dependent variable R) is expressed in terms of the uncertainties (ω_{r_i})in the primary measurement (independent variables r_i) by

$$\omega_R^2 = \sum_{i=1}^{k} \left[\left(\partial R / \partial r_i \right) \omega_{r_i} \right]^2$$

where $R = R(r_1, r_2, \ldots, r_k)$.

The derivatives $\partial R/\partial r_i$ were approximated by finite differences obtained by perturbating the primary quantities, r_i, from their originally measured values and calculating the corresponding R utilizing the computer program developed for reduction of the experimental data.

Uncertainties in the primary quantities, estimated for a confidence level of 95%, are summarized below:

copper test plate segment thermocouples	± 0.1K
jet plenum air temperature	± 0.1K

initial crossflow plenum air temperature	± 0.1K
room air temperature	± 2K
thermal resistance for segment heater back loss	± 15%
segment heater power inputs	± 1%
specific heat of air	± 1%
thermal conductivity of air	± 1.5%
jet hole diameters	± 1.5%
segment heat transfer surface areas	± 1%
total jet flow rate	± 2%
total initial crossflow rate	± 2%
normalized individual jet mass flux $(G_j/\bar{G}_j)$	± 2%

All thermocouples were calibrated relative to each other, so the uncertainties indicated for temperature measurements are to be considered as applying on a relative, not an absolute, scale. This is appropriate since it is temperature differences not absolute temperatures which strongly influence the data reduction. The larger uncertainty associated with room temperature accounts for possible drift during a given test series. This temperature affects the determination of the back heat losses which were normally several percent or less. The flow rates, in the case of the overall array domain, or mass fluxes, in the case of the individual row domain, affect the determination of the mixed-mean total temperatures of the crossflow through the energy balances.

For the main sets of results in terms of individual row parameters, presented in Sections 6 and 8, composite uncertainty ranges on η_r, Nu_r, and r_r are shown as vertical bars attached to the data point symbols in the plots. For the results in terms of array parameters presented in Section 7, composite uncertainty ranges on η and Nu are specified in the opening paragraphs of the section.

6. RESULTS IN TERMS OF INDIVIDUAL SPANWISE ROW PARAMETERS

In applications involving cooling of gas turbine components with impinging jets in the presence of a crossflow, surface-to-fluid temperature differences are typically large enough and coolant flow velocities low enough such that recovery effects are negligible. Thus, in applying equations in the form of Eqs. (2.4) and (2.8), or similar forms, precise information on recovery factors is not required. Since Eqs. (2.4) and (2.8) are formulated in terms of total fluid temperatures for the jet flow and the crossflow, neglecting the term containing the recovery factor is equivalent to assuming a recovery factor of unity. Therefore, though typically small (or negligible), recovery effects are still accounted for to a good approximation since the recovery factors ordinarily are close to unity.

Nusselt numbers $(Nu \text{ or } Nu_r)$ and fluid temperature difference influence factors $(\eta \text{ or } \eta_r)$, or equivalent results, are the primary parameters required. In Sections 6 and 7 experimentally determined results for regional average temperature difference influence factors and Nusselt numbers for the jet array geometries summarized in Table 4.1 are presented in graphical form. The results were determined according to the procedures outlined in Section 5. Results for these two quantities defined in terms of individual spanwise row parameters (η_r and Nu_r) are presented in Section 6, followed by results for the same two quantities defined in terms of overall array parameters (η and Nu) presented in Section 7. Corresponding results are presented in tabular form in the Appendices.

The significance of recovery effects on the determination of the temperature difference influence factors and Nusselt numbers for the test conditions utilized in this study is illustrated in Section 8.1. Recovery factor results for all of the jet array geometries are then presented in graphical form in Section 8.2. Because precise recovery factor values should not normally be required in the gas turbine application of these heat transfer characteristics, tabular results for recovery factors have not been included in the Appendices.

Before proceeding to the presentation of the major results just delineated it should be noted here that heat transfer coefficients measured in

the initial crossflow channel of the test facility (Fig. 4.1), which may be considered in an idealized sense as a parallel plate channel with one side heated and the other adiabatic, were compared by Florschuetz et al. (1982) with prior data from several other investigators for similar conditions. The good consistency of this data provided confidence in the test rig and associated instrumentation.

Now, considering the domain associated with an individual spanwise row (see Section 2.2 for overview, and Section 3 for details), it was shown that the row parameters Nu_r and η_r may be considered as functions of the geometric parameters (x_n/d, y_n/d, z_n/d) and the flow parameters (Re_j, G_c/G_j, Pr) as well as the normalized velocity and temperature distributions at the entrance to the domain. All results for η_r and Nu_r presented in the present section are based on the same raw test data as the results for Nu and η to be presented in Section 7. η_r and Nu_r were evaluated with the term related to recovery effects (ε_r) retained in Eq. (2.5) as discussed in Section 5.1. The significance of recovery effects in evaluating η_r and Nu_r is examined in Section 8.1. In the present section we first consider the influence of Re_j and G_c/G_j on the dependent parameters Nu_r and η_r. Then the effects of the normalized velocity and temperature profiles at the upstream control surfaces of the individual row domains are examined. These normalized profiles depend, of course, on the history of the flow upstream of the row being considered which, in turn, depends on the position of the row within the array. Understanding the significance of these effects is of primary importance in assessing the validity of applying individual row heat transfer characteristics measured for a given array to individual rows of other arbitrary arrays (i.e., longer or shorter or nonuniform arrays) for a given individual row parameter set (Re_j, G_c/G_j, x_n/d, y_n/d, z_n/d). Examination of these effects also answers the following question: What is the minimum number of spanwise rows needed for testing in order to apply the results with confidence to downstream rows within larger arrays? Finally, the effects of the geometric parameters are considered.

Values of Re_j and G_c/G_j are based on the previously reported measurements and the validated flow distribution model developed by Florschuetz et al. (1982) [or see Florschuetz and Isoda (1983)]. An example for a geometry with

a very nearly uniform distribution is reproduced in Fig. 6.1, and one for a highly nonuniform flow distribution in Fig. 6.2. Experimental values for flow conditions corresponding either exactly or very nearly to those for each heat transfer test were available. In those cases where the test conditions for the flow distribution results did not match those for the heat transfer results exactly, the small adjustments required were made using the validated model. For experimental uncertainties associated with the values of $G_j/\bar{G}_j$ (on which Re_j is based) and G_c/G_j see Florschuetz et al. (1982). Tabular values for all η_r and Nu_r data presented in this section are given in Appendix A as a function of Re_j and G_c/G_j.

In reducing the test data to determine η_r and Nu_r it was necessary to determine the mixed-mean total temperature $T_{m,n}$ at the entrance to each individual spanwise row domain. These temperatures were determined on the basis of energy balances as previously described in Section 5.1. For illustrative purposes, typical profiles of $T_{m,n}$ in normalized form are shown in Figs. 6.3 and 6.4 for two different array geometries, each at two different initial crossflow rates. As one proceeds downstream, the continuing injection of cooler jet air more than compensates for the heat addition at the impingement surface, so that $T_{m,n}$ decreases. The geometry of Fig. 6.3 has a nearly uniform jet flow distribution, even for the largest m_c/m_j of unity, with G_c/G_j increasing in the downstream direction (see Fig. 6.1). Note that the rate of decrease of $T_{m,n}$ becomes smaller downstream. The geometry of Fig. 6.4 with $m_c/m_j = 0.20$ (upper plot) has a more highly nonuniform flow distribution than both cases shown in Fig. 6.3, but G_c/G_j still increases downstream (see Fig. 6.2); the behavior of $T_{m,n}$ is also seen to be similar to that in Fig. 6.3. For m_c/m_j near unity (lower plot, Fig. 6.4) this geometry has a highly nonuniform flow distribution (Fig. 6.2) with G_c/G_j decreasing markedly from upstream to downstream. This accounts for the change in curvature of the $T_{m,n}$ profiles in this case as compared with the other cases.

6.1 Effect of Jet Reynolds Number

The bulk of the tests were conducted at a mean jet Reynolds number of 10^4. However, the geometry B(5,4,2)I at $m_c/m_j = 0.20$ and the geometries B(5,8,2)I, B(5,8,3)I, and B(10,8,2)I at $m_c/m_j = 0.50$ were tested at three

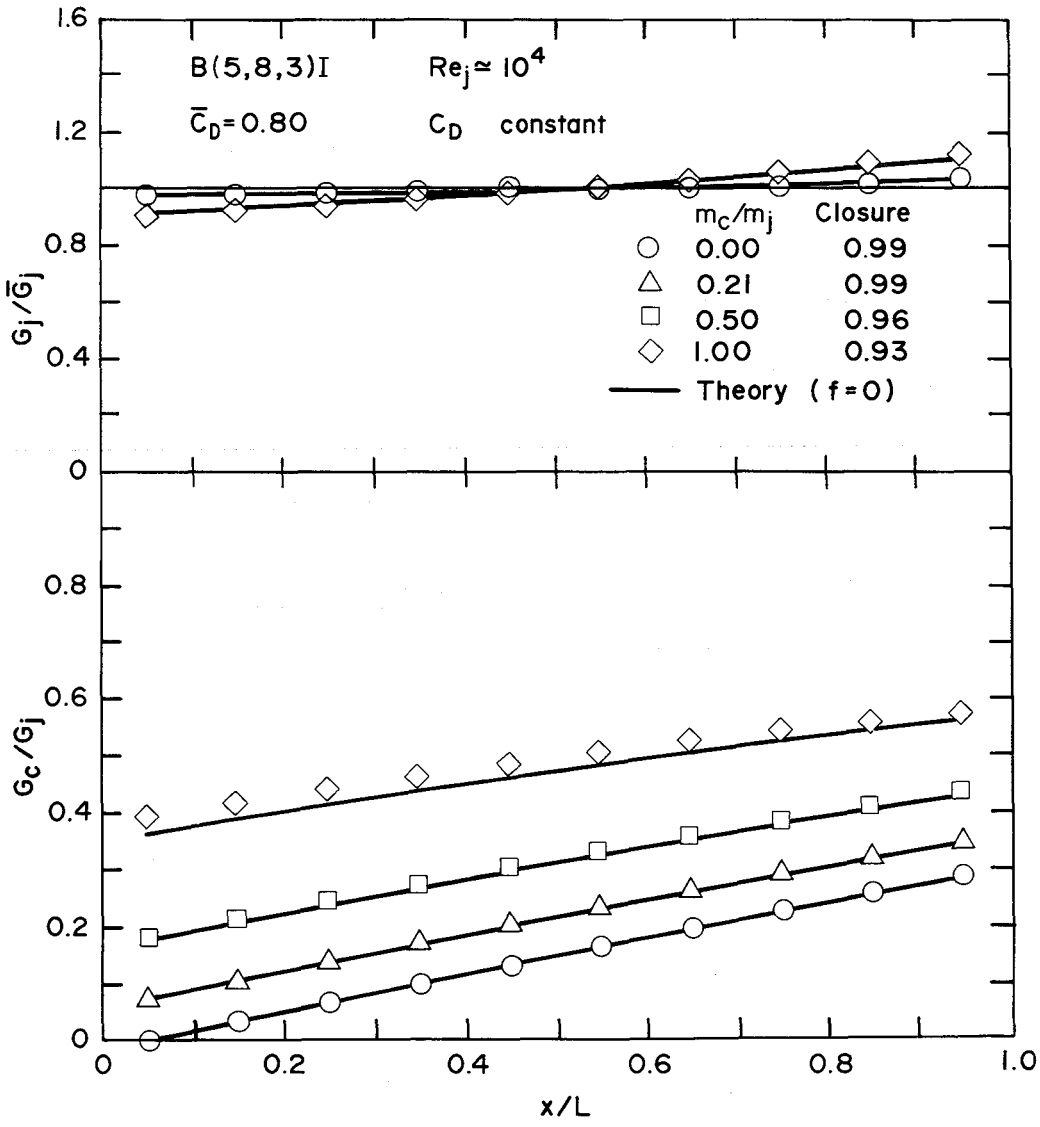

Fig. 6.1 Effect of initial crossflow on jet array flow distribution for B(5,8,3)I geometry - experimental data compared with theoretical model [Florschuetz and Isoda (1983)].

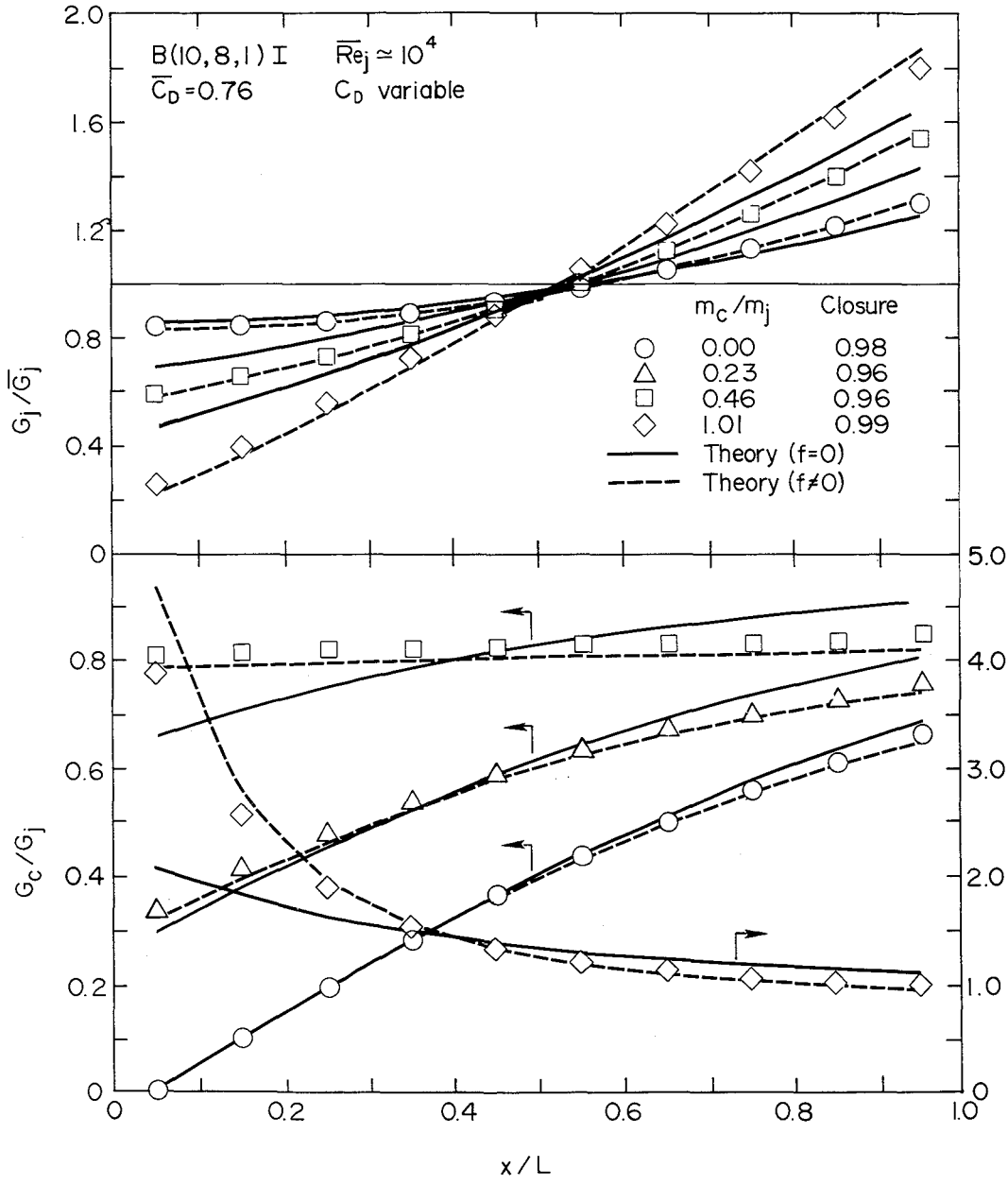

Fig. 6.2 Effect of initial crossflow on jet array flow distribution for B(10,8,1)I geometry - experimental data compared with theoretical model [Florschuetz and Isoda (1983)].

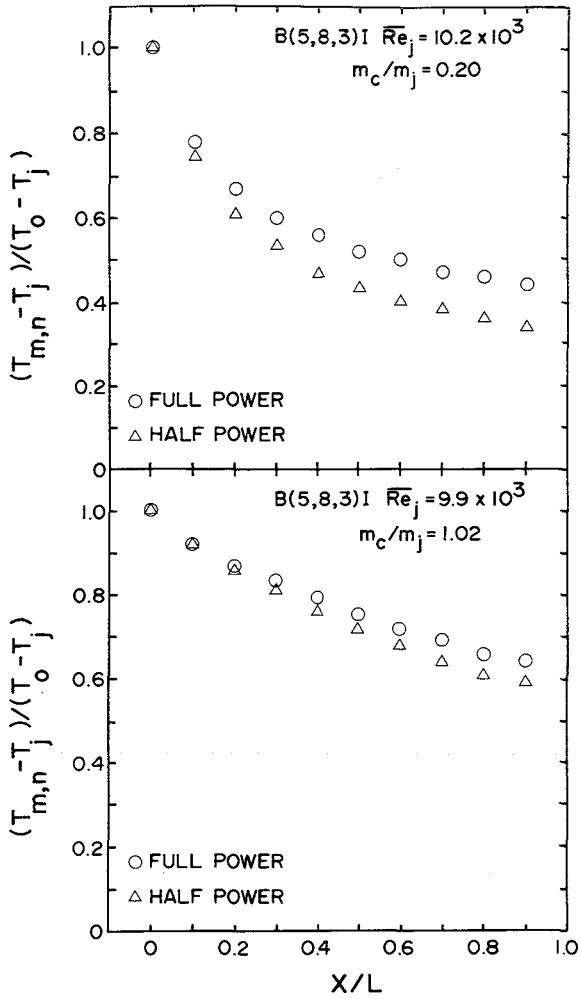

Fig. 6.3 Mixed-mean total temperature profiles for B(5,8,3)I geometry.

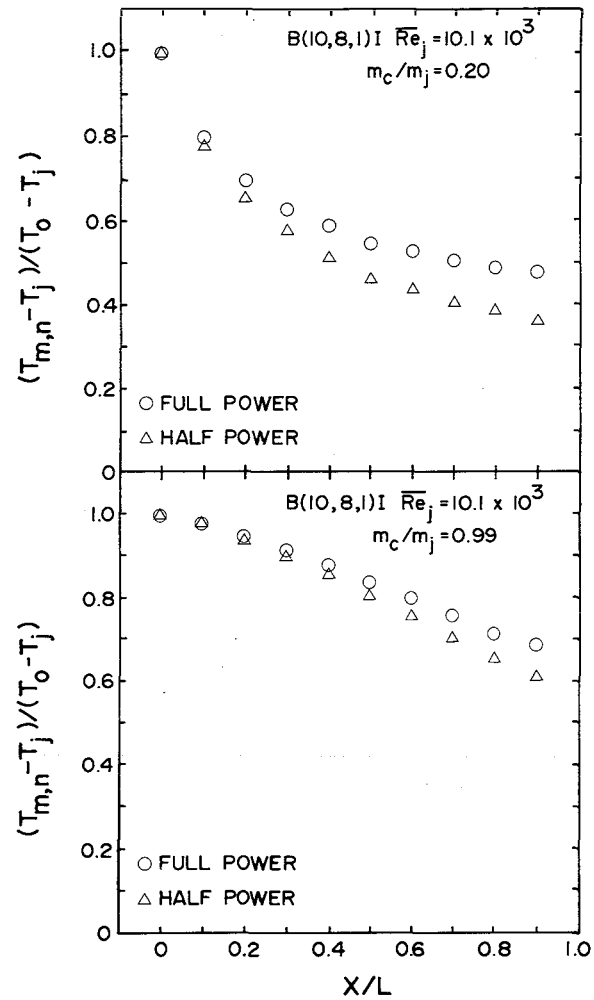

Fig. 6.4 Mixed-mean total temperature profiles for B(10,8,1)I geometry.

nominal mean jet Reynolds numbers of 6 x 10^3, 10^4, and 2 x 10^4. The results for η_r and Nu_r are shown in Figs. 6.5 to 6.8. All of these results are for standard arrays with L/x_n = 10 (10 row arrays). However, data for only the first seven rows was obtained, because prior to these particular tests the test plate segment heater opposite row 9 developed an open circuit (burned out) and because of the design of the test plate could not be replaced or repaired. Hence the segment opposite row 8 had to be used as the downstream guard heater, permitting the acquisition of useful data only through row 7.

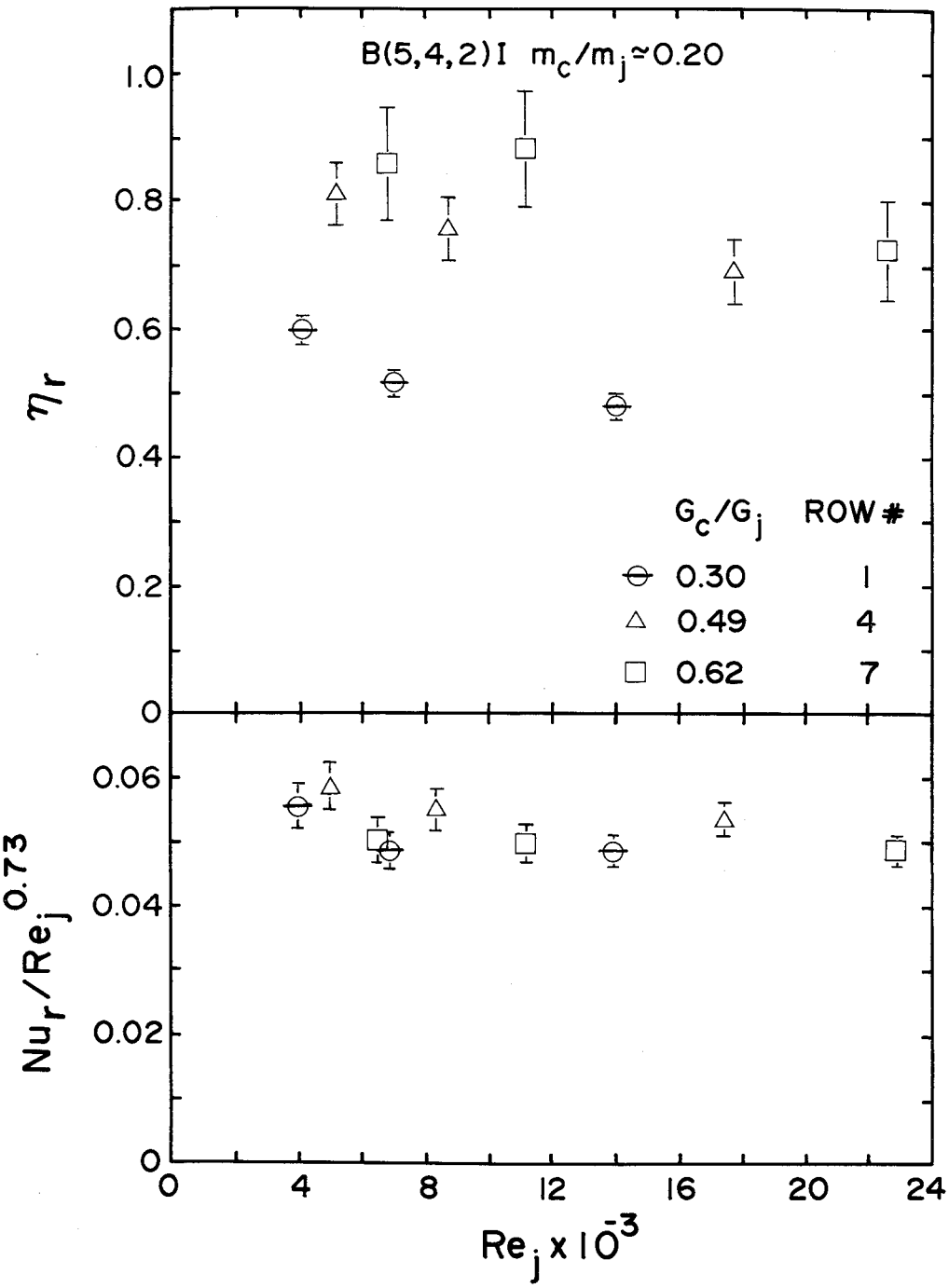

Fig. 6.5 Effect of jet Reynolds number on η_r and Nu_r for B(5,4,2)I geometry.

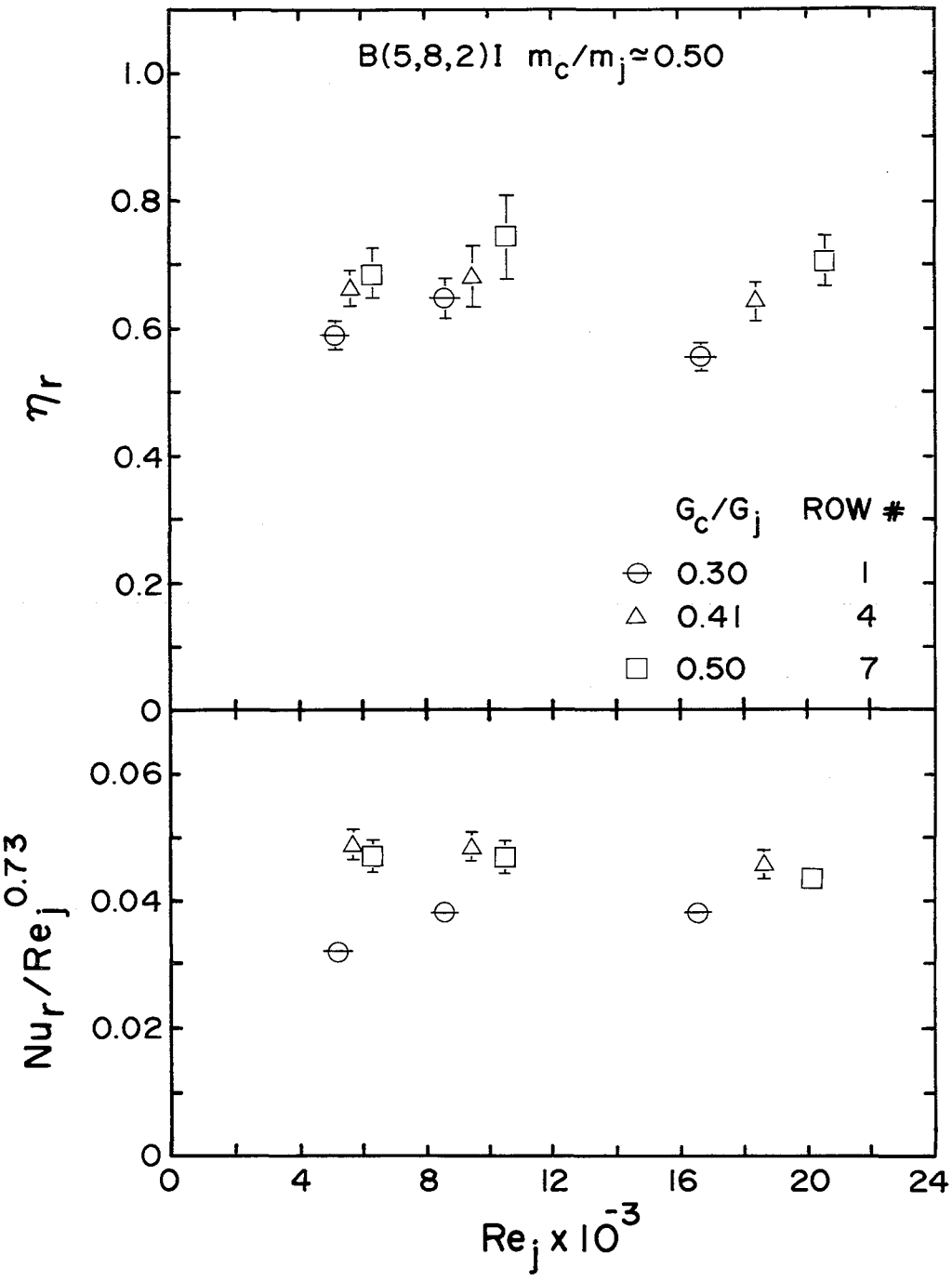

Fig. 6.6 Effect of jet Reynolds number on η_r and Nu_r for B(5,8,2)I geometry.

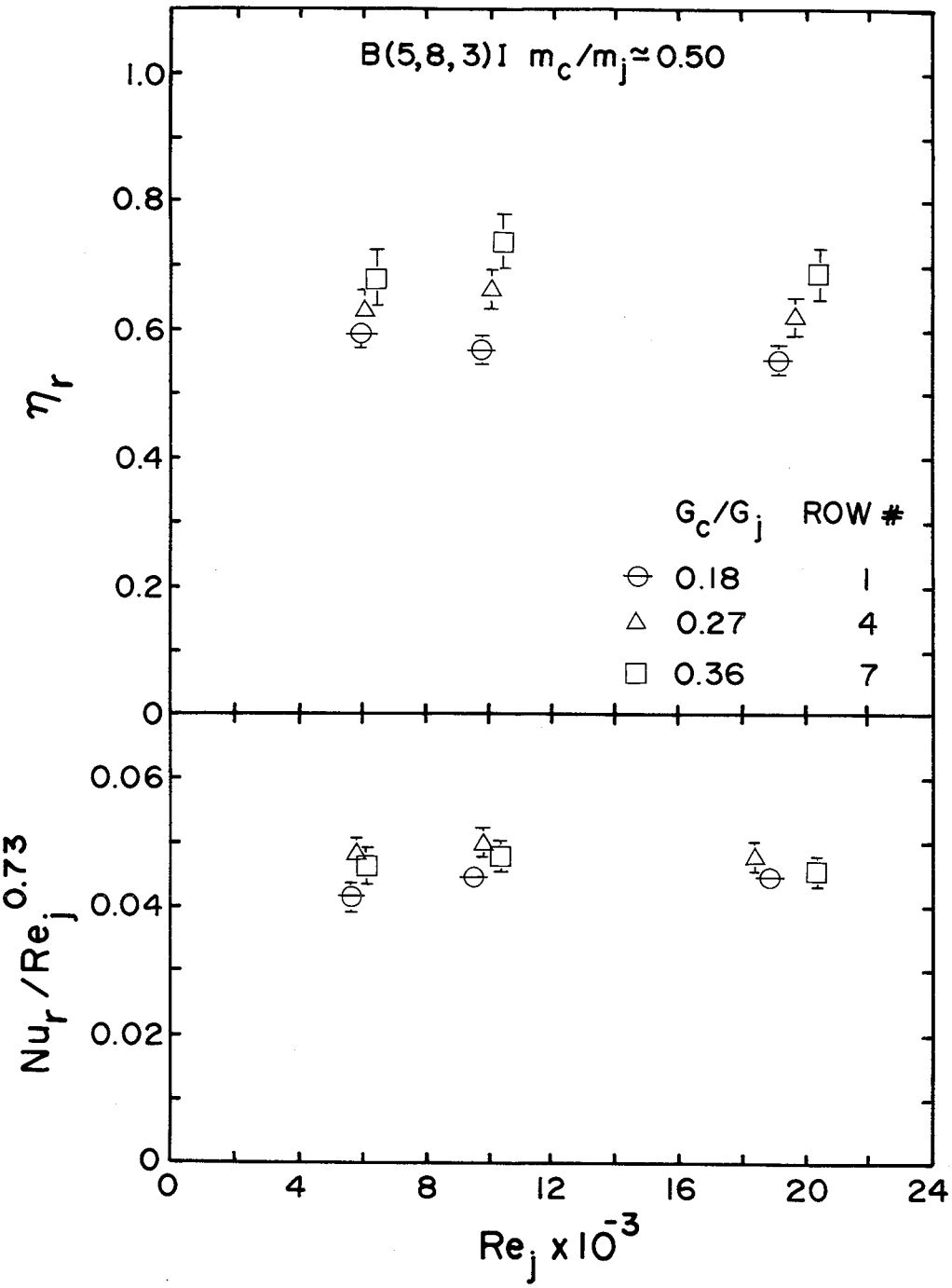

Fig. 6.7 Effect of jet Reynolds number on η_r and Nu_r for B(5,8,3)I geometry.

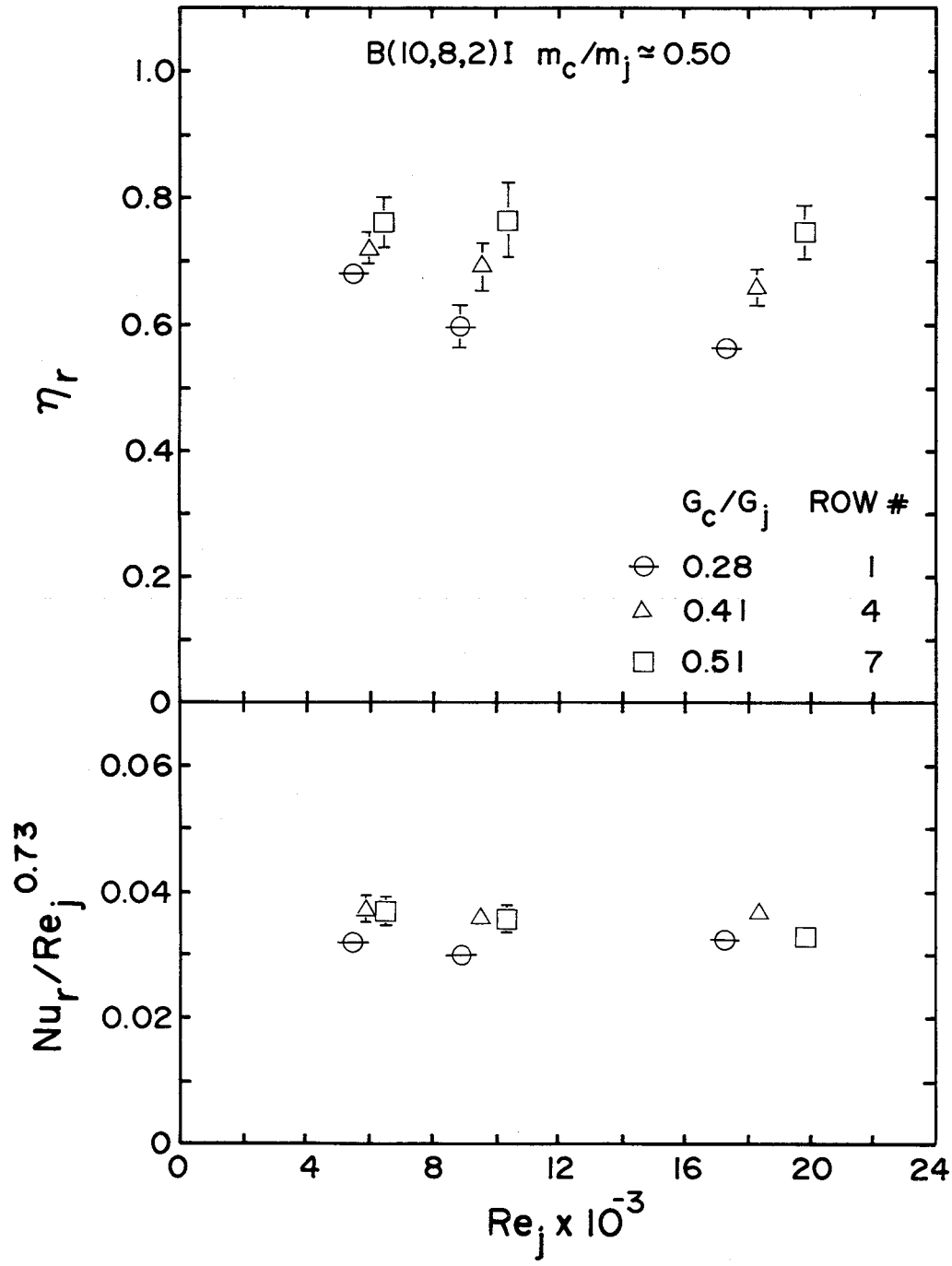

Fig. 6.8 Effect of jet Reynolds number on η_r and Nu_r for B(10,8,2)I geometry.

For clarity, only the results based on data for rows 1, 4, and 7 are presented in the figures. Results for all seven rows are included in Appendix A.

This information was entirely adequate to check the dependence of η and Nu on Re_j. The Nu values were normalized by $Re_j^{0.73}$ for direct comparison. The exponent on Re_j is from the previous noninitial crossflow jet array impingement correlation reported by Florschuetz, et al. (1981a, 1981b). Considering experimental uncertainty, the η_r values appear to be relatively insensitive to Re_j, while the Reynolds number dependence of $Re_j^{0.73}$ accounts quite well for the Nusselt number variation. Results based on data from the remaining rows (not shown in the figures) also support this general conclusion. Variations, though still small, are sometimes more noticeable at upstream rows and smaller values of Re_j.

The composite uncertainties for $Nu/Re_j^{0.73}$ indicated in Figs. 6.5 through 6.8 were calculated based on an uncertainty in Re_j of ± 3%. Composite uncertainty ranges (Section 5.2) in plots throughout Section 6 are indicated by vertical bars attached to the data point symbols.

6.2 Effect of Crossflow-to-Jet Mass Flux Ratio

A complete set of plots for η_r and Nu_r for all twelve geometries is shown in Figs. 6.9 to 6.20. Each figure shows the dependence of η_r and Nu_r on G_c/G_j. The values of Nu_r were adjusted to $Re_j = 10^4$ according to $Nu_r \alpha Re_j^{0.73}$. The values of η_r were plotted for the Re_j at which they were measured, since as discussed in the preceding paragraph η_r is relatively insensitive to Re_j. The values of the independent overall array parameters and the range of Re_j for the test conditions are shown in the legend. Values of Nu_r at $G_c/G_j = 0$ are for the first row of the zero initial crossflow tests. η_r at the first row of an array with no initial crossflow is by definition zero. Values of Nu_r and η_r at downstream rows cannot be obtained from data for zero initial crossflow tests since the crossflow mixed-mean temperatures approaching individual rows cannot be varied independently when the jet flow is from a single plenum and the type of thermal boundary condition at the impingement surface is fixed. Horizontal lines are added to the symbols for data from row 1 of the array. This permits one to more easily identify from which row each data point was obtained since the points lie in sequence to the

right or left of the first row point depending on whether G_c/G_j increased or decreased from upstream to downstream. The figures include twelve different geometric configurations - the first ten for the inline arrays and the last two for the staggered arrays.

Consider first the plots for η_r. On theoretical grounds we should expect that as G_c/G_j goes to zero η_r also goes to zero and that as G_c/G_j increases η_r asymptotically approaches one. Furthermore, if all the parameters $(x_n/d, y_n/d, z_n/d, Re_j, Pr)$ plus the normalized velocity and temperature profiles at the entrance to each individual row domain (or the flow history) were in fact held constant we would expect a single smooth curve for η_r vs. G_c/G_j joining the two limits. An important observation is that, allowing for experimental uncertainty, the bulk of the data points for η_r in Figs. 6.9 through 6.20 appear to fit the above pattern.

For Nu_r vs. G_c/G_j we would expect a finite value of Nu_r for $G_c/G_j = 0$ which then decreases with increasing G_c/G_j, since we normally expect the presence of a crossflow to diminish the heat transfer capability of an impinging jet. If G_c/G_j is increased far enough, however, we would expect Nu_r to increase again eventually approaching values for a fully developed channel flow, as the crossflow completely dominates. Examining Figs. 6.9 through 6.20, it appears that the bulk of the data points for Nu_r do indeed follow these overall trends.

For every geometric configuration there are some data points which clearly do not follow the overall trends described above and some which only marginally fall in the overall trend of the bulk of the data points. It may be noted again that the data points for η_r were plotted for the corresponding spanwise row jet Reynolds numbers which existed for the test condition. Though it was previously shown that η_r is not very sensitive to Re_j (Figs. 6.5 through 6.8), it should be kept in mind that some small variations in the trend of the η_r data points could be associated with Re_j variations. The same is not true of the Nu_r data points since based on experimental correlation, as previously described, it was possible to adjust these to the same Re_j in order to examine the effect of G_c/G_j.

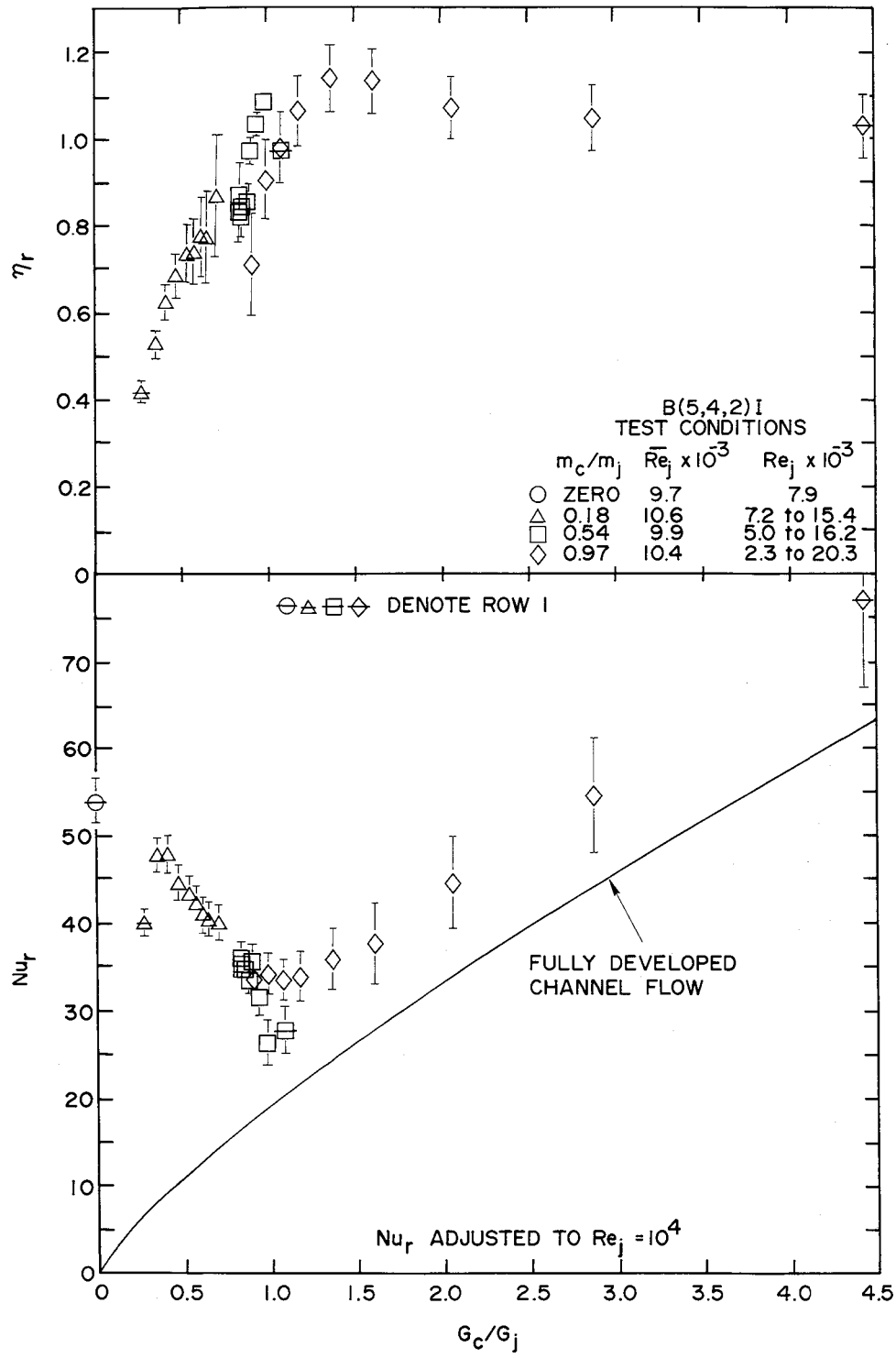

Fig. 6.9 Effect of crossflow-to-jet mass flux ratio on η_r and Nu_r for B(5,4,2)I geometry.

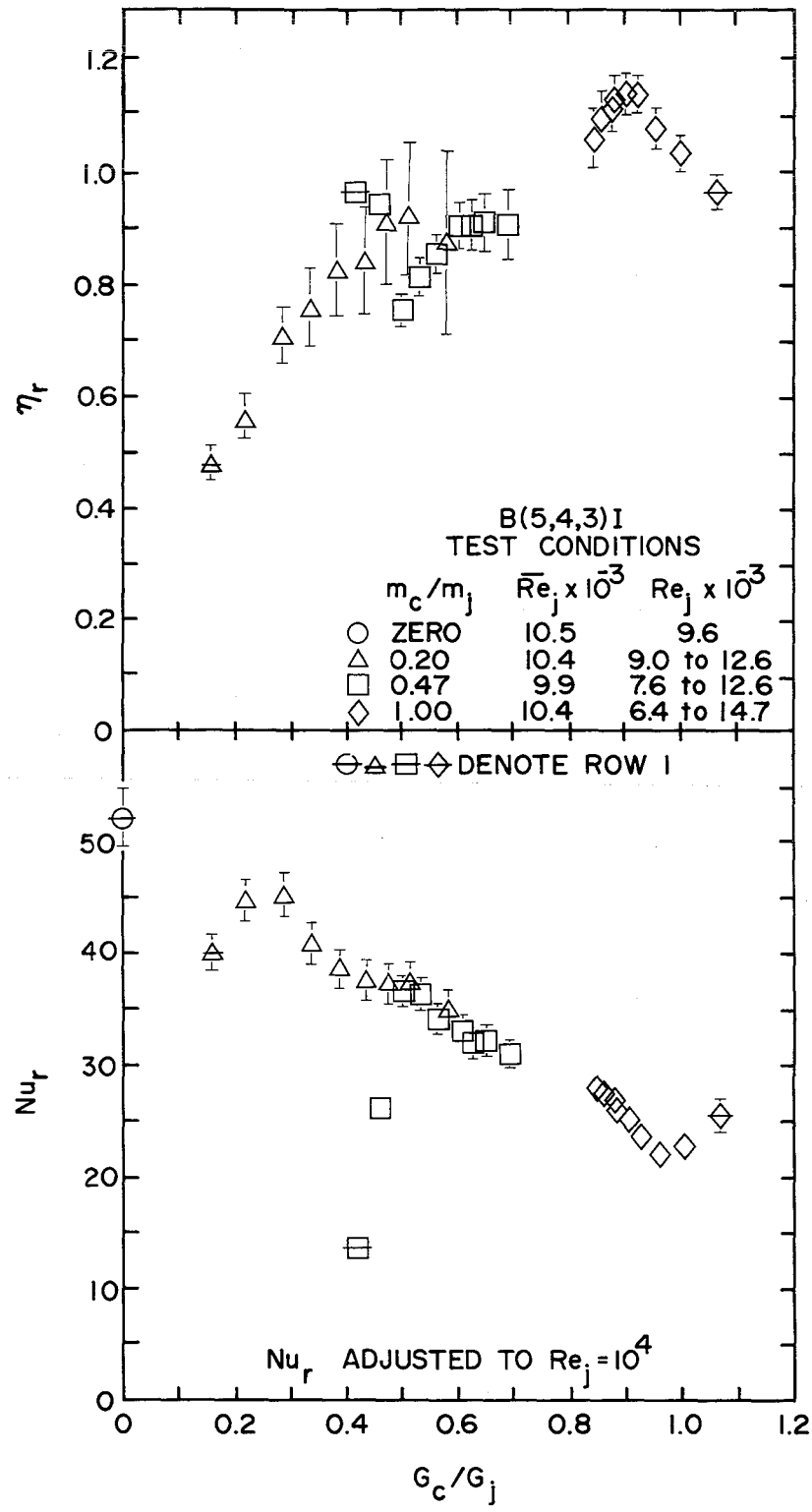

Fig. 6.10 Effect of crossflow-to-jet mass flux ratio on η_r and Nu_r for B(5,4,3)I geometry.

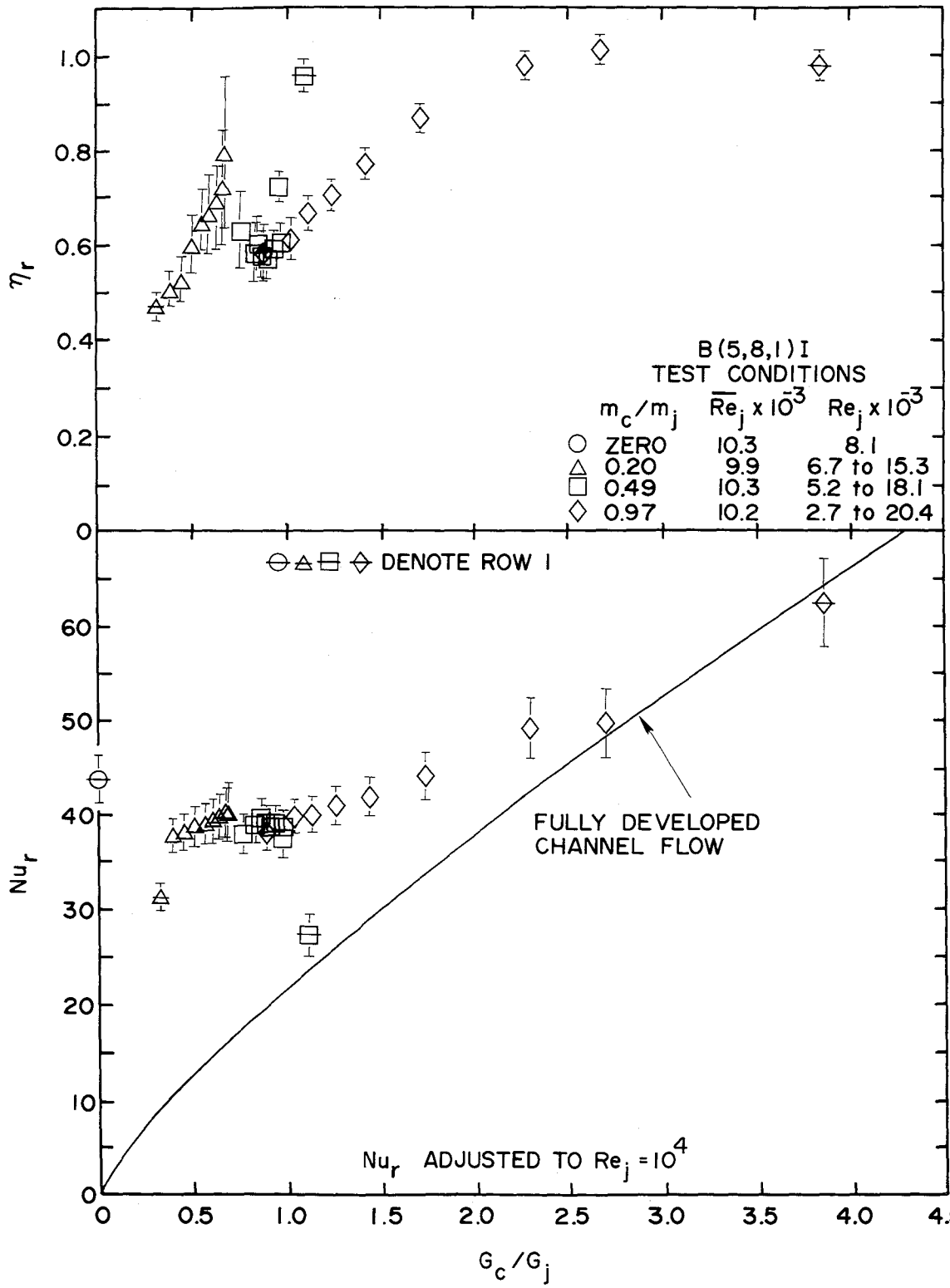

Fig. 6.11 Effect of crossflow-to-jet mass flux ratio on η_r and Nu_r for B(5,8,1)I geometry.

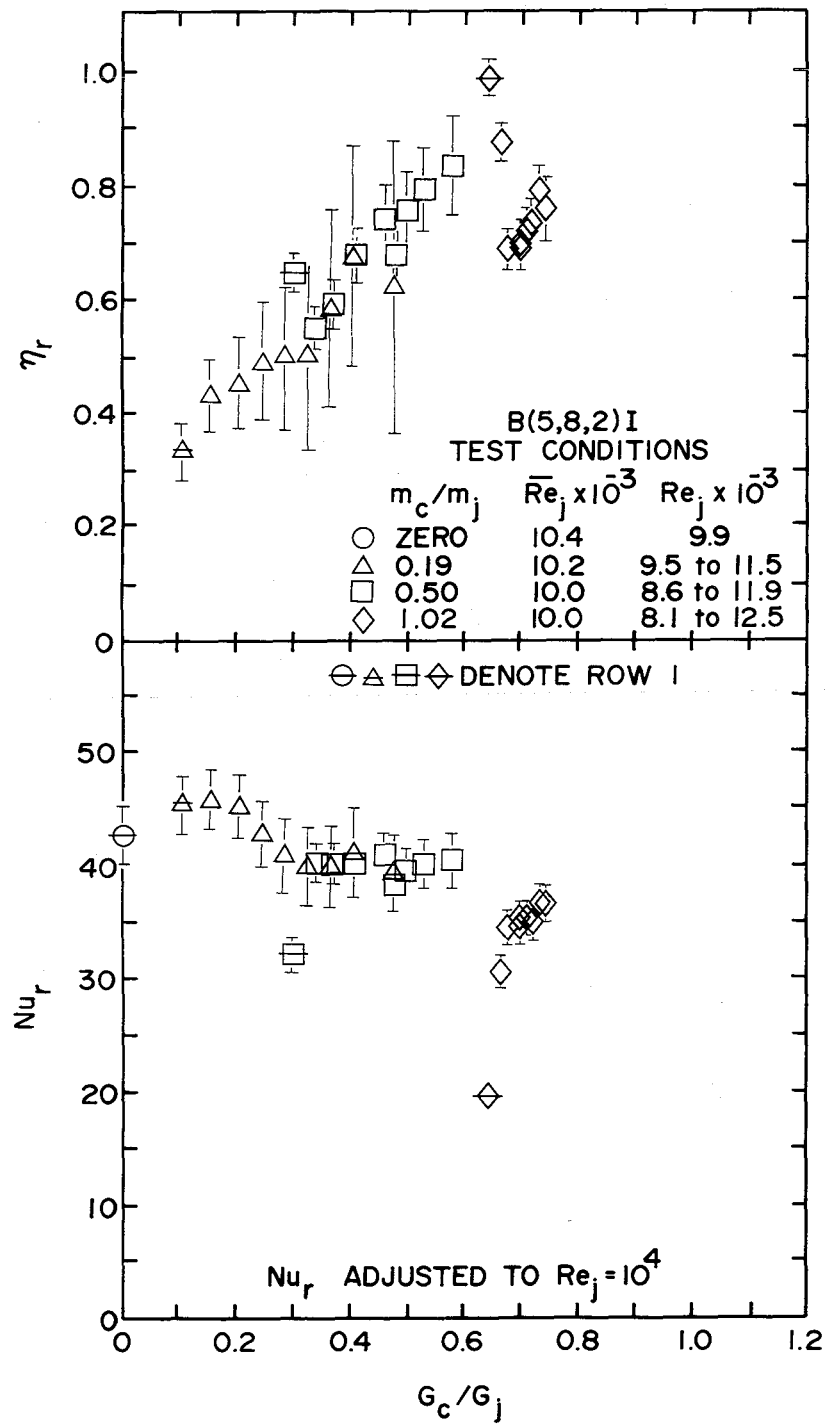

Fig. 6.12 Effect of crossflow-to-jet mass flux ratio on η_r and Nu_r for B(5,8,2)I geometry.

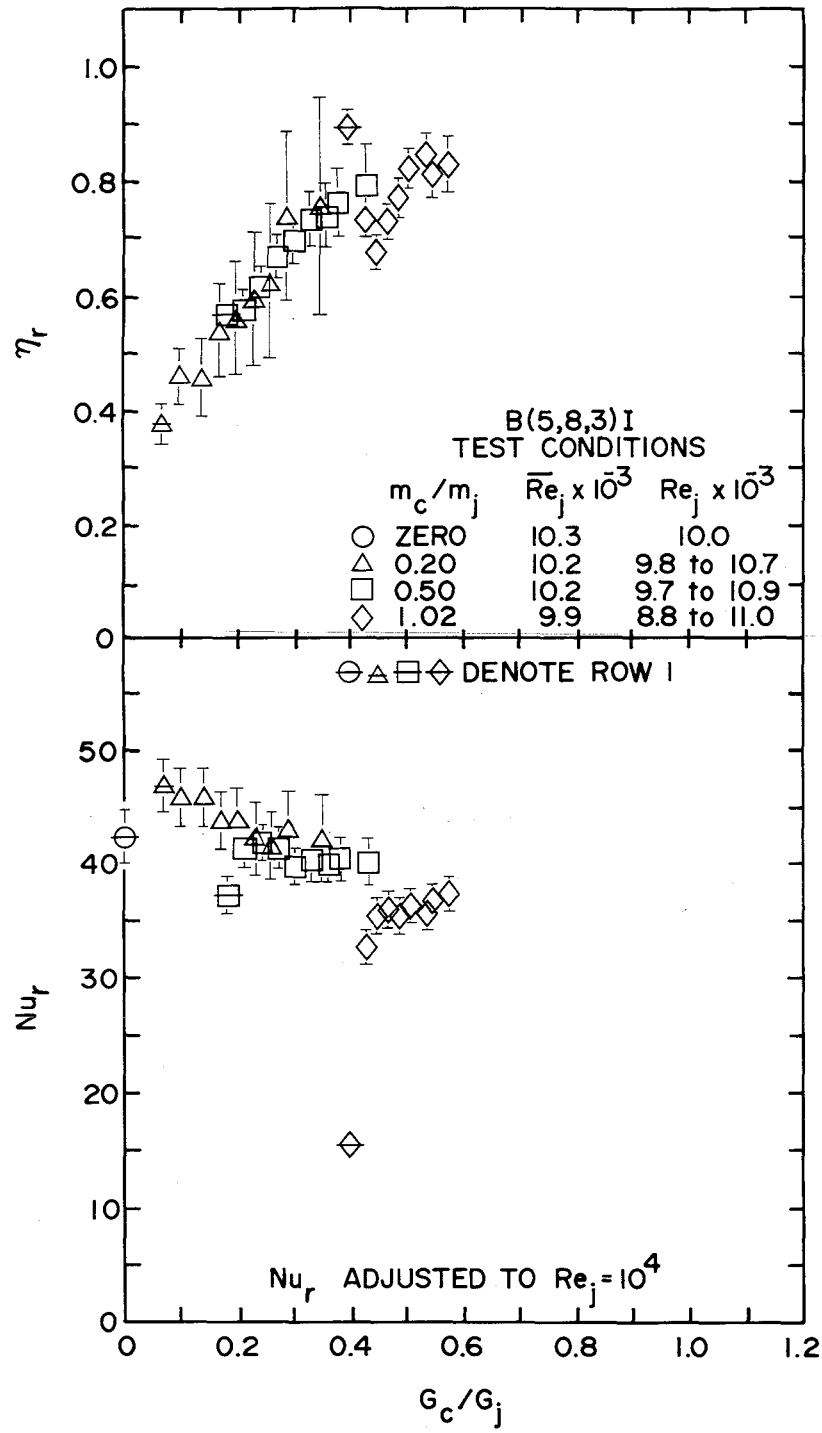

Fig. 6.13 Effect of crossflow-to-jet mass flux ratio on η_r and Nu_r for B(5,8,3)I geometry.

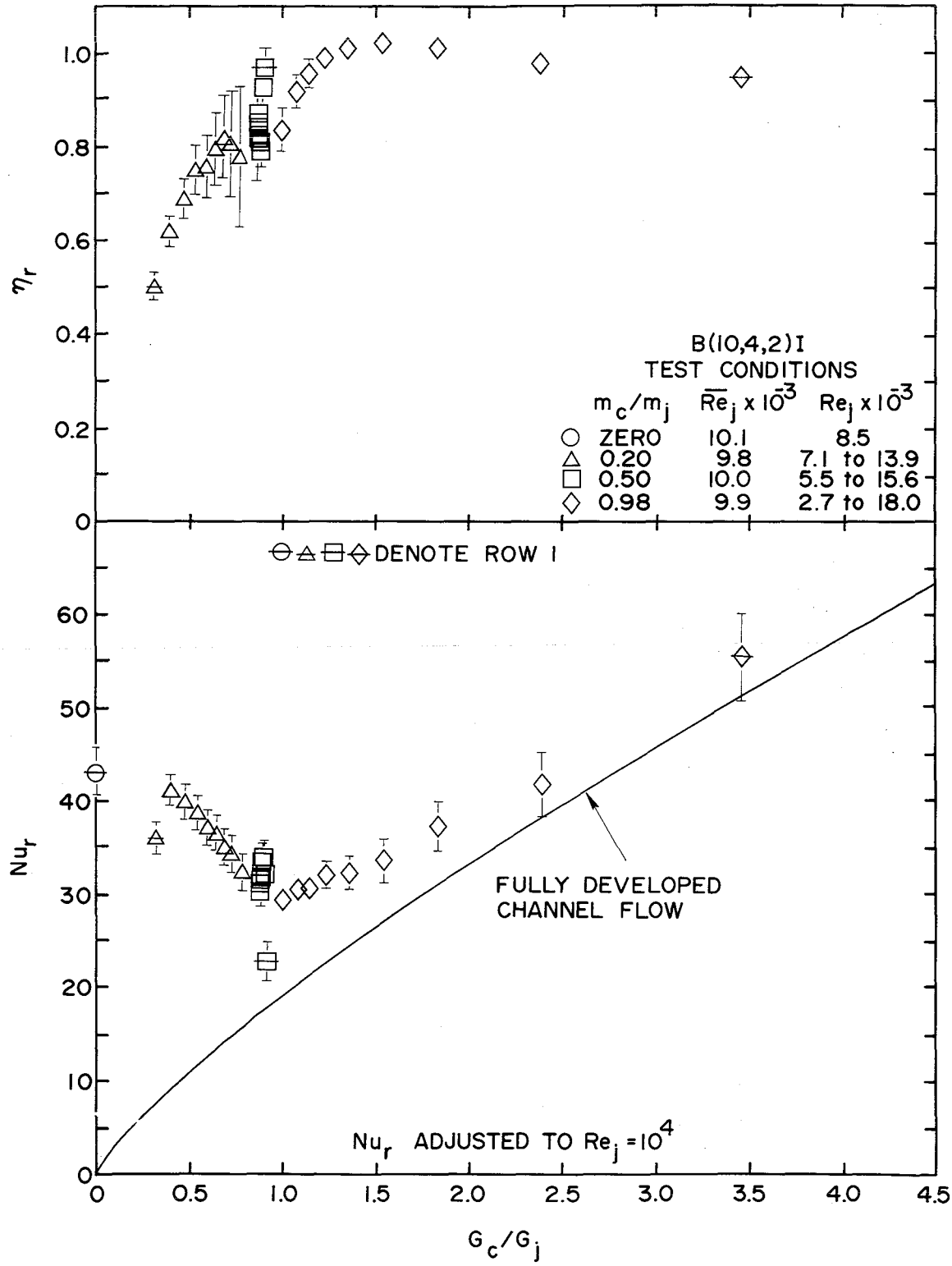

Fig. 6.14 Effect of crossflow-to-jet mass flux ratio on η_r and Nu_r for B(10,4,2)I geometry.

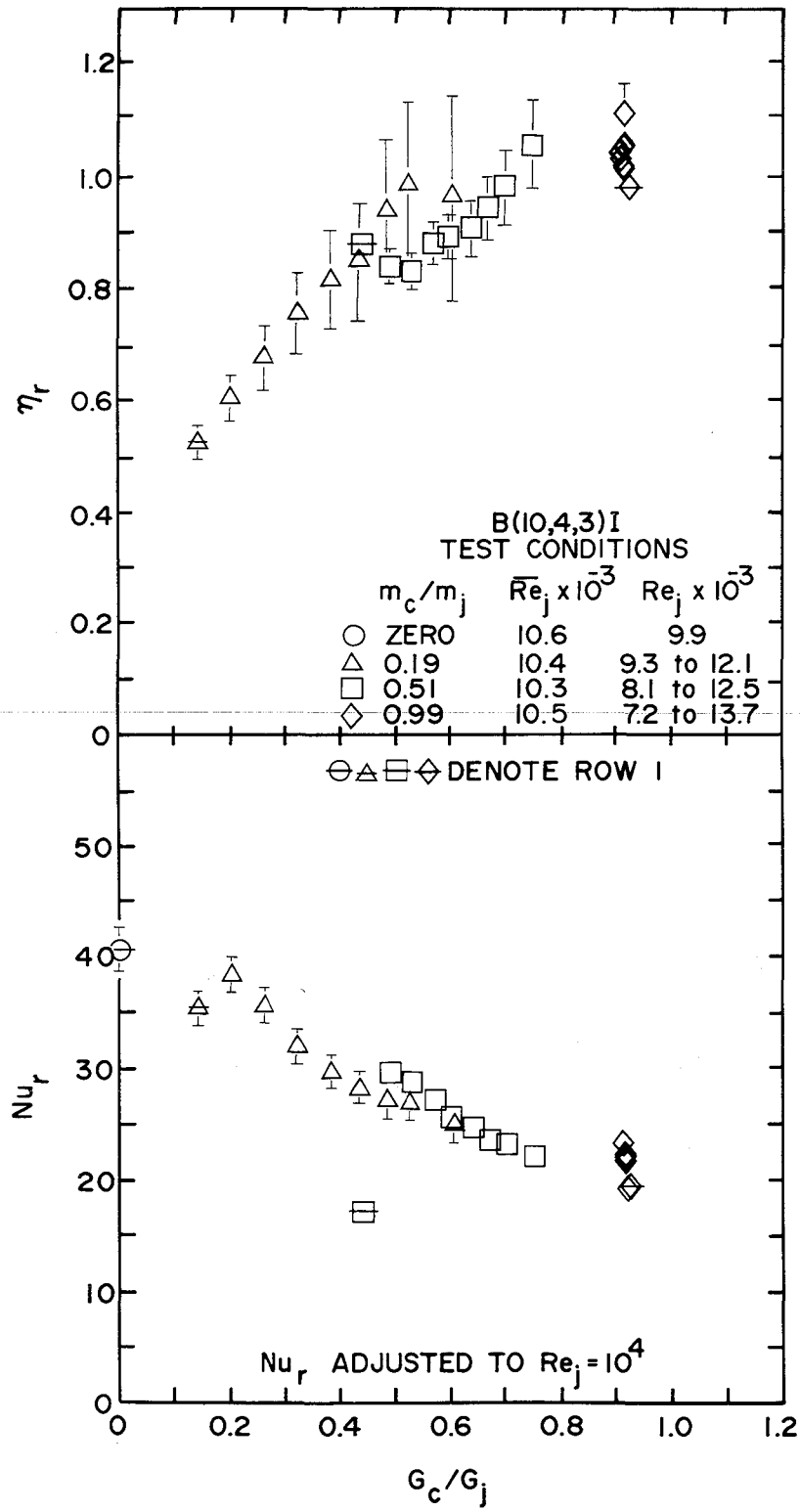

Fig. 6.15 Effect of crossflow-to-jet mass flux ratio on η_r and Nu_r for B(10,4,3)I geometry.

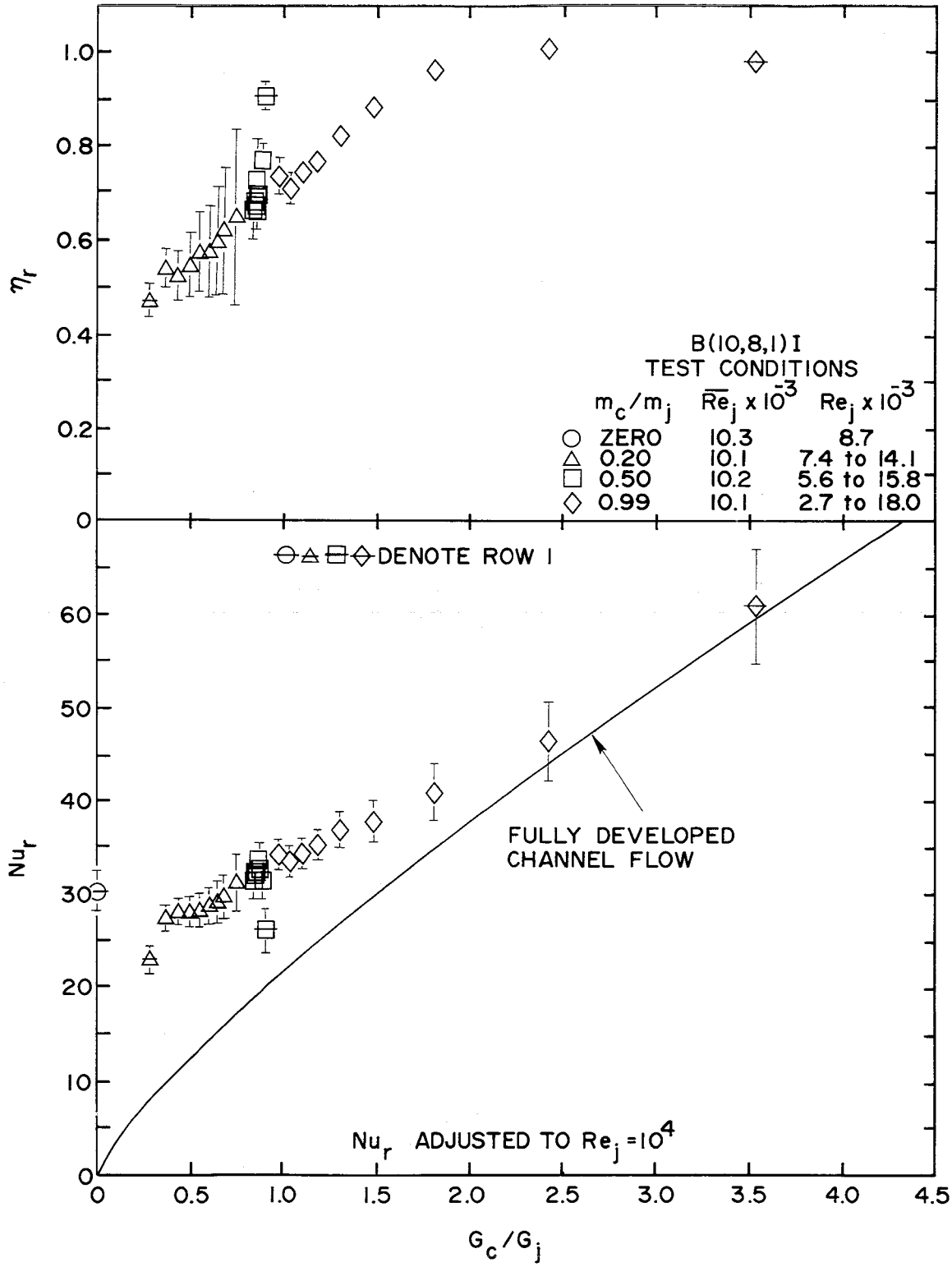

Fig. 6.16 Effect of crossflow-to-jet mass flux ratio on η_r and Nu_r for B(10,8,1)I geometry.

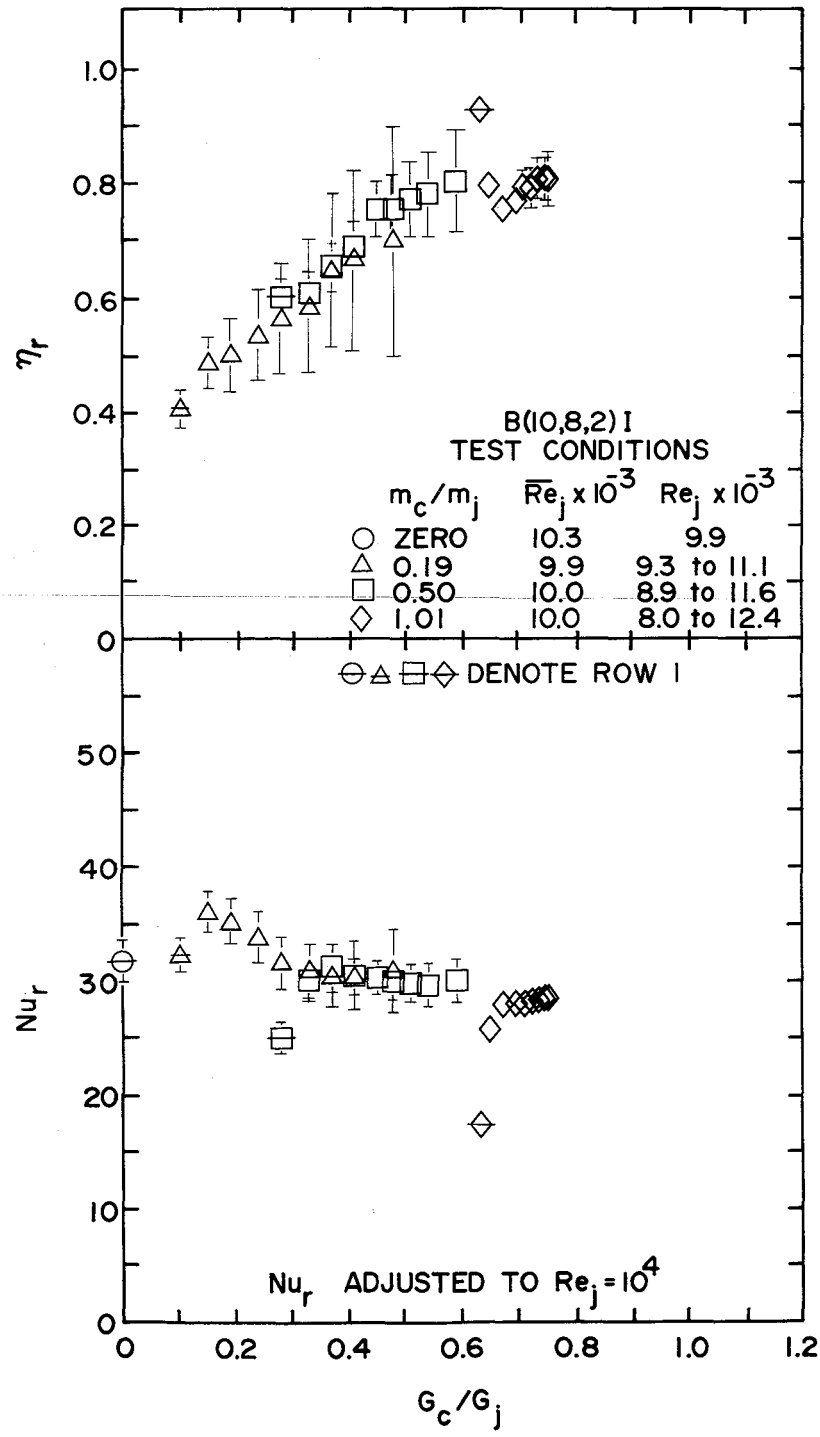

Fig. 6.17 Effect of crossflow-to-jet mass flux ratio on η_r and Nu_r for B(10,8,2)I geometry.

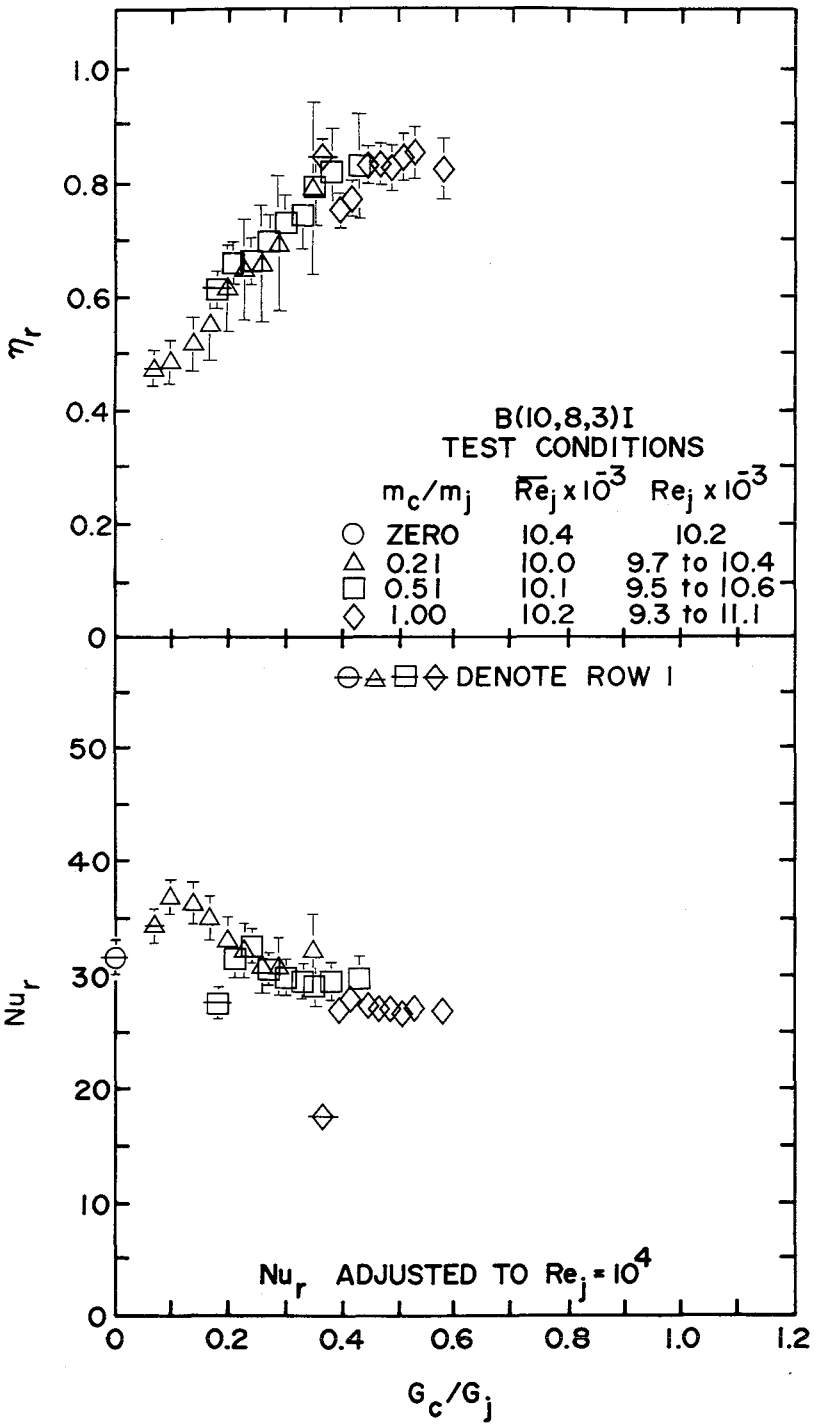

Fig. 6.18 Effect of crossflow-to-jet mass flux ratio on η_r and Nu_r for B(10,8,3)I geometry.

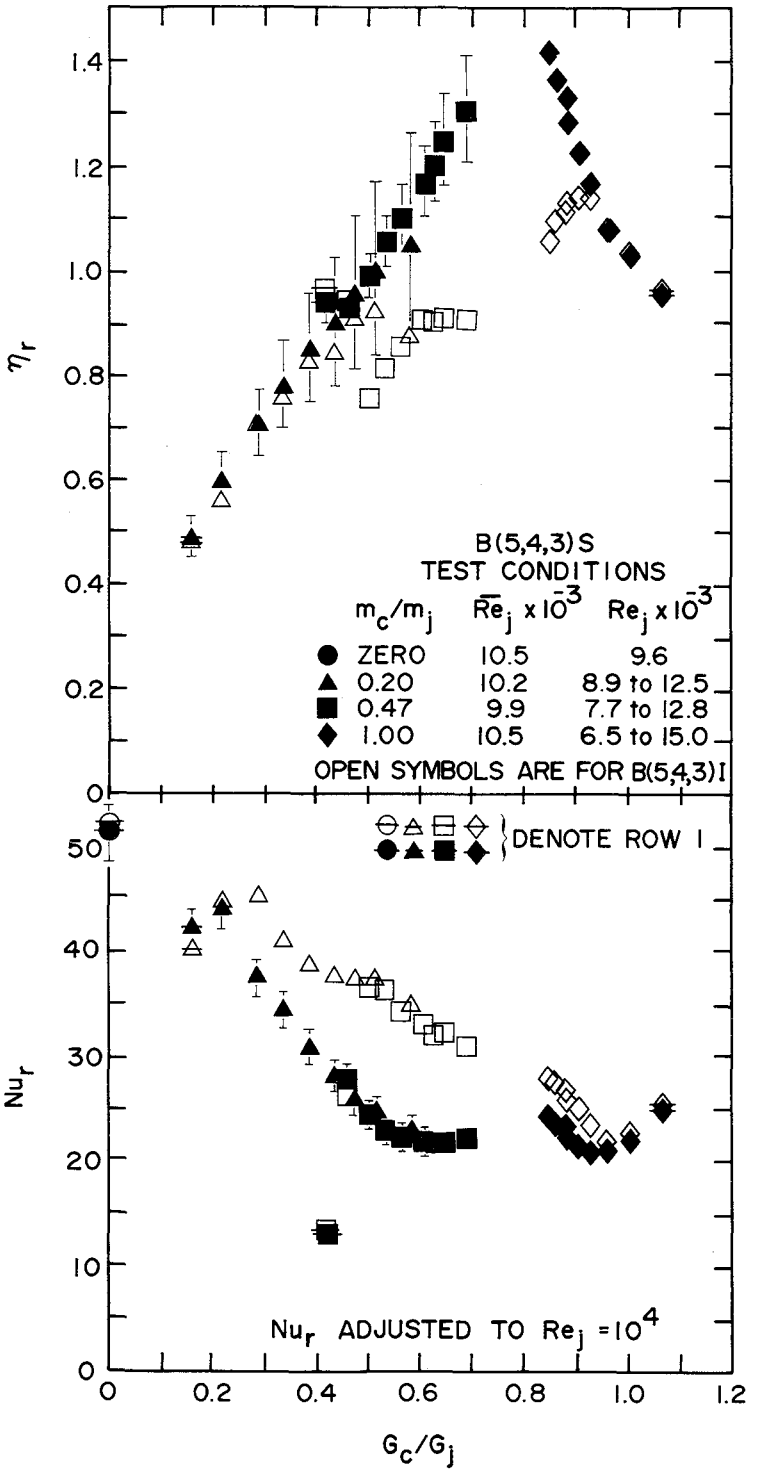

Fig. 6.19 Effect of crossflow-to-jet mass flux ratio on η_r and Nu_r for B(5,4,3)S geometry - comparison with inline case.

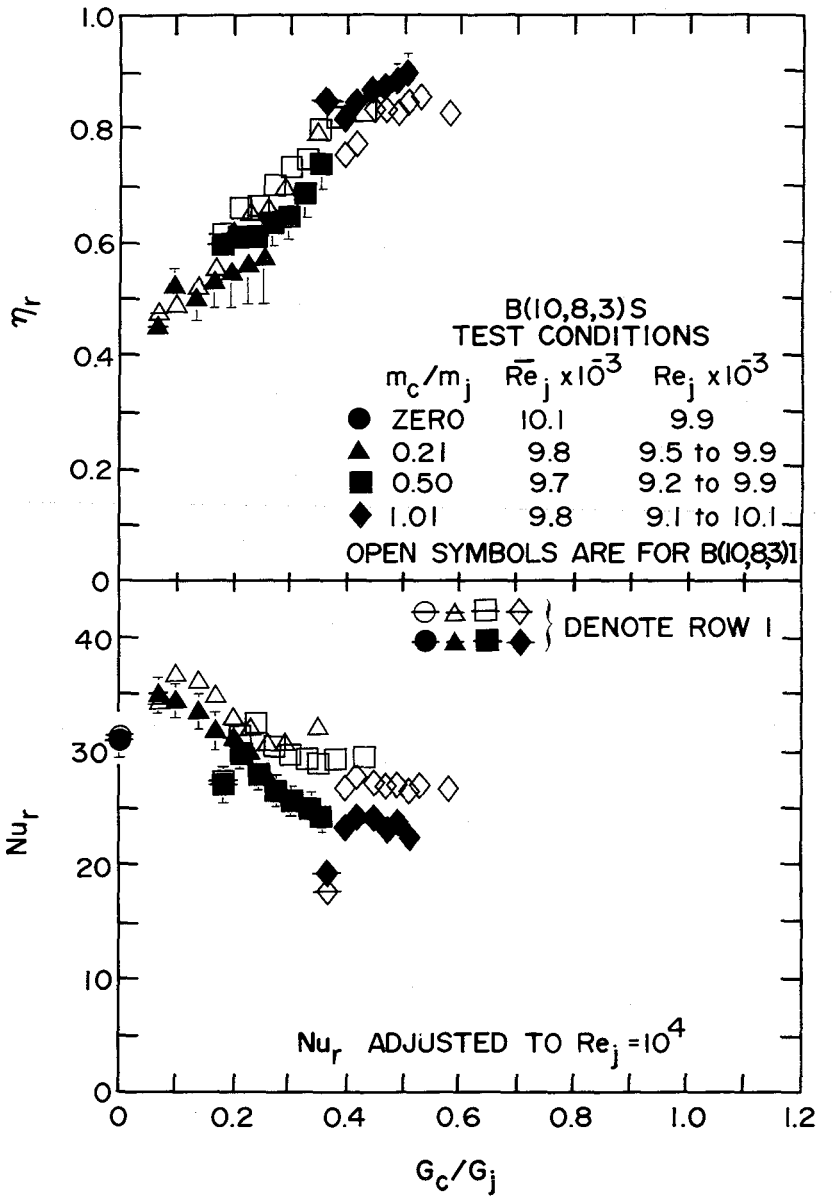

Fig. 6.20 Effect of crossflow-to-jet mass flux ratio on η_r and Nu_r for B(10,8,3)S geometry - comparison with inline case.

For both η_r and Nu_r the data points which deviate most clearly from the overall trends of the other points are always for the upstream rows of the array, primarily row 1 and to a lesser extent row 2. This result may be attributed to the differences in the normalized velocity and temperature profiles at the entrances to the individual row domains (flow history effects), which should be most pronounced for row 1 as compared with downstream rows. This is clearly illustrated in Fig. 6.21 for the (5,4,2) I geometry. The basic set of data points for this case was displayed in Fig. 6.9, but Fig. 6.21 includes more data points at smaller increments of G_c/G_j for rows 1 and 2 obtained from several extra tests conducted for this particular geometry. These extra tests were for various combinations of the following array parameter values: nominal $\overline{Re}_j = 6 \times 10^3$ and 10^4, and m_c/m_j = 0, 0.07, 0.15, 0.20, 0.25, 0.30, 0.35, and 0.54.

These results show that for small values of G_c/G_j the trend of both η_r and Nu_r is independent of the row number (and therefore the flow history). However, as G_c/G_j increases the trends for row 1 clearly begin to separate from those for the downstream rows. The effects of individual spanwise row normalized entrance profiles are discussed in more detail in Section 6.3.

Returning to the primary set of plots (Figs. 6.9 through 6.20), several additional observations are in order. Values of η_r greater than unity occurred in the case of four geometric configurations (Figs. 6.9, 6.10, 6.15, and 6.19). These occur only for G_c/G_j of order unity or larger when the crossflow exerts a dominant influence on the impingement surface heat flux. Consider the interpretation of η_r in terms of the reference temperature defined for a zero regional average heat flux, Eq. (2.11). η_r greater than unity occurs for $T_{ref,r}$ greater than the mixed-mean total temperature $T_{m,n}$. After the row where $T_{ref,r}$ becomes equal to $T_{m,n}$ ($\eta_r = 1$), the crossflow is controlling the heat flux. Proceeding downstream $T_{ref,r}$ may decrease very slowly because the temperature of the jet flow can now influence $T_{ref,r}$ only after mixing with the crossflow since it no longer impinges directly on the heat transfer surface, while $T_{m,n}$ will have decreased more since its value is independent of the degree of mixing between the two flow streams. Thus η_r may become larger than unity. As a practical matter knowledge of these values of η_r would normally not be required since jet array designs in which the

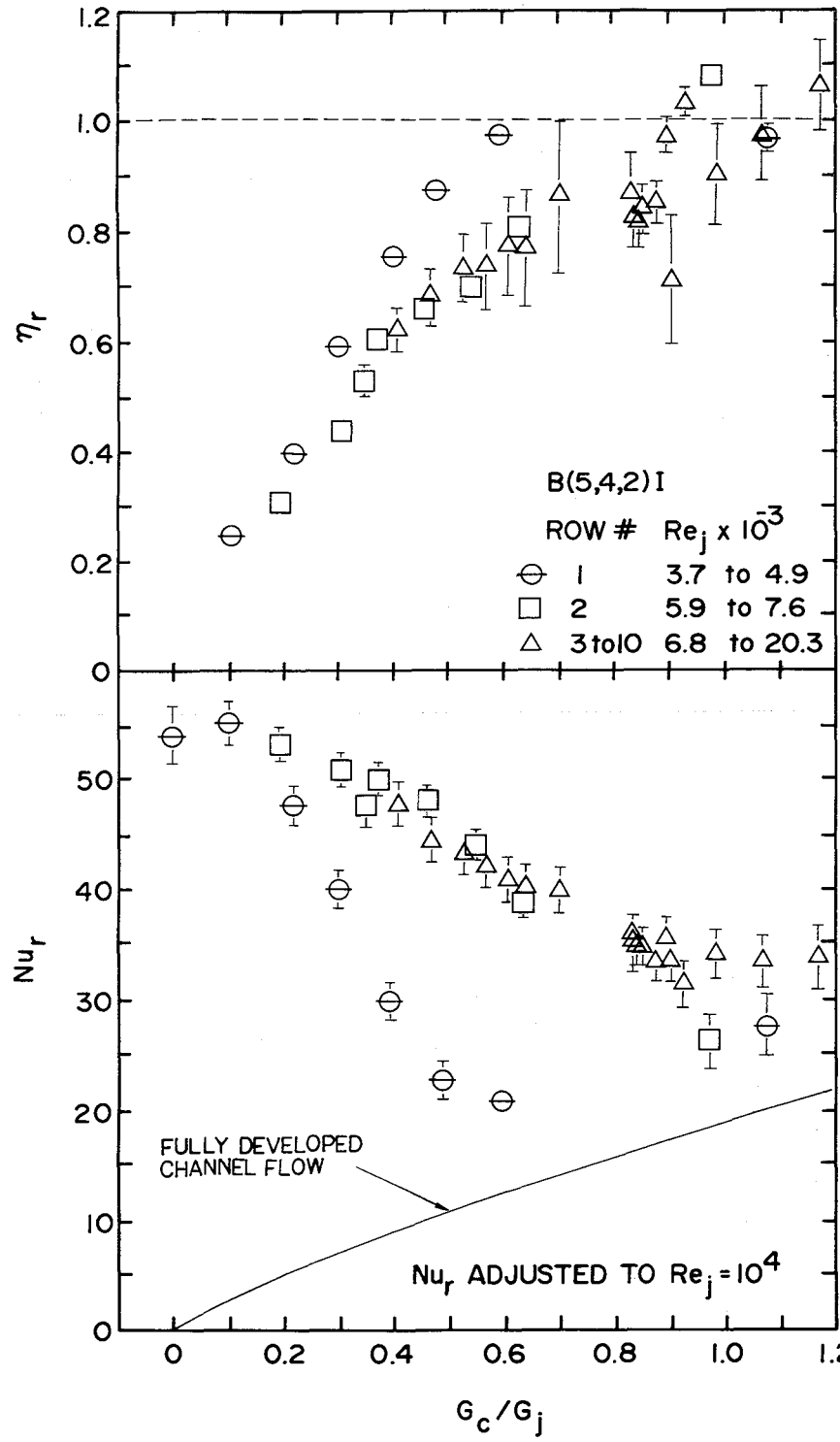

Fig. 6.21 Effect of crossflow-to-jet mass flux ratio on η_r and Nu_r by row number.

crossflow negates the cooling effect of the jet would not be utilized. It is useful for design purposes, however, to know the point at which (Figs. 6.12, 6.13, 6.17, 6.18, and 6.20) the presence of the jet is rendered useless by the crossflow.

The Nu_r data indicates that for some configurations (Figs. 6.12, 6.13, 6.17, 6.18 and 6.20) the presence of a small crossflow increases Nu_r slightly relative to the zero crossflow value before it begins to decrease with further increases in G_c/G_j. It appears that in these cases a direct contribution to the heat transfer rate by a small crossflow outweighs any degradation of the heat transfer contribution of the impinging jet caused by the small crossflow. Further increases in G_c/G_j then cause a decline in Nu_r which then tends to level off. If in these cases G_c/G_j were increased even more, Nu_r would presumably begin to increase again ultimately approaching heat transfer rates equivalent to those of a fully developed channel flow, as in fact was observed in some of the other cases.

6.3 Flow History Effects

The individual spanwise row heat transfer parameters (Nu_r and η_r) have been presented as functions of the independent parameters for the row domain (x_n/d, y_n/d, z_n/d, Re_j, G_c/G_j). While these formulations account for the effects of both the average mass flux G_c and the mixed-mean total temperature of the crossflow at the entrance to an individual spanwise row (regional) domain, there is also, in general, a dependence of the heat transfer parameters on the normalized velocity and temperature profiles at the control surface which marks the entrance to the domain [see Section 3, in particular Eqs. (3.38) and (3.39)]. These normalized profiles depend in turn, of course, on the details of the flow history upstream of the domain. Two domains having identical values for the independent parameter sets noted above may have different flow histories. In the interests of generalizing the applicability of the individual row parameters Nu_r and η_r, it is important to consider the sensitivity of these parameters to the flow history.

For the array geometries under consideration here it is reasonable to consider the available flow development length upstream of the entrance to a given domain to extend from the control surface marking the entrance of the

domain to the nearest upstream spanwise row of jet holes. In the present tests this length for the initial crossflow channel upstream of the overall array domain was fixed (Table 4.1). It ranged from 16 to 95 hydraulic diameters depending on the channel height. Channel heat transfer coefficients just upstream of the entrance to the array were in good agreement with prior results for large aspect ratio rectangular ducts with one large side heated [Florschuetz et al. (1982)]. It may therefore be assumed that the velocity and temperature profiles at the entrance to the array were spanwise uniform.

Now consider the individual row domains. The available development length upstream of the domain associated with row 1 is the same as that for the overall array. For rows downstream of row 1, it ranges from 5/12 ($\approx$ 0.4) for geometries with (x_n/d, z_n/d) = (5,3) to 2.5 for geometries with (x_n/d, z_n/d) = (10,1). For the present test geometries these available development lengths are 38 times smaller than those upstream of row 1 (and of the array).

For the data base available in the present study, flow hisotry effects for an individual spanwise row domain (i.e., the effect of the normalized velocity and temperature profiles at the entrance to the domain) arise, and can be considered, in three categories. First, inline vs. staggered hole patterns under otherwise identical conditions result in differing flow histories for a given spanwise row. Second, conditions exist where for a given array geometry at a certain initial crossflow-to-total jet flow ratio (m_c/m_j), G_c/G_j is uniform (or nearly so) along the array making it possible to compare η_r and Nu_r values along the array, where the only significant variable is the flow history resulting from the position of a row within the array. Third, for a given array geometry, varying flow histories for individual rows occur for the several different m_c/m_j magnitudes at which measurements were made, while the ranges of values of G_c/G_j resulting from the several m_c/m_j magnitudes may overlap. The varying flow histories for otherwise identical conditions at an individual row are then the result of a combination of effects - row position within the array and the magnitude of m_c/m_j. Each of these three categories will now be considered in turn.

Results for the staggered arrays tested are plotted in Figs. 6.19 and 6.20. Data points for the corresponding inline arrays are included for comparison. Uncertainty intervals for the inline array data points are

omitted in these figures for the sake of clarity (see the individual plots of this inline data, Figs. 6.10 and 6.18, for these uncertainty intervals). The η_r data points for the array with large hole spacing (10,8,3), Fig. 6.20, are essentially independent of hole pattern to within experimental uncertainty, while the staggered array Nu_r data begins to fall noticeably below the inline array data as G_c/G_j increases. For the array with closer hole spacing (5,4,3), Fig. 6.19, η_r is independent of hole pattern for smaller values of G_c/G_j but for increasing G_c/G_j the η_r data points for the staggered array fall significantly above those for the inline array with values rising above unity, then decreasing to unity again as G_c/G_j approaches one, with the points again coinciding with those for the inline array. An explanation for η_r greater than one was discussed in a preceding paragraph. Apparently η_r for the (5,4,3) staggered array falls above that for the inline array because increased mixing between the crossflow and jet streams for the staggered array causes the crossflow to begin to dominate at smaller values of G_c/G_j (about 0.5) than for the inline case. This is also indicated by the comparison of the Nu_r data. The more rapid decrease of Nu_r for the staggered array is arrested near $G_c/G_j = 0.5$ while the slower decrease of Nu_r for the inline array continues. Then as G_c/G_j approaches unity the crossflow becomes dominant for both the inline and staggered arrays and both η_r and Nu_r for the two arrays again coincide as they do for small values of G_c/G_j. Because of the complexity of the flow fields involved explanations of observed heat transfer characteristics for staggered arrays relative to inline arrays must remain speculative. Hippensteele et al. (1983) presented a comparison of an inline and a staggered array using thermal visualization with liquid crystals which also indicated higher heat rates for the inline array.

Now consider test results for a given array geometry at a given initial crossflow-to-total jet flow ratio (m_c/m_j). For a given array geometry, as m_c/m_j is increased a value is reached for which the crossflow-to-jet mass flux ratio G_c/G_j becomes uniform over all spanwise rows of the array [see e.g., Fig. 6.2, B(10,8,1)I at $m_c/m_j = 0.46$]. This condition occurred, at least approximately, for several of the test runs in the present study, thus providing, in each of these cases, heat transfer results from a single test having a uniform G_c/G_j, but with varying flow history (depending on row

number). Since the individual row Reynolds number increases from upstream to downstream Nu_r values were adjusted to correspond to $Re_j = 10^3$ according to $Nu_r \propto Re_j^{0.73}$. It may also be recalled that η_r was found to be relatively insensitive to Re_j. Thus, we have results from individual test cases for which, to a good approximation, the only remaining independent parameter that may affect η_r or Nu_r is the flow history (i.e., row number).

Results of this type for η_r and Nu_r as a function of row number for four different array geometries are shown in Figs. 6.22 and 6.23. Generally these results indicate that η_r and Nu_r become relatively insensitive to any changes in the normalized velocity and temperature profiles after the first two rows of the array. Or stated another way, a reasonable entrance length for the array appears to be two rows. These results imply further that the application of test results obtained for a crossflow approaching a single line of jets to individual downstream jet rows within a two-dimensional array could result in serious errors, but that results based on the third row of an array could be applied as a good approximation for rows downstream of the third row. That is, for such application, test results for an array having at least three rows should be obtained. These figures show clearly (as did Figs. 6.9 through 6.21) that Nu_r at row 1 is often significantly smaller than at downstream rows for the same Re_j and G_c/G_j because the entire crossflow interacts directly with the jets at row 1, whereas for any given downstream row the bifurcation of the crossflow caused by upstream jets tends to decrease the direct interaction of the crossflow with jets in the given downstream row. This effect is more pronounced for inline arrays than for staggered arrays as is indicated by the comparisons in Figs. 6.19 and 6.20. There, for intermediate values of G_c/G_j (large enough to have a significant effect but still small enough so the crossflow is not dominating), staggered vs. inline Nu_r values for the same G_c/G_j are identical at row 1, whereas for downstream rows Nu_r for the staggered arrays is larger than at row 1 by a smaller increment than for the inline arrays. The crossflow bifurcation is less significant in decreasing direct interaction between jets and crossflow for the staggered case because of the offset of the jets immediately upstream of the row in question. For conditions where significant differences exist, η_r tends to be larger at row 1 than at downstream rows (except where the crossflow is

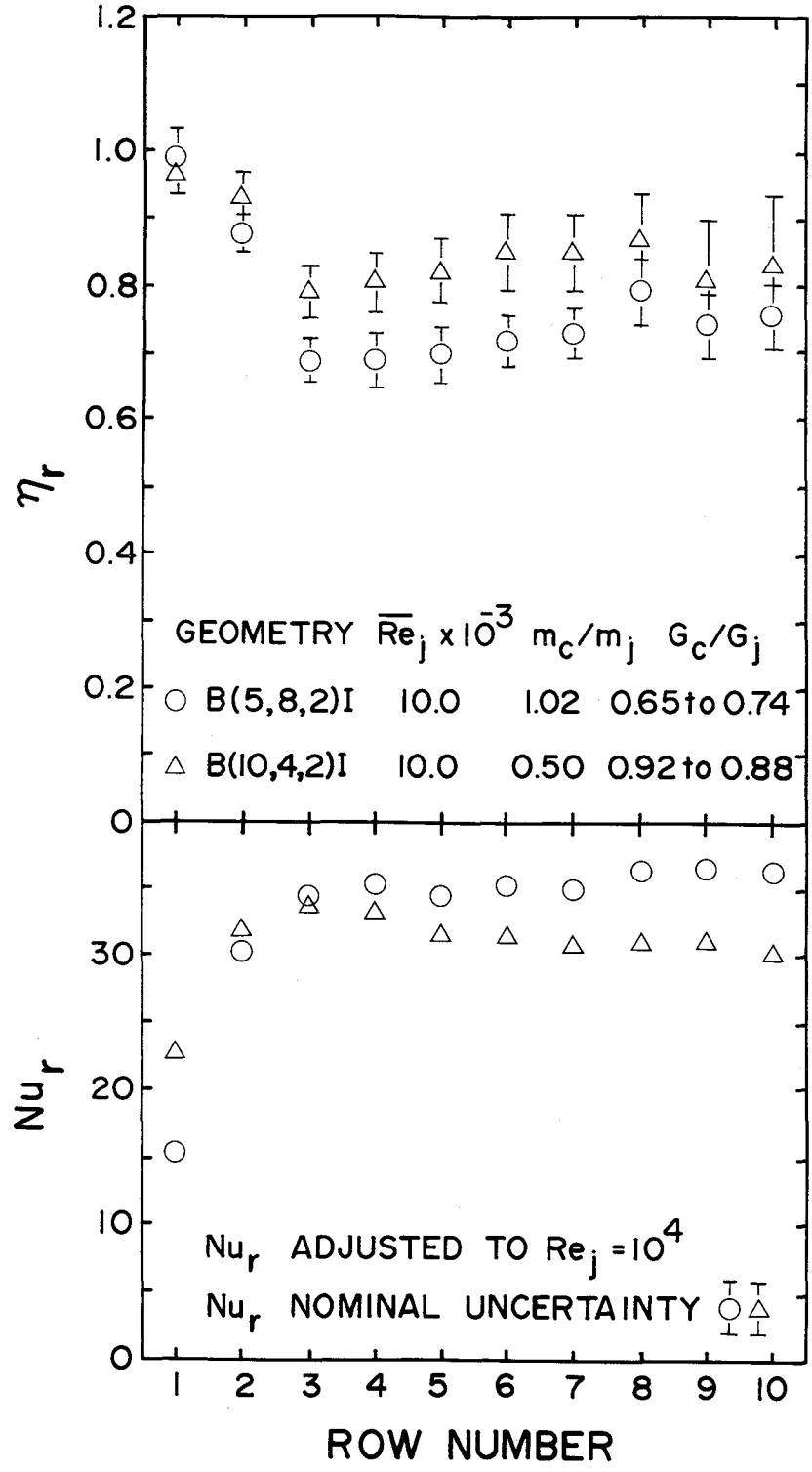

Fig. 6.22 Effect of flow history on η_r and Nu_r for B(5,8,2)I and B(10,4,2)I geometries.

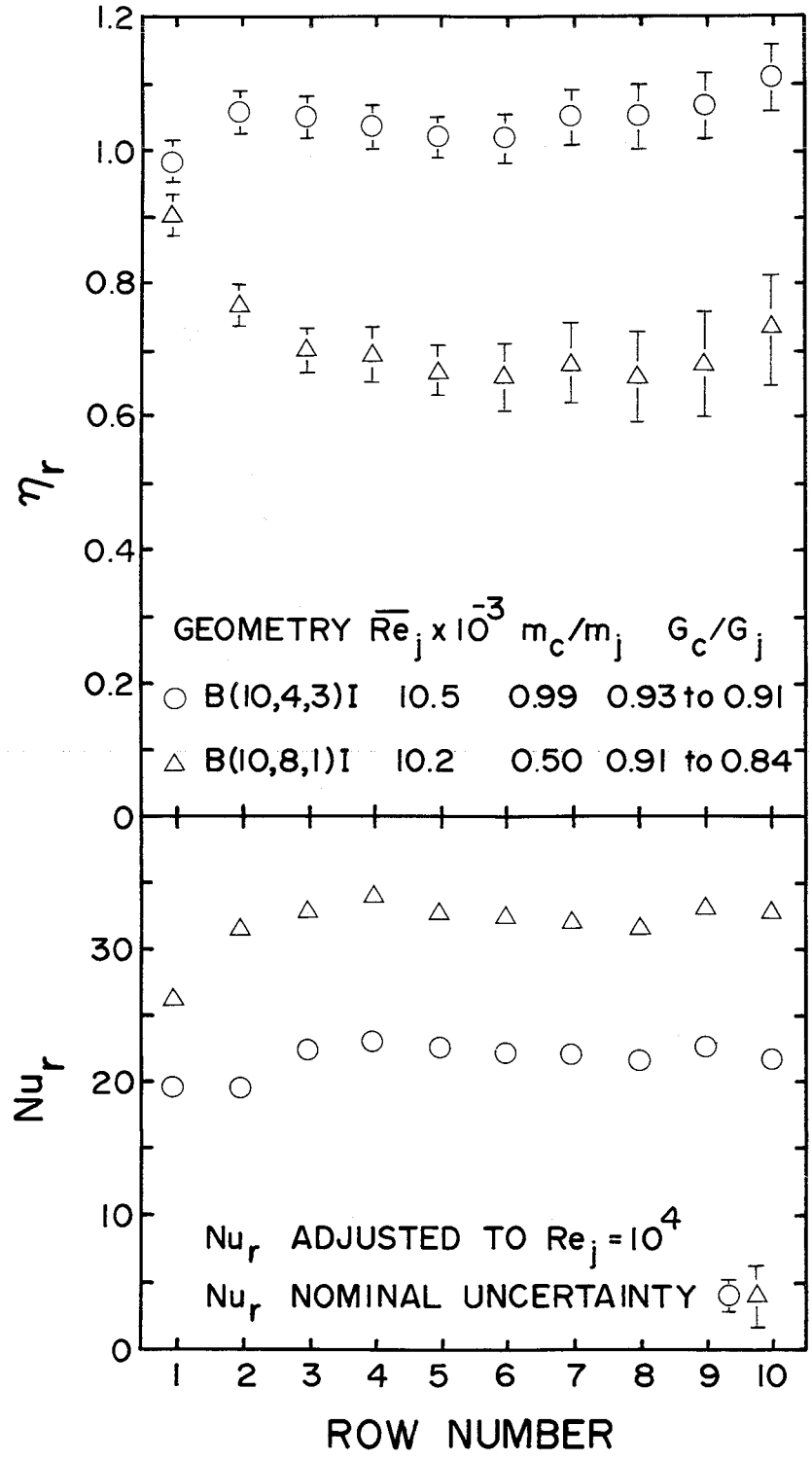

Fig. 6.23 Effect of flow history on η_r and Nu_r for B(10,4,3)I and B(10,8,1)I geometries.

dominant) and for staggered arrays than for inline arrays, presumably for the same reasons suggested above in connection with Nu_r.

Finally, it is appropriate to re-examine η_r and Nu_r results in Figs. 6.9 through 6.20 considering possible effects of flow history. Each of these figures applies for a specific array geometry and includes test results obtained at three different initial crossflow rates. When, for a given geometry, the ranges of G_c/G_j from tests at different m_c/m_j overlap, the sets of Nu_r data points from the different tests are generally quite consistent; and when the ranges of G_c/G_j do not overlap it appears that the sets of points are also generally quite consistent in that they lie on or close to a single smooth curve which could be drawn through them. Thus, with the important exception of row 1 and sometimes row 2 and then only at intermediate values of G_c/G_j, the flow history effects on Nu_r may be neglected.

Turning to η_r, for a given geometry the different sets of points which result from tests at different m_c/m_j do not appear overall as consistent for most geometries as they are for Nu_r, though the larger experimental uncertainties for some of the η_r data points at downstream rows make it more difficult to draw precise conclusions. In Fig. 6.10, the η_r points from the $m_c/m_j = 0.47$ test (squares), beginning at row 1 and proceeding downstream, first drop below the points from the $m_c/m_j = 0.20$ test (triangles), then at row 3 (the third square point) the trend reverses with the points appearing to asymptotically approach an imaginary line extrapolated from the $m_c/m_j = 0.20$ set (triangles). Similar trends are present in Figs. 6.12, 6.13, 6.14, 6.17 and 6.18.

These trends may be explained by flow history effects. Approaching row 1 the crossflow is entirely initial crossflow. For succeeding rows considered at the same G_c/G_j and mixed-mean total temperature, the further downstream the row, the larger the fraction of the crossflow which originated from upstream jets, but at the same time a larger fraction of the crossflow originating from upstream jets becomes more thoroughly mixed in the crossflow stream before reaching the row. Thus, for rows immediately following row 1 the zero regional average heat flux surface temperature $T_{ref,r}$ (Section 2.3) is directly influenced by the cooler part of the crossflow originating from upstream jets and is smaller relative to the mixed-mean temperature than at

row 1. For rows further downstream $T_{ref,r}$ is again larger relative to the mixed-mean temperature because more of the jet contribution to the crossflow has mixed with the crossflow stream before interacting with the surface.

As additional evidence that the observed pattern of the η_r data points under discussion may be attributed to flow history effects, one may compare the data sets for the smaller x_n/d with those for larger x_n/d, other parameters being held constant. For example, the behavior of the square set of data points for η_r in Fig. 6.10 ($x_n/d = 5$) attributed above to flow history effects is much less pronounced in Fig. 6.15 ($x_n/d = 10$) presumably because of the increase in available flow development length between rows for the latter case. Compare also Fig. 6.9 with 6.14, 6.11 with 6.16, 6.12 with 6.17, and 6.13 with 6.18.

6.4 Effects of Geometric Parameters

Since the flow history effects sometimes render the results for η_r and Nu_r at row 1, and to a lesser extent row 2, different from those for the downstream rows, the geometric parameter effects will be examined at row 1 separately from effects for rows beyond row 2. Figs. 6.24 and 6.25 show the values of η_r and Nu_r as a function of G_c/G_j for three different channel heights ($z_n/d = 1,2,$and 3) for jet plate (10,8)I. Fig. 6.24 applies for row 1 and Fig. 6.25 for rows 3 to 10. The trends with z_n/d are similar in both figures. η_r increases noticeably with increasing z_n/d while Nu_r is relatively insensitive to it. It seems reasonable that an increase in the path length for the jet to impinge on the surface would tend to cause a smaller influence of jet temperature on the heat flux relative to the influence of crossflow temperature thus increasing η_r. Apparently the very small to negligible effect of z_n/d on Nu_r is a result of the fact that the z_n/d range covered is well within the potential core length for circular jets.

The effects of jet hole spacings, x_n/d and y_n/d, on η_r and Nu_r for $z_n/d = 2$ is shown in Figs. 6.26 and 6.27. In contrast to the effect of z_n/d, Nu_r is more sensitive to hole spacing than η_r. Nu_r clearly decreases with hole spacing, the effect tending to diminish with increasing G_c/G_j. For smaller G_c/G_j, η_r increases slightly with hole spacing. For downstream rows at intermediate G_c/G_j the apparent dependence of η_r on hole spacing (Fig. 6.27)

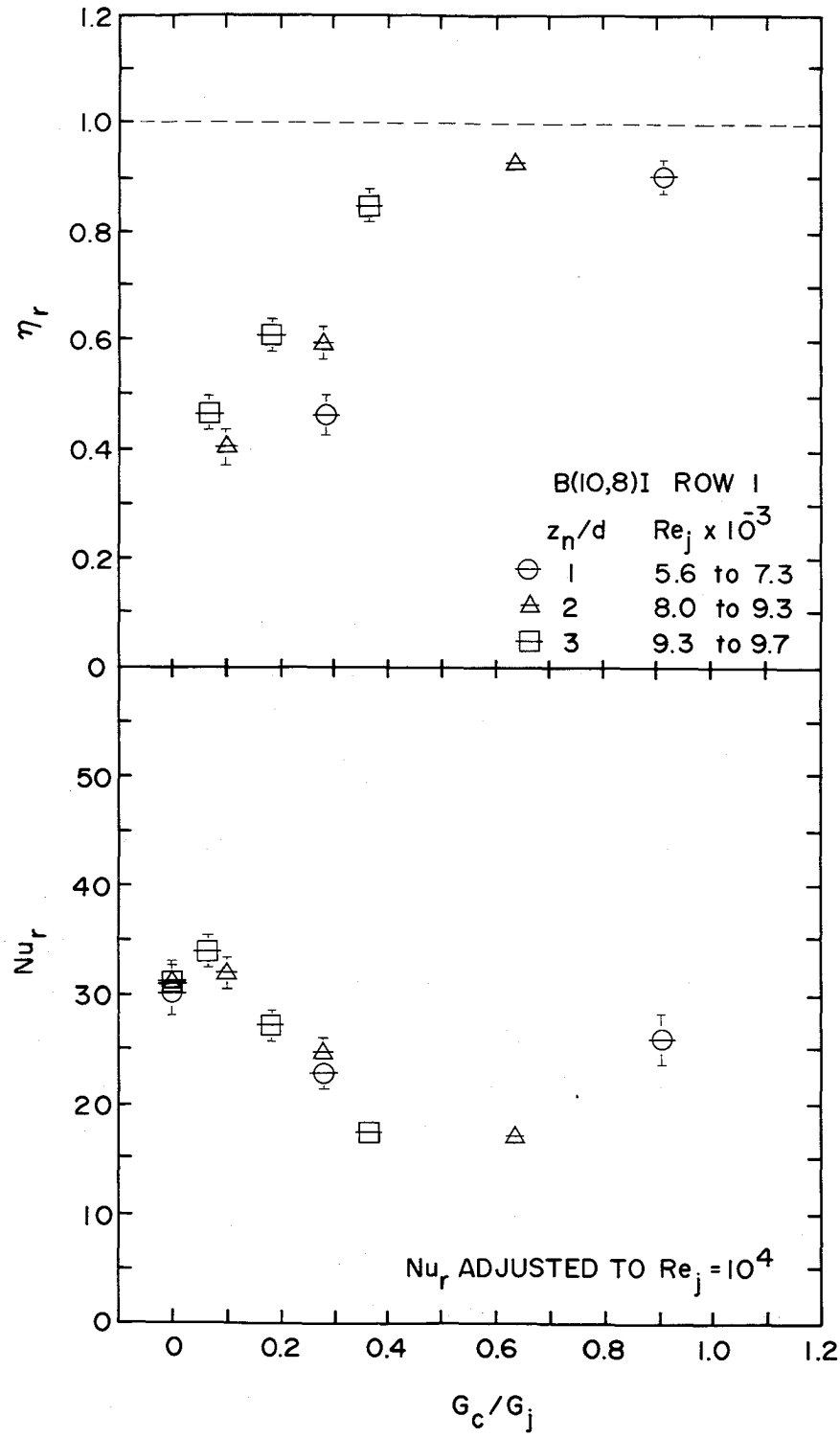

Fig. 6.24 Effect of channel height on η_r and Nu_r at the first row of B(10,8)I jet plate.

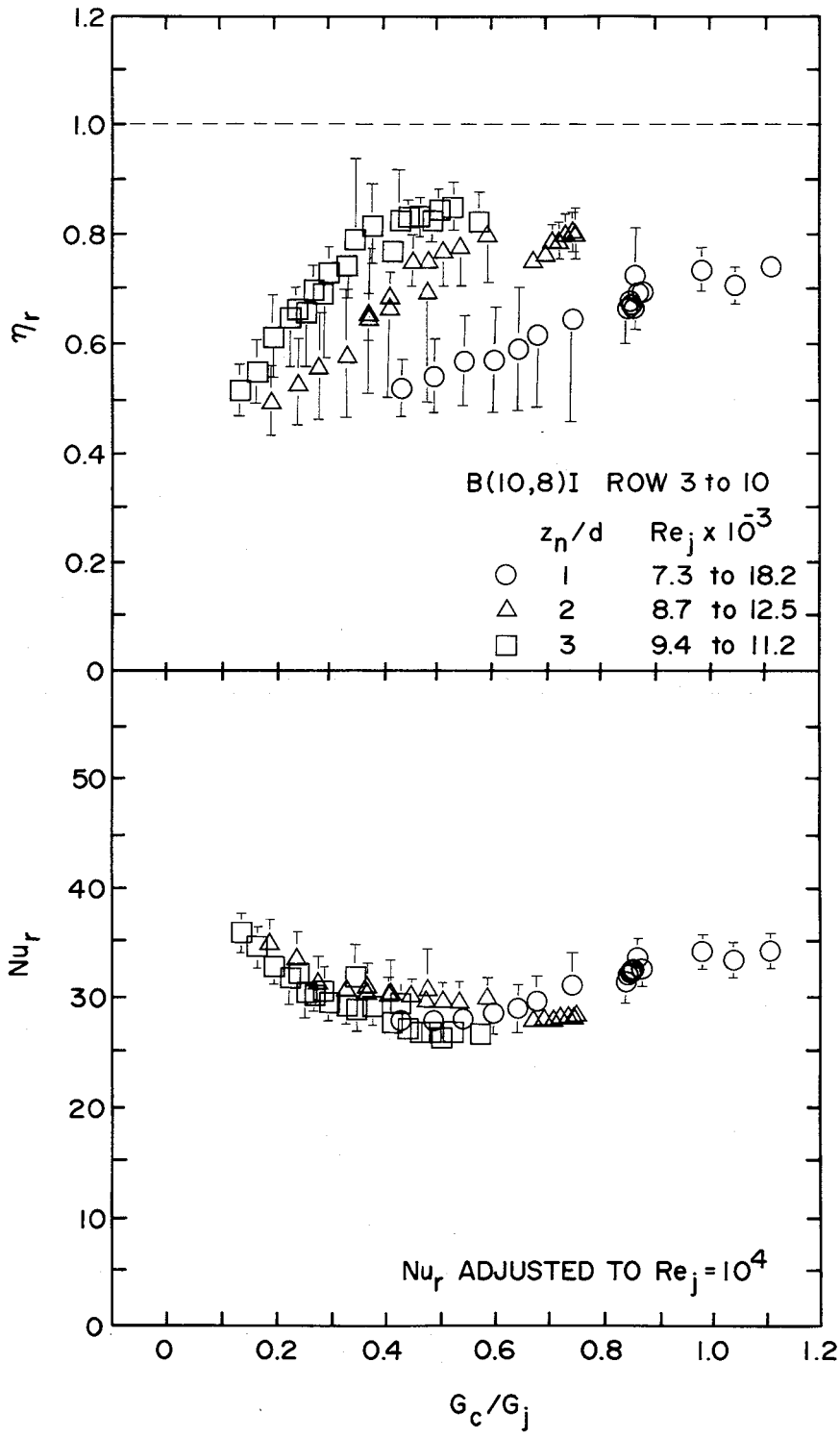

Fig. 6.25 Effect of channel height on η_r and Nu_r beyond the second row of B(10,8)I jet plate.

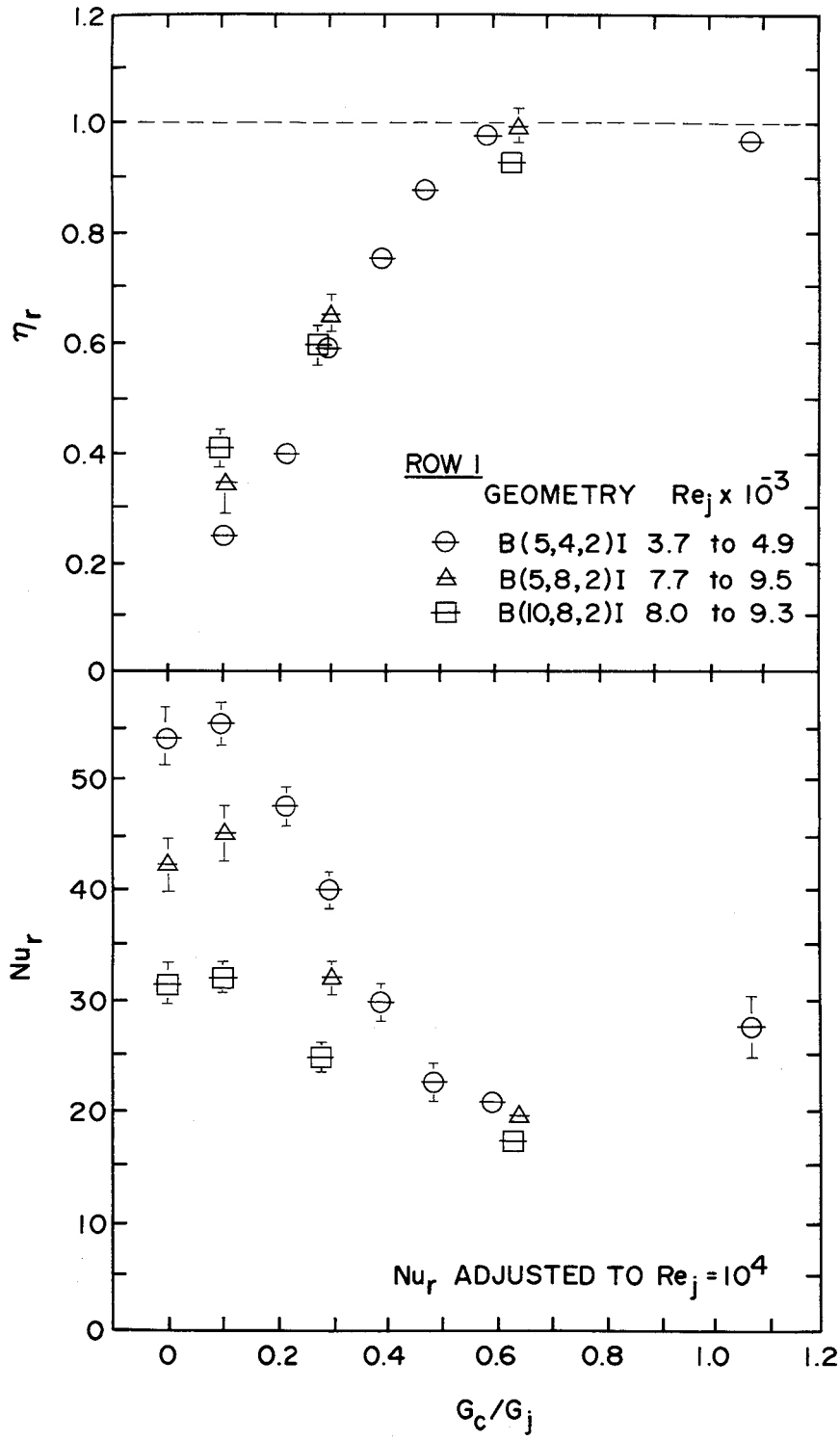

Fig. 6.26 Effect of jet hole spacings on η_r and Nu_r at the first row for $z_n/d = 2$.

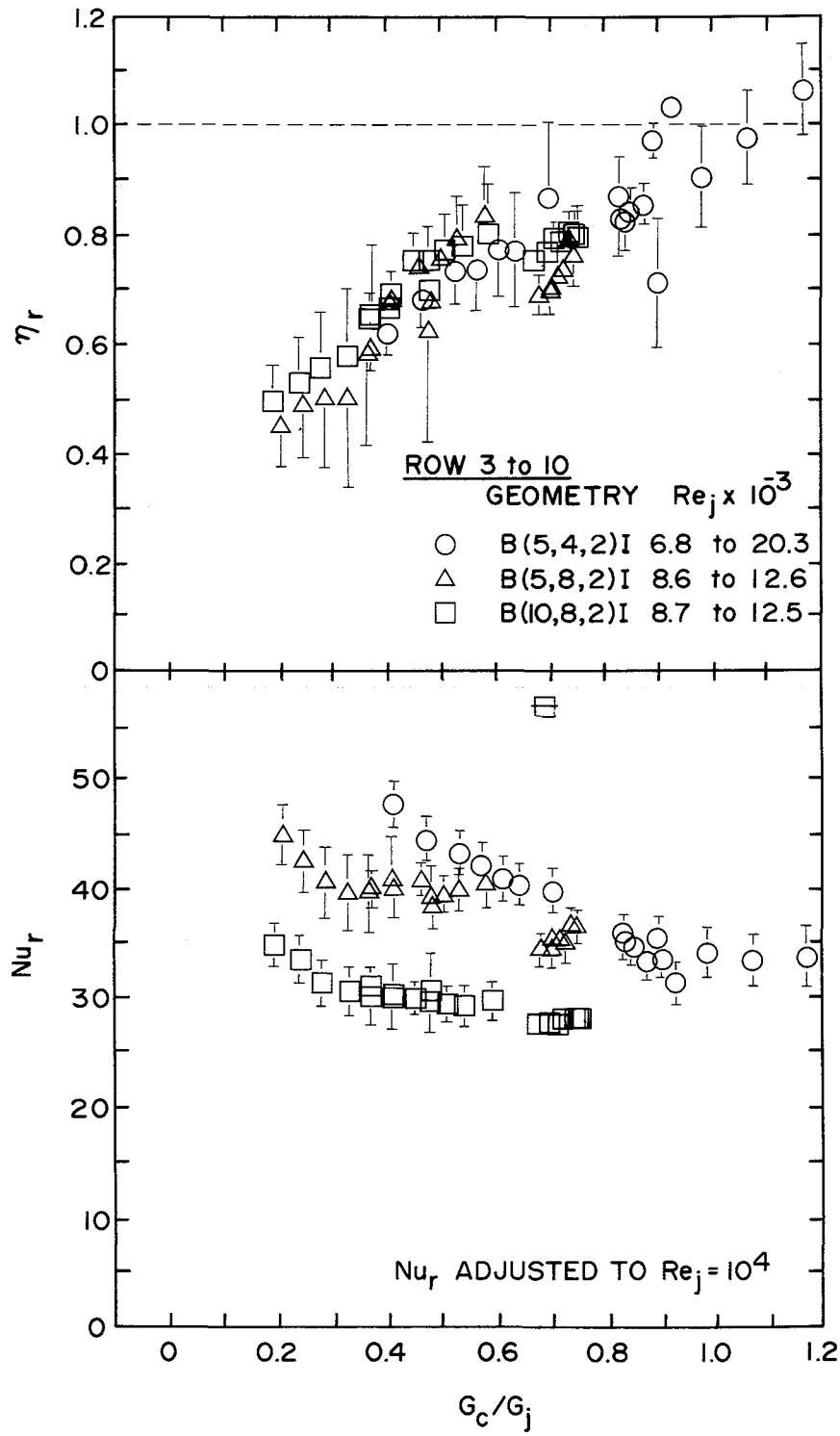

Fig. 6.27 Effect of jet hole spacings on η_r and Nu_r beyond the second row for $z_n/d = 2$.

though still quite small is perhaps confounded to some degree by the flow history effects discussed in the prior section.

7. RESULTS IN TERMS OF OVERALL ARRAY PARAMETERS

Considering the domain associated with the overall array (see Section 3.3 for details, or Section 2.1 for overview), it was shown that the parameters Nu and η depend on the streamwise position (x/L), the geometric parameters (x_n/d, y_n/d, z_n/d, L/x_n), the flow parameters ($\bar{\bar{Re}}_j$, m_c/m_j, Pr), and the normalized velocity and temperature distributions at the array entrance (x=0). In addition, there may be an effect of jet hole pattern. All of the η and Nu results presented in this section are based on the same raw test data as the η_r and Nu_r results given in Section 6.1 and were determined with the term related to recovery effects (ε) retained in Eq. (2.1) as discussed in Section 5.1. The significance of recovery effects in evaluating η and Nu is examined in Section 8.1. For the range of geometries and flow conditions considered here recovery effects are negligible in the evaluation of Nu, and also in the evaluation of η except for a small effect in those cases having highly nonuniform flow distributions. Therefore, the set of streamwise profiles of η and Nu to be presented in section 7.1 differs little overall from the results in terms of array parameters previously reported [Florschuetz et al., 1982]. The set is included here for completeness and to provide a set of results in terms of array parameters which is entirely consistent with the set of results in terms of row parameters presented earlier in Section 6 of the present report.

7.1 Streamwise Profiles of Heat Transfer Parameters

A complete set of plots for η and Nu as a function of x/L for the twelve geometries tested is shown in Figs. 7.1 through 7.12. Each figure is for a specified array geometry (x_n/d, y_n/d, z_n/d). The number of spanwise rows of holes, L/x_n, was fixed at 10. The first ten figures are for inline arrays and the last two for staggered arrays. The profiles of η and Nu are paired in each figure to emphasize that in order to appropriately relate the impingement surface heat flux and the fluid temperatures both parameter values are needed. The nominal mean jet Reynolds number, $\bar{\bar{Re}}_j$, was 10^4. For each geometry profiles are shown for m_c/m_j at nominal values of 0.2, 0.5 and 1.0. The Nu profiles for initial crossflow configurations at $m_c = 0$ are also shown as a

reference case for comparison. In the heat flux equation Eq. (2.1), η is defined as zero when the initial crossflow rate is zero. In addition to the points shown within the jet array region, three additional points are included for the initial crossflow channel immediately upstream of the array and one point immediately downstream of the array. Because the power measurements for the heater opposite row 9 developed a small intermittent random variation, the results at row 9, though they fit the overall pattern quite well, are not presented in the figures, but are included in the tables of Appendix B for reference. This heater later burned out. Therefore the data beyond row 7 were not obtained for B(10,8,3)S.

Composite uncertainties were computed for individual data points (Section 5.2). The composite uncertainties in η varied from $\pm$ 0.02 to $\pm$ 0.07 and were normally within $\pm$ 0.04. The composite uncertainties in Nu ranged from $\pm$ 4.1% to $\pm$ 8.8% for $\eta < 0.9$, and $\pm$ 5.7% to $\pm$ 12.5% for $\eta > 0.9$. For these results in terms of array parameters the uncertainty intervals are not shown directly on the plots.

As explained in the introductory paragraph of Section 7, this set of results differs little from the set presented in an earlier report [Florschuetz et al., 1982]. Therefore, the discussion provided in that report still applies. Attention is directed here, however, to Figs. 7.11 and 7.12 comparing staggered array results with their inline counterparts. Results for the (5,4,3)S array (Fig. 7.11) were included in the earlier report but were not compared directly on the same plot to the corresponding inline array results. Significant effects of hole pattern for this case are apparent as previously reported. The results for the (10,8,3)S array (Fig. 7.12) with initial crossflow were obtained subsequent to the prior report. For this array with larger hole spacings the effects of hole pattern are much less significant than for the (5,4,3) case with an initial crossflow present, just as they were for the noninitial crossflow configurations [Florschuetz et al., 1980a].

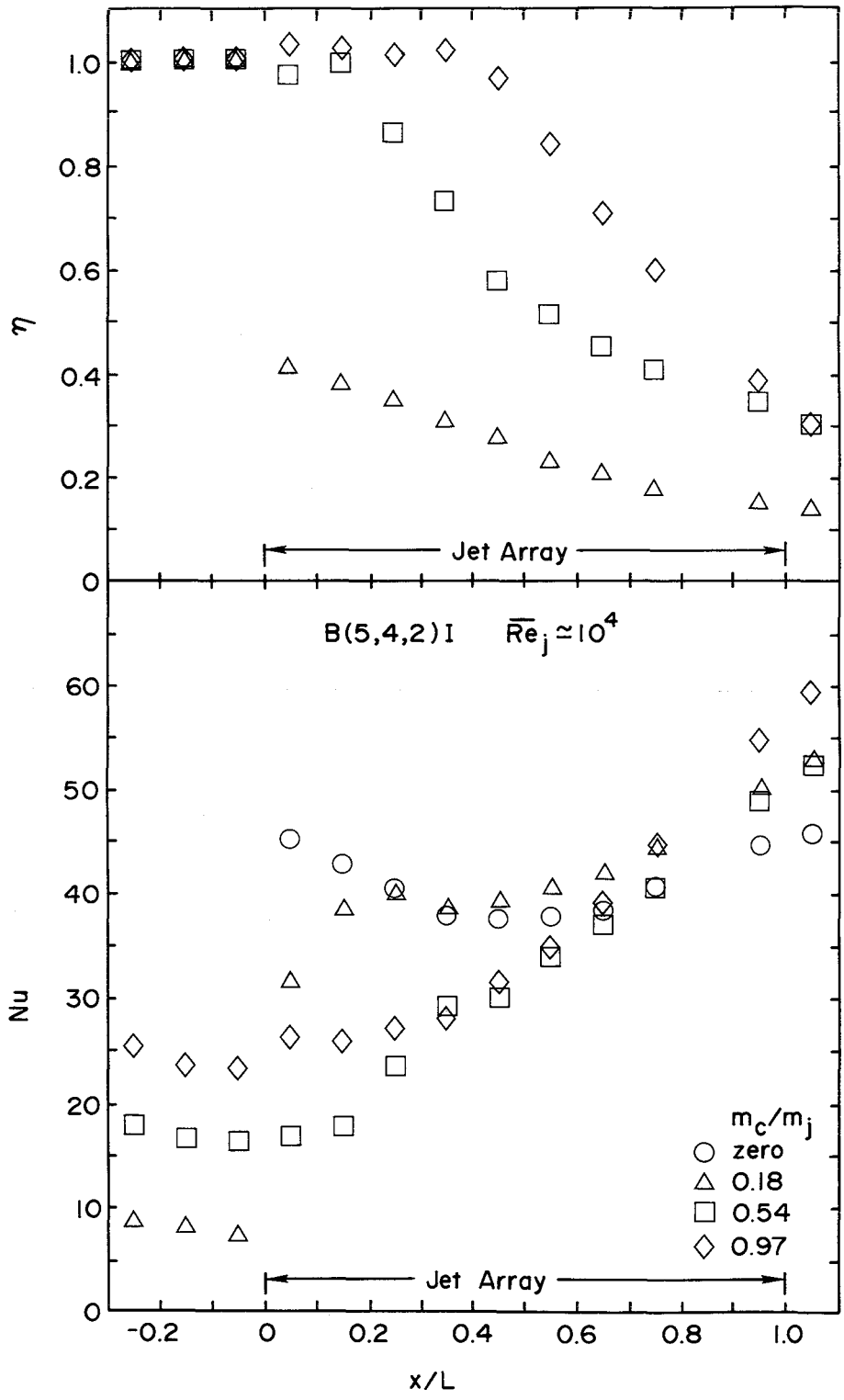

Fig. 7.1 Effect of initial crossflow rate on η and Nu profiles for B(5,4,2)I geometry.

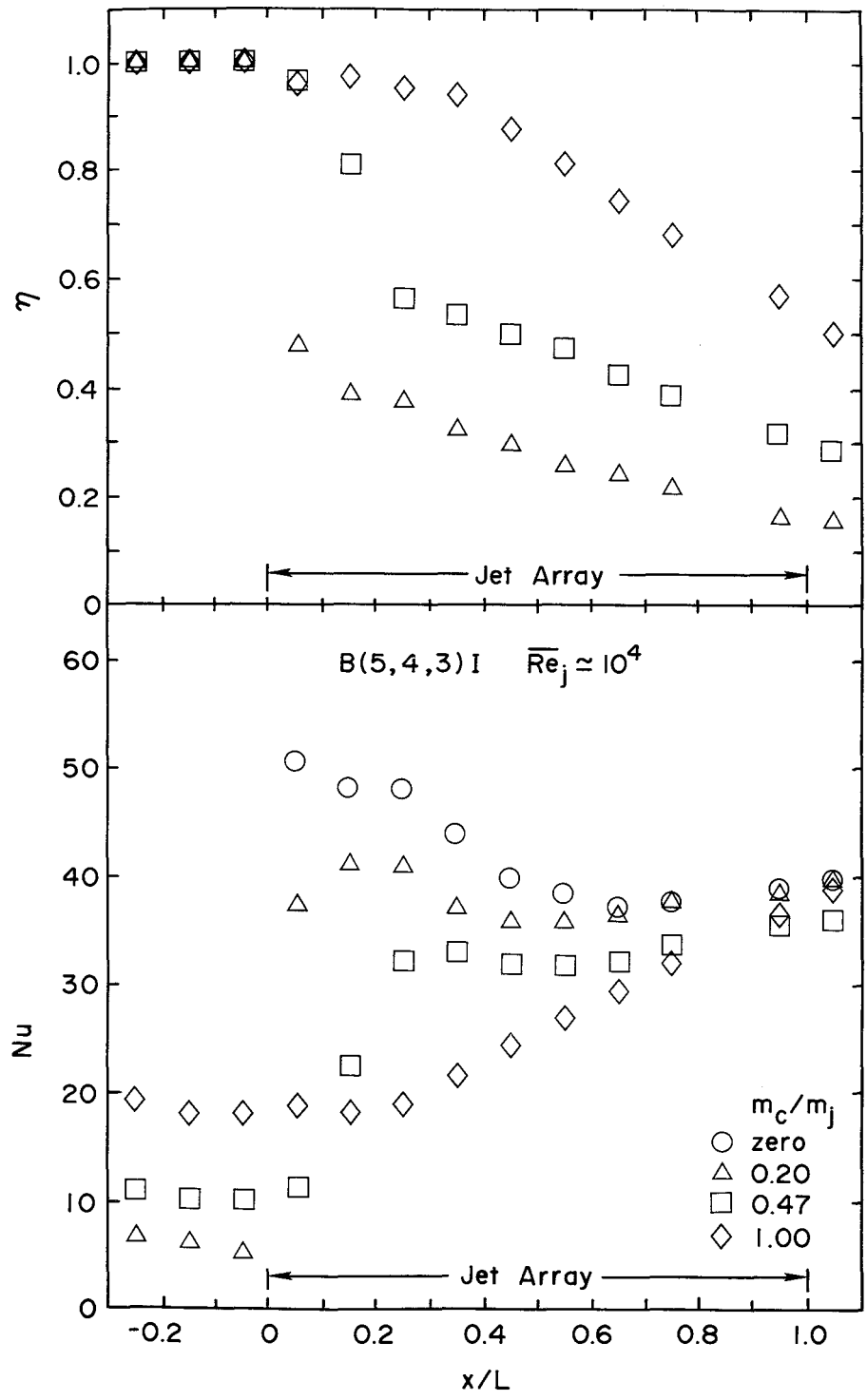

Fig. 7.2 Effect of initial crossflow rates on η and Nu profiles for B(5,4,3)I geometry.

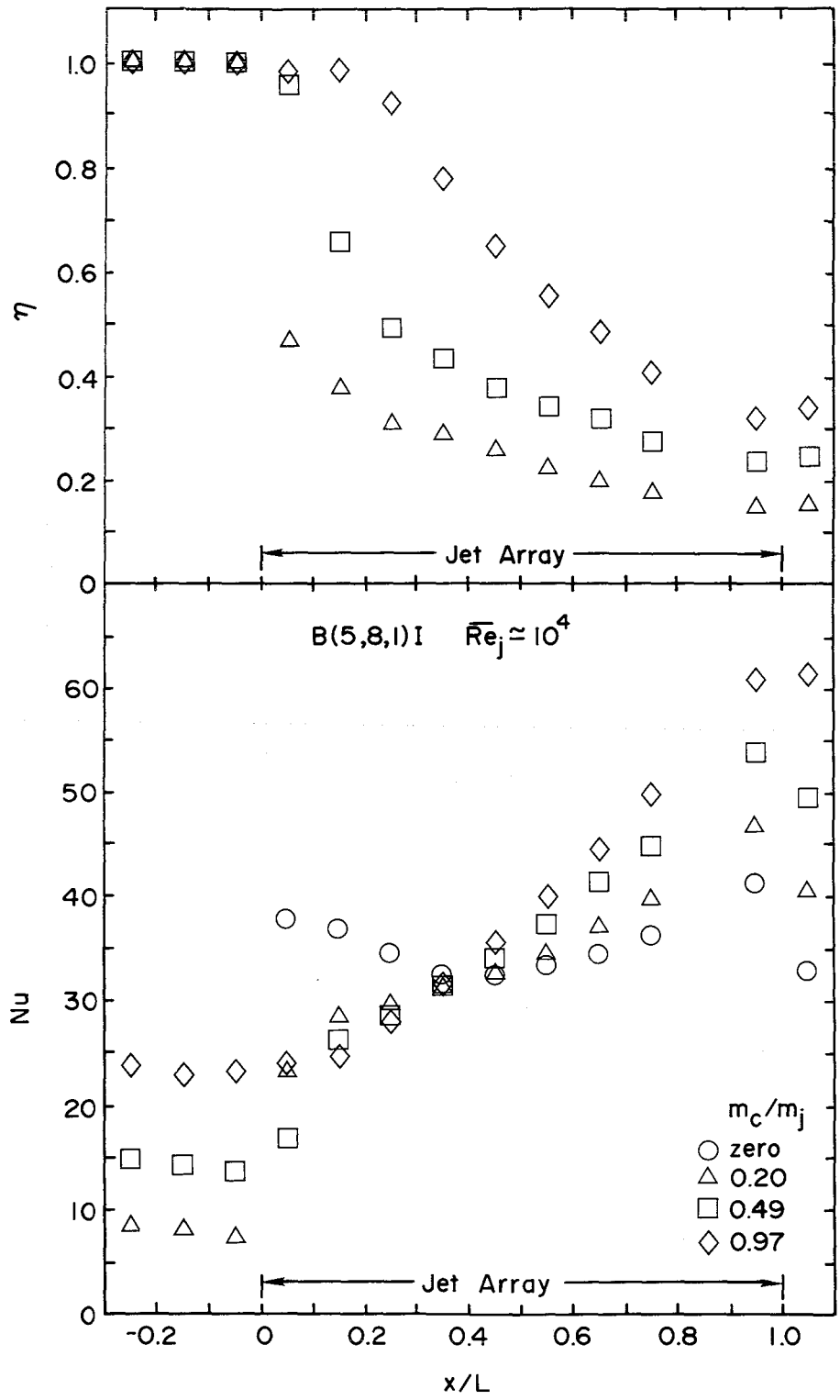

Fig. 7.3 Effect of initial crossflow rate on η and Nu profiles for B(5,8,1)I geometry.

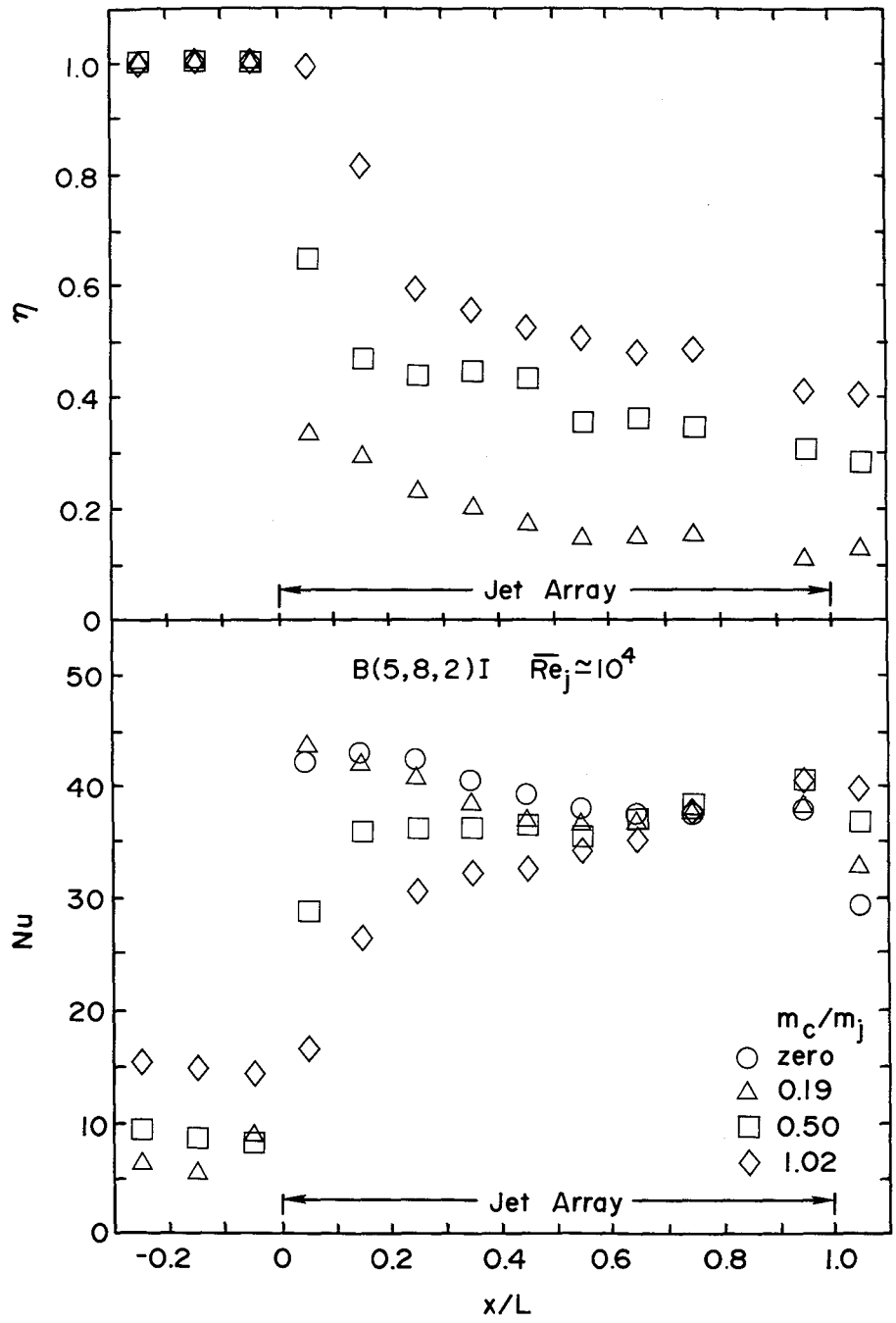

Fig. 7.4 Effect of initial crossflow rates on η and Nu profiles for B(5,8,2)I geometry.

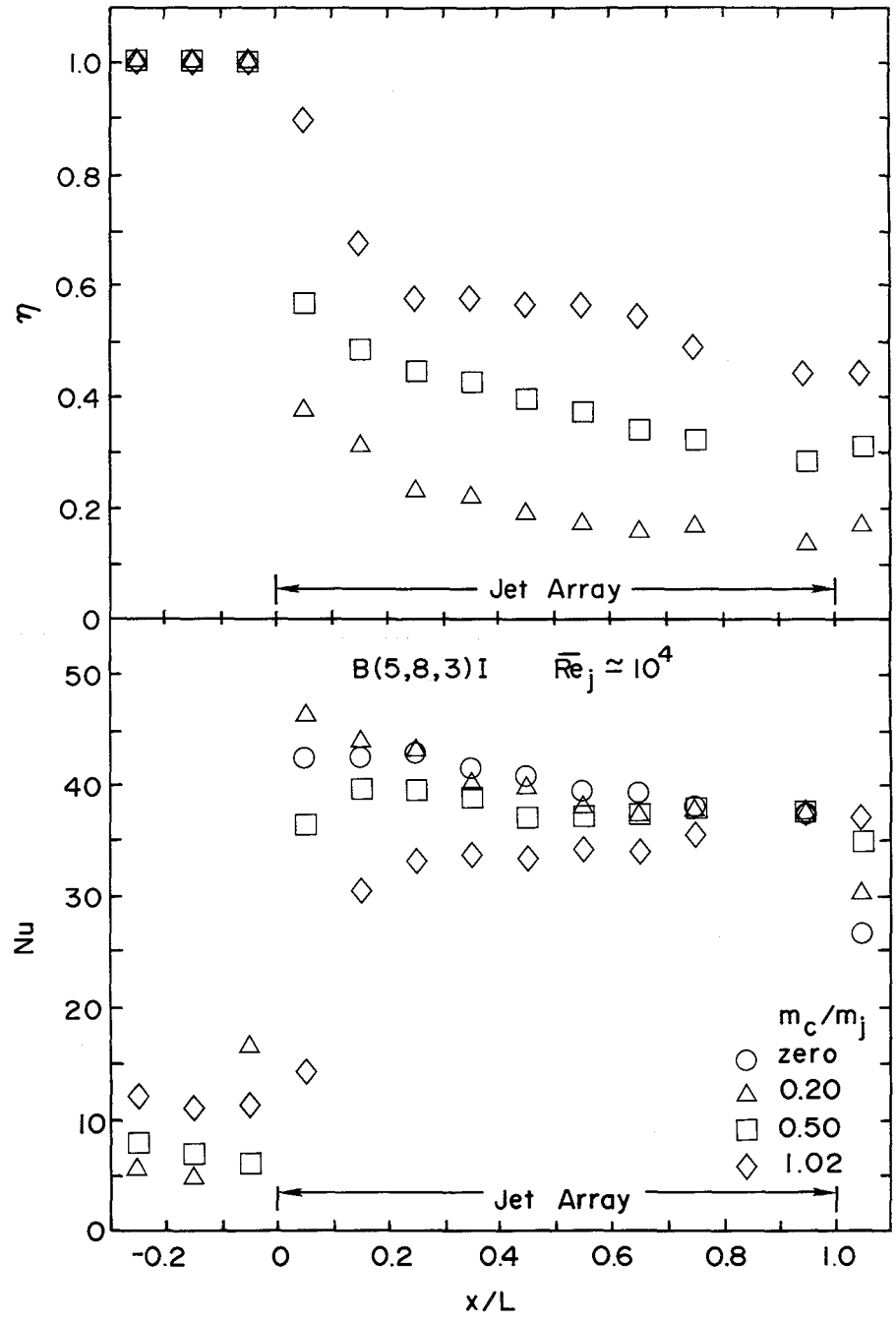

Fig. 7.5 Effect of initial crossflow rate on η and Nu profiles for B(5,8,3)I geometry.

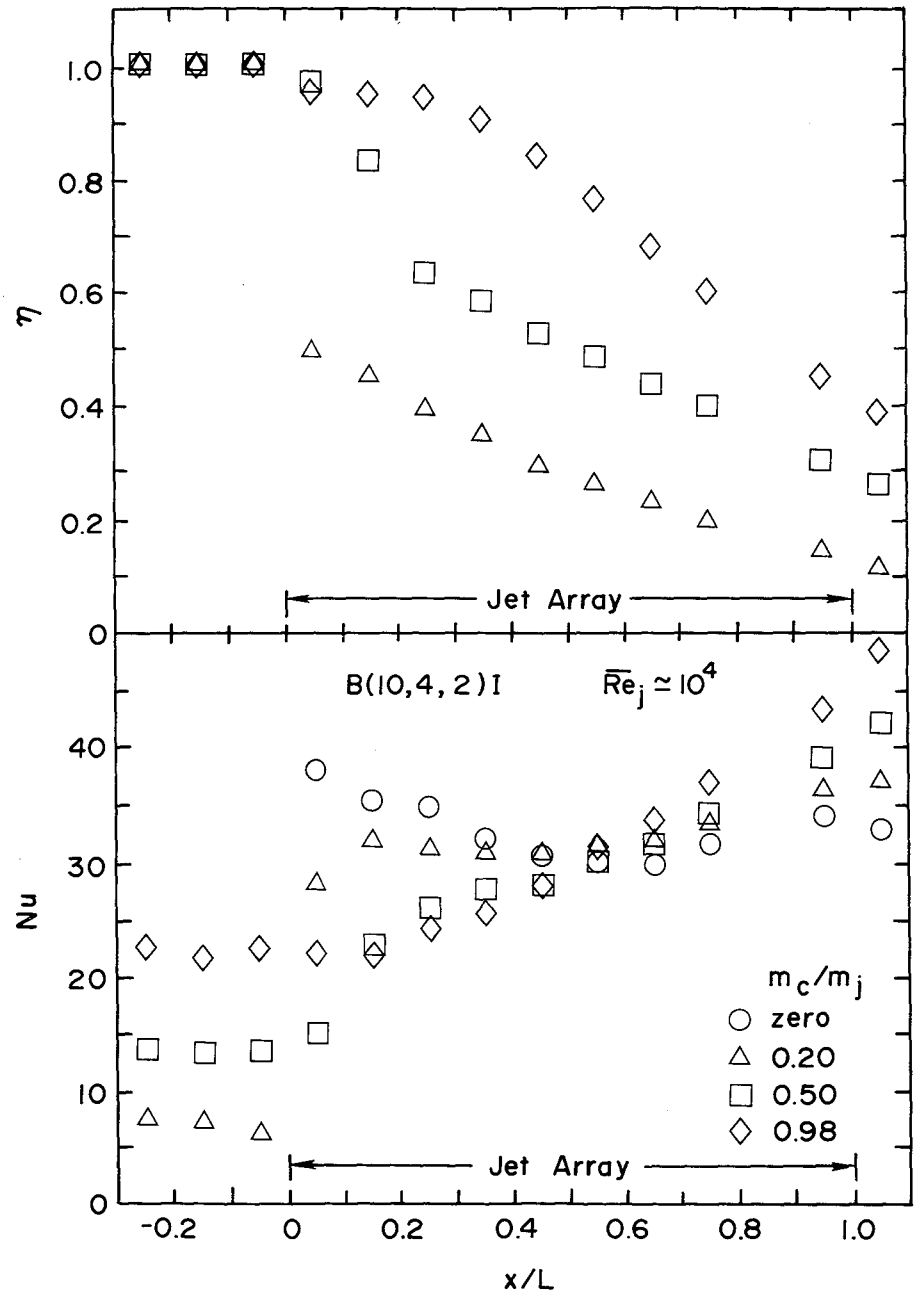

Fig. 7.6 Effect of initial crossflow rates on η and Nu profiles for B(10,4,2)I geometry.

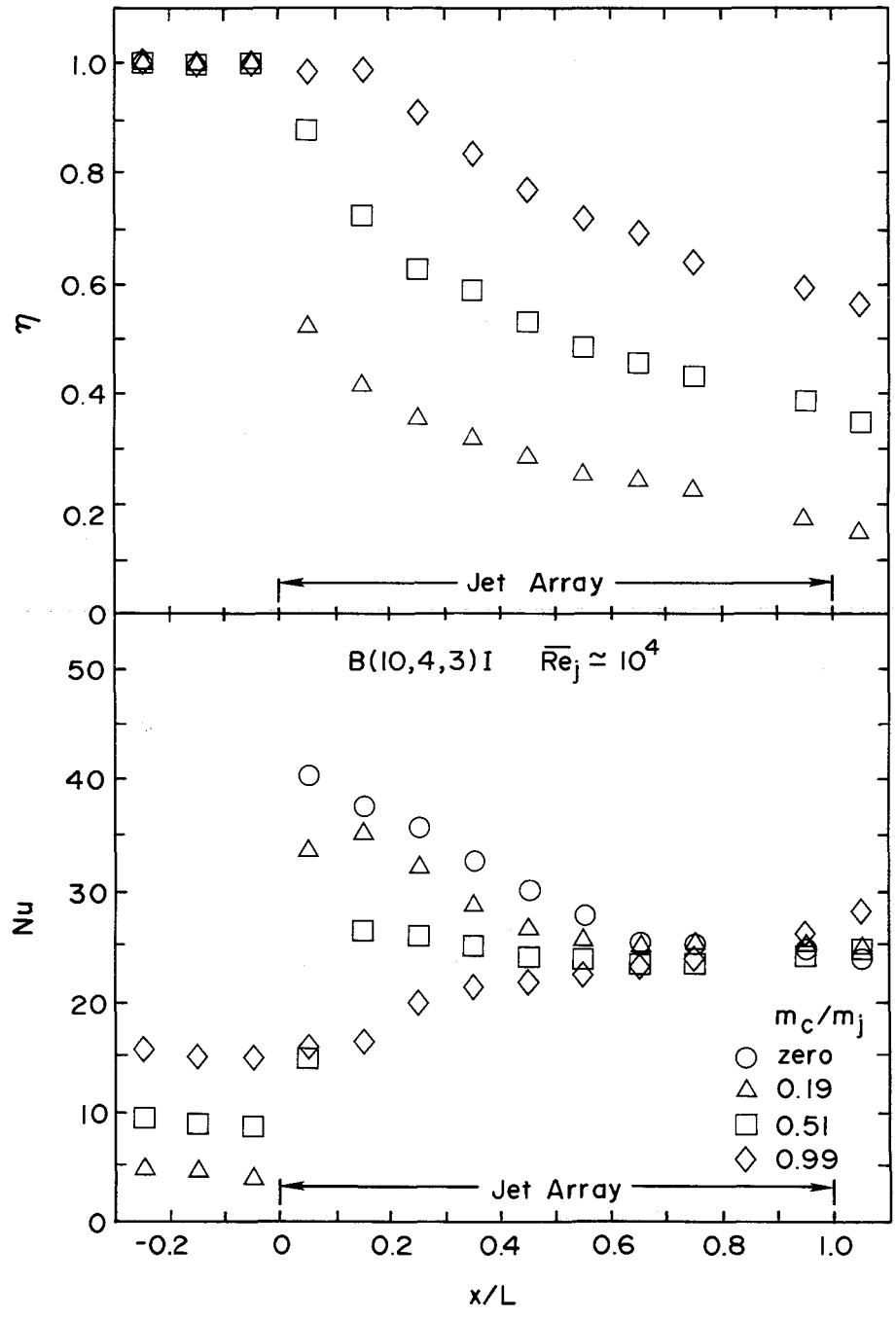

Fig. 7.7 Effect of initial crossflow rate on η and Nu profiles for B(10,4,3)I geometry.

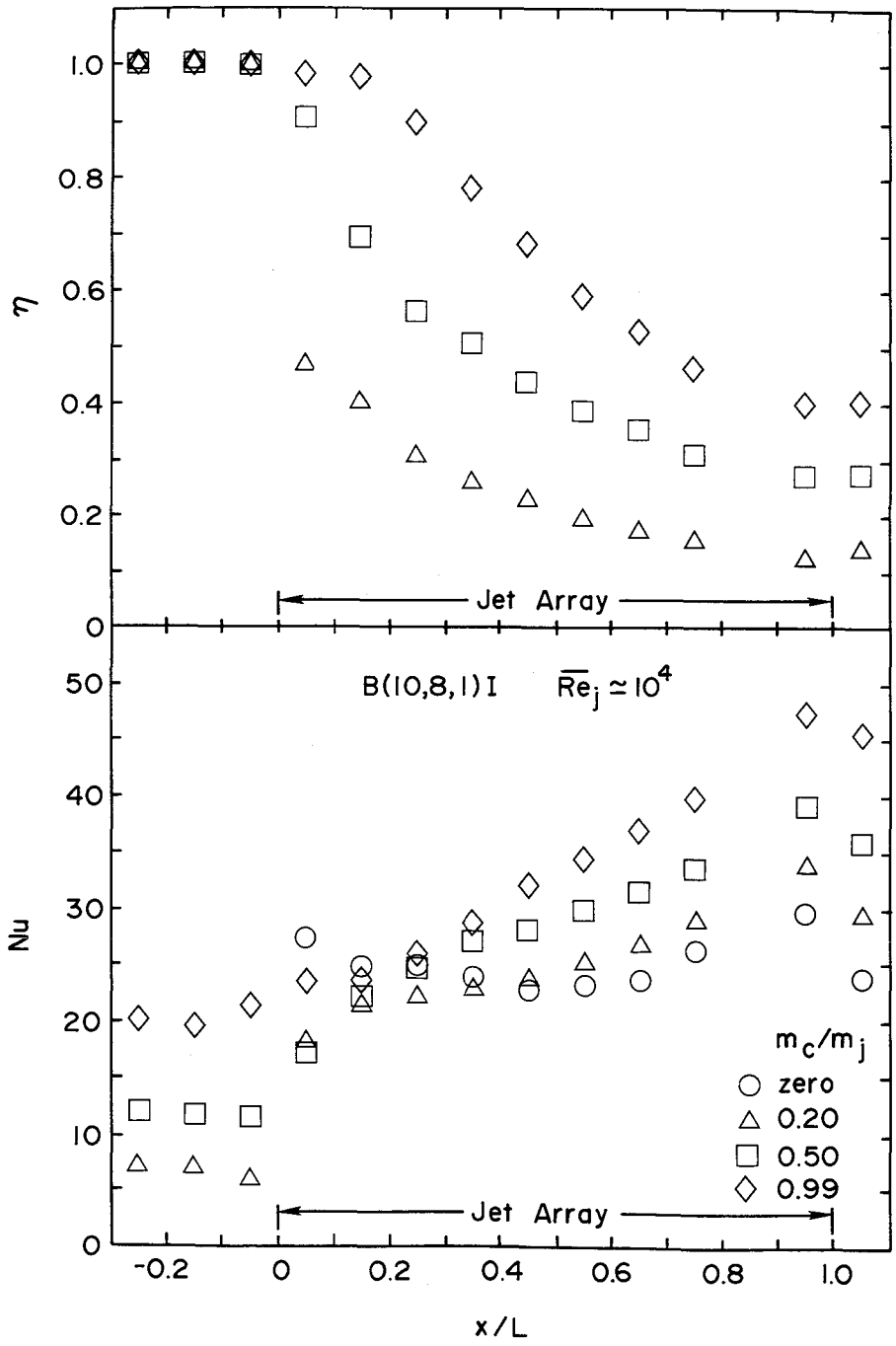

Fig. 7.8 Effect of initial crossflow rates on η and Nu profiles for B(10,8,1)I geometry.

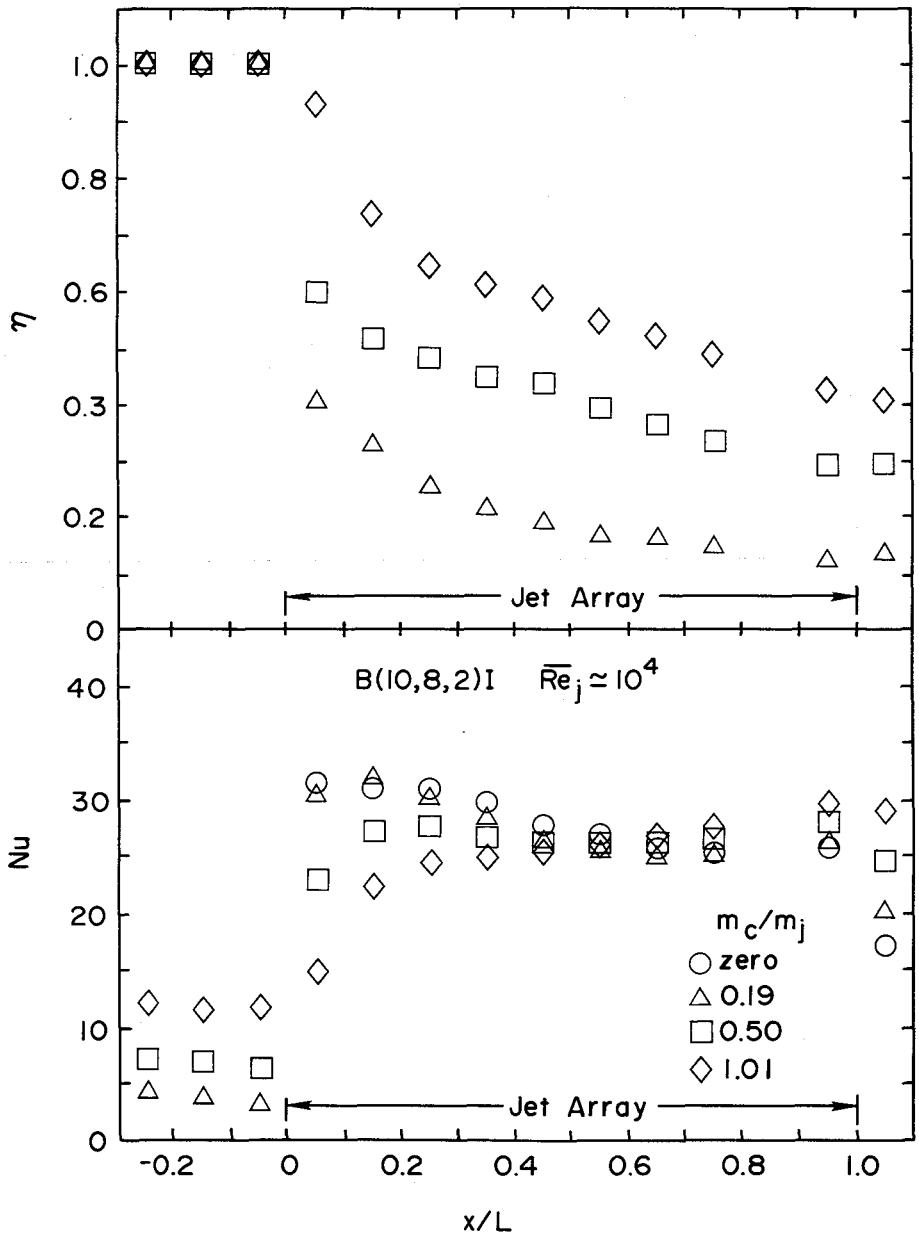

Fig. 7.9 Effect of initial crossflow rates on η and Nu profiles for B(10,8,2)I geometry.

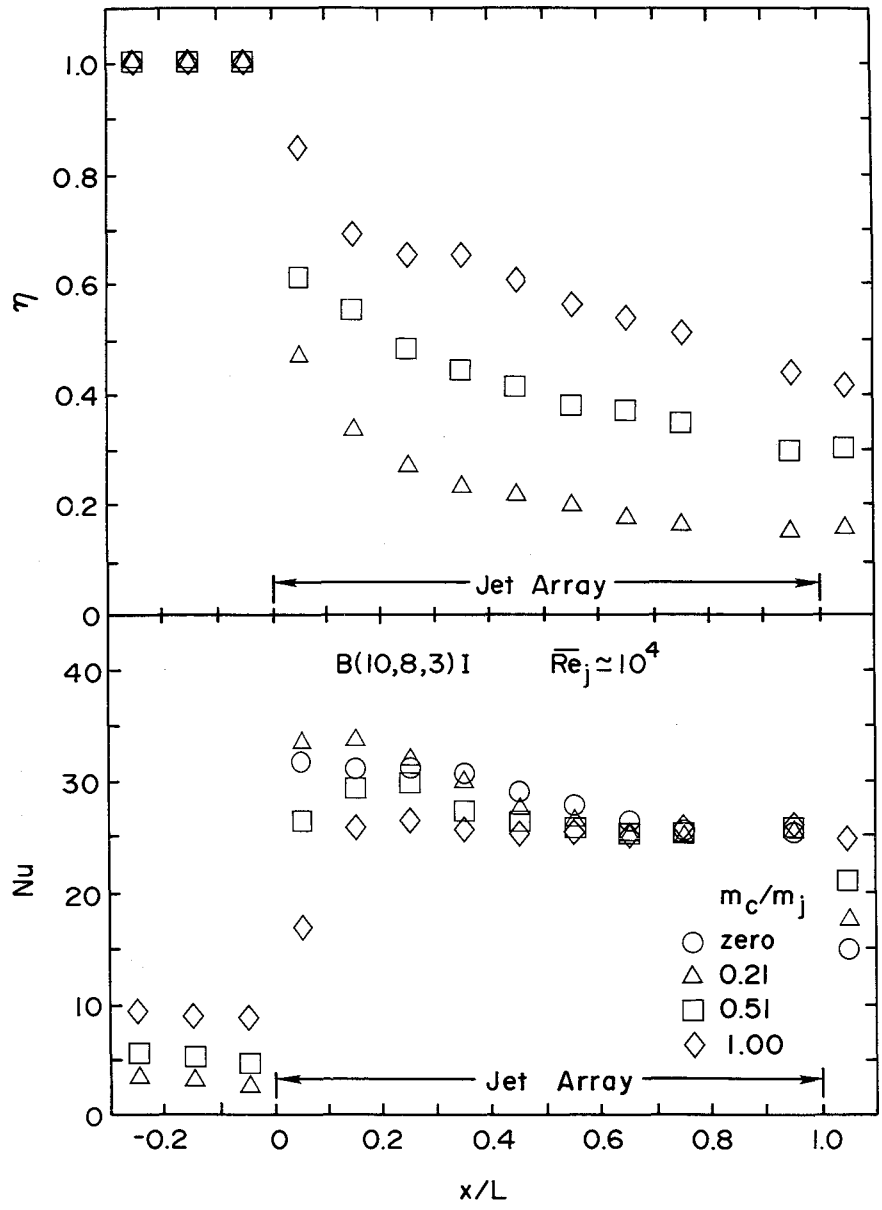

Fig. 7.10 Effect of initial crossflow rate on η and Nu profiles for B(10,8,3)I geometry.

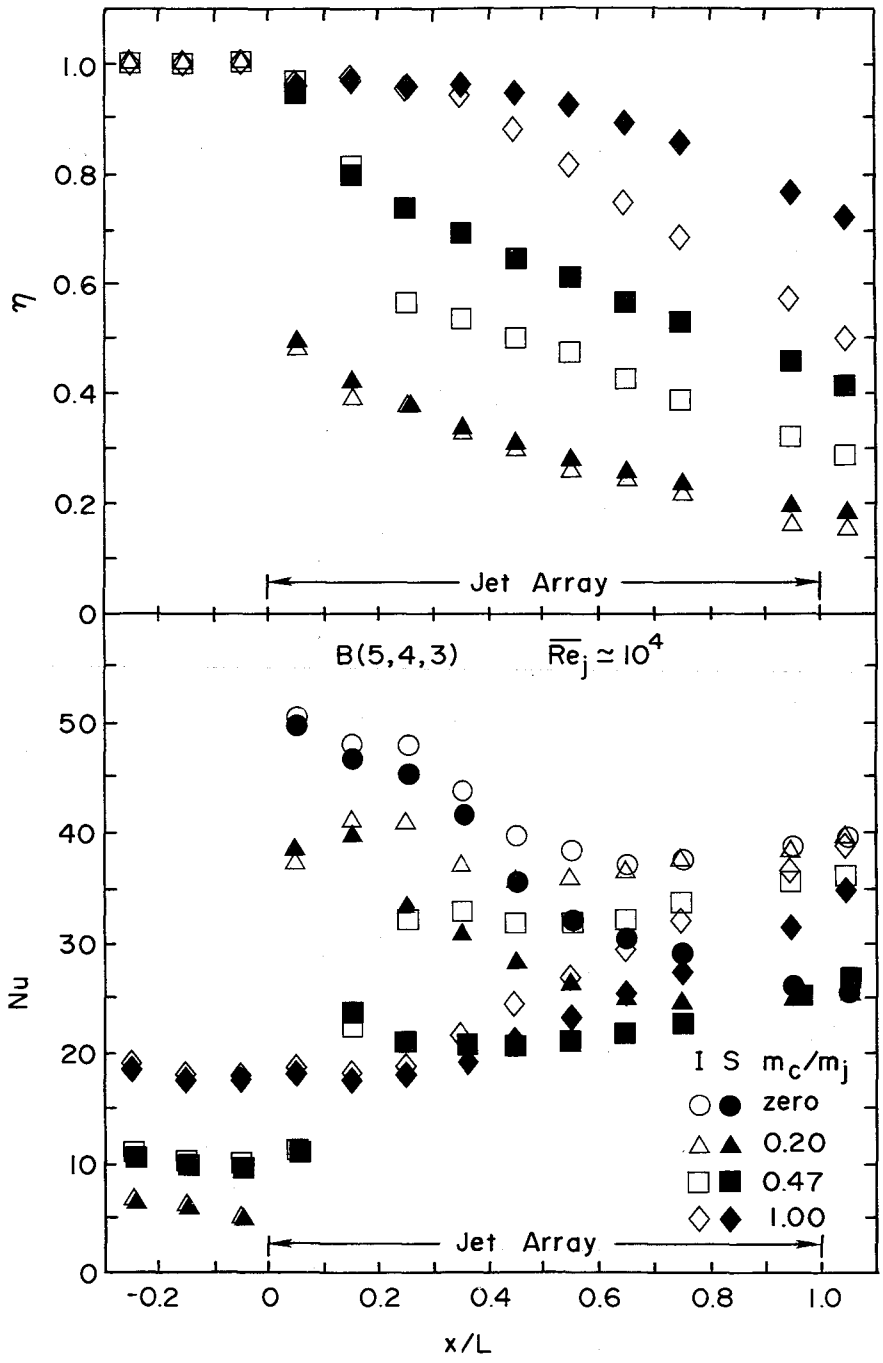

Fig. 7.11 Effect of initial crossflow rates on η and Nu profiles for B(5,4,3) geometry: I = inline pattern, S = staggered pattern.

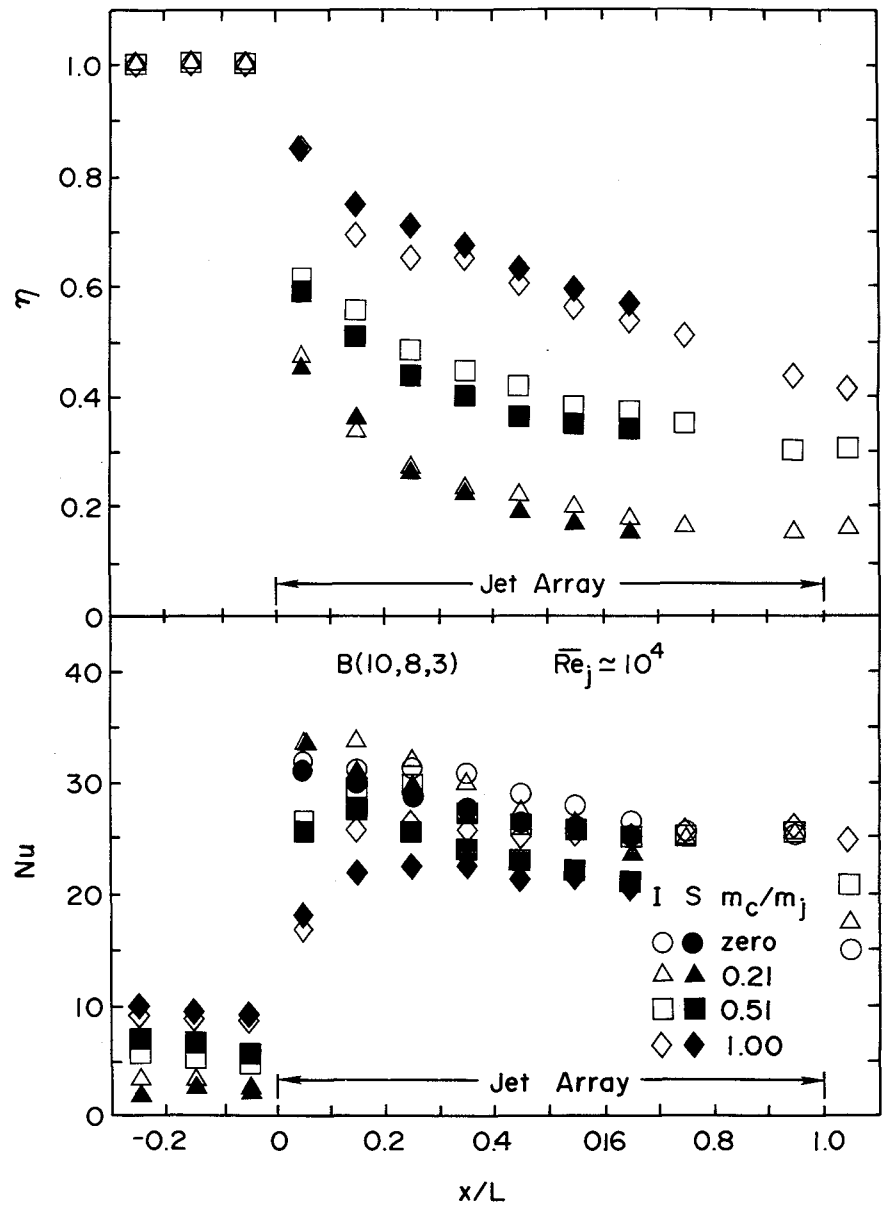

Fig. 7.12 Effect of initial crossflow rates on η and Nu profiles for B(10,8,3) geometry: I = inline pattern, S = staggered pattern.

7.2 Effect of Mean Jet Reynolds Number

The geometry B(5,4,2)I at m_c/m_j = 0.20 and the geometries B(5,8,2)I, B(5,8,3)I, and B(10,8,2)I at m_c/m_j = 0.50 were tested at nominal mean jet Reynolds numbers of 6 x 10^3, 10^4, and 2 x 10^4. The results for η and Nu are shown in Figs. 7.13 to 7.16 and also listed in Appendix B.

All of these results are for standard arrays with L/x_n = 10 (10 row arrays). however, data for only the first seven rows was obtained, because prior to these particular tests the test plate segment heater opposite row 9 developed an open circuit (burned out) and because of the design of the test plate could not be replaced or repaired. Hence the segment opposite row 8 had to be used as the downstream guard heater, permitting the acquisition of useful data only through row 7. This information was entirely adequate to check the dependence of η and Nu on $\overline{Re}_j$. The Nu values were normalized by $\overline{Re}^{0.73}$ for direct comparison. The exponent on $\overline{Re}_j$ is from the previous noninitial crossflow jet array impingement correlation reported by Florschuetz, et al. (1981a, 1981b). Considering experimental uncertainty, the η values appear to be relatively insensitive to $\overline{Re}_j$, while the Reynolds number dependence of $\overline{Re}_j^{0.73}$ accounts quite well for the Nusselt number variation. The composite uncertainties for $Nu/\overline{Re}_j^{0.73}$ indicated in Figs. 7.13 through 7.16 were calculated based on an uncertainty in $\overline{Re}_j$ of ± 3%.

7.3 Effect of Array Length (Number of Spanwise Rows).

The governing independent parameters for Nu and η are the geometric parameters (x/L, x_n/d, y_n/d, z_n/d, L/x_n) and hole pattern, the flow parameters ($\overline{Re}_j$, m_c/m_j) and the normalized velocity and temperature profiles at the array entrance (Sections 2.1 and 3.3). For the arrays in the present study the standard array length N_c(= L/x_n) was ten spanwise rows of holes. Consider now a domain extending over the first N upstream rows of a standard array (i.e., N < N_c). The results for η and Nu over these first N rows should be applicable to an overall array with a total of N rows having the same (x_n/d, y_n/d, z_n/d)

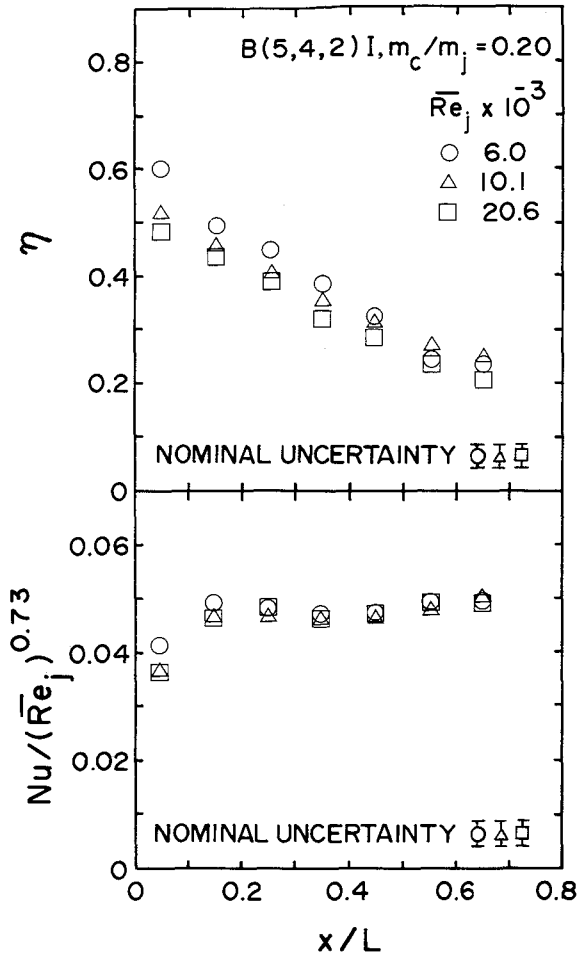

Fig. 7.13 Effect of mean jet Reynolds number on η and Nu for B(5,4,2)I geometry.

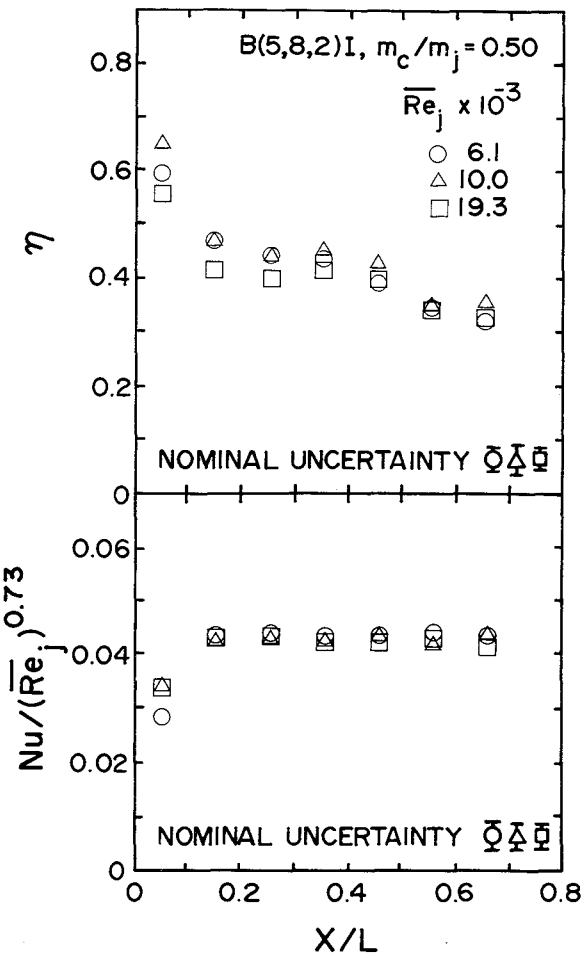

Fig. 7.14 Effect of mean jet Reynolds number on η and Nu for B(5,8,2)I geometry.

and hole pattern, but only for the appropriate $\overline{Re}_j$ and m_c/m_j evaluated for the first N rows of the standard array. To verify this assumption the B(5,4,2)I geometry was selected for a special test. For the B(5,4,2)I standard 10 row array test which had $\overline{Re}_j = 9.8 \times 10^3$ and $m_c/m_j = 0.54$ for the overall array, the values considering the domain of the first five rows were calculated as $\overline{Re}_{j,5} = 6.8 \times 10^3$ and $(m_c/m_j)_{,5} = 1.56$. These values were calculated using the measured flow distribution results [Florschuetz and Isoda (1983)]. The standard 10 row array was converted to a five row array by plugging five rows of holes. A heat transfer test was then conducted with the five row array at the above stated conditions; the actual conditions achieved were $\overline{Re}_{j,5} = 6.9$

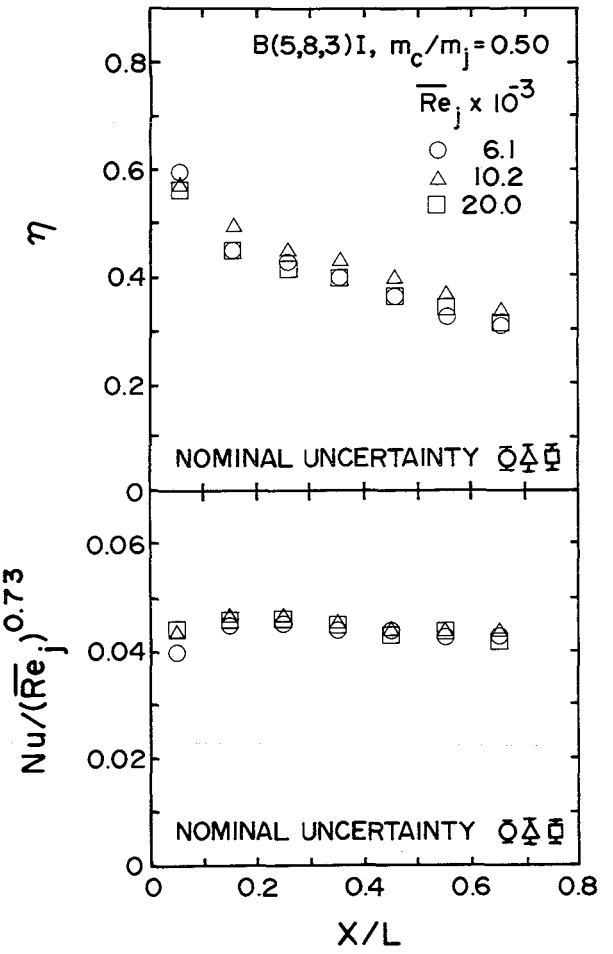

Fig. 7.15 Effect of mean jet Reynolds number on η and Nu for B(5,8,3)I geometry.

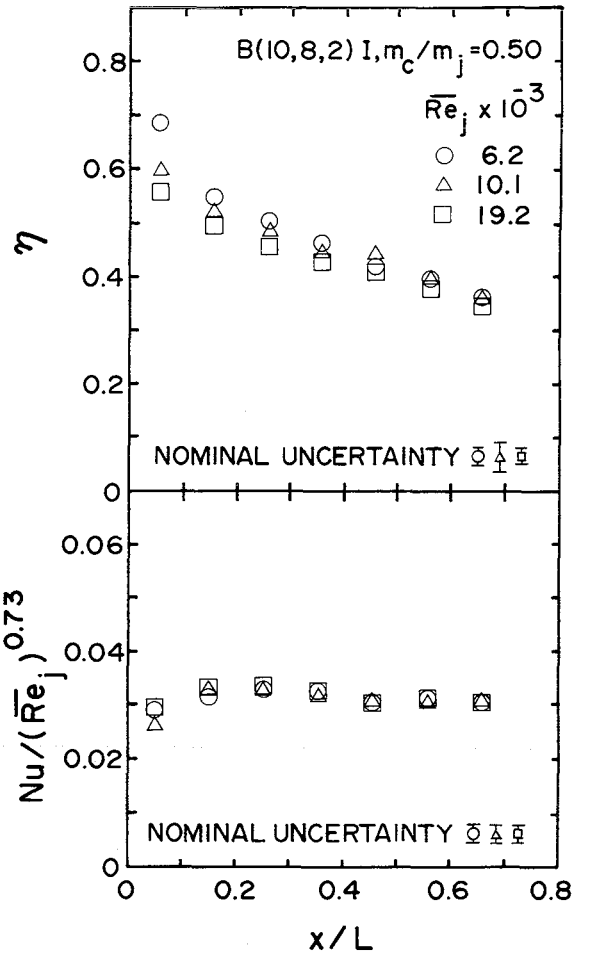

Fig. 7.16 Effect of mean jet Reynolds number on η and Nu for B(10,8,2)I geometry.

$\times 10^3$ and $(m_c/m_j)_{,5} = 1.51$. The measured heat transfer parameters η and Nu for the five row overall array length are compared with those for the first five rows of the standard 10 row overall array length in Fig. 7.17. For both η and Nu the values are consistent to within experimental uncertainty.

Relying on the confidence engendered by the above verification test, values of $\overline{Re}_{j,N}$ and $(m_c/m_j)_{,N}$ have been calculated and included with the tabular results in Appendix B.

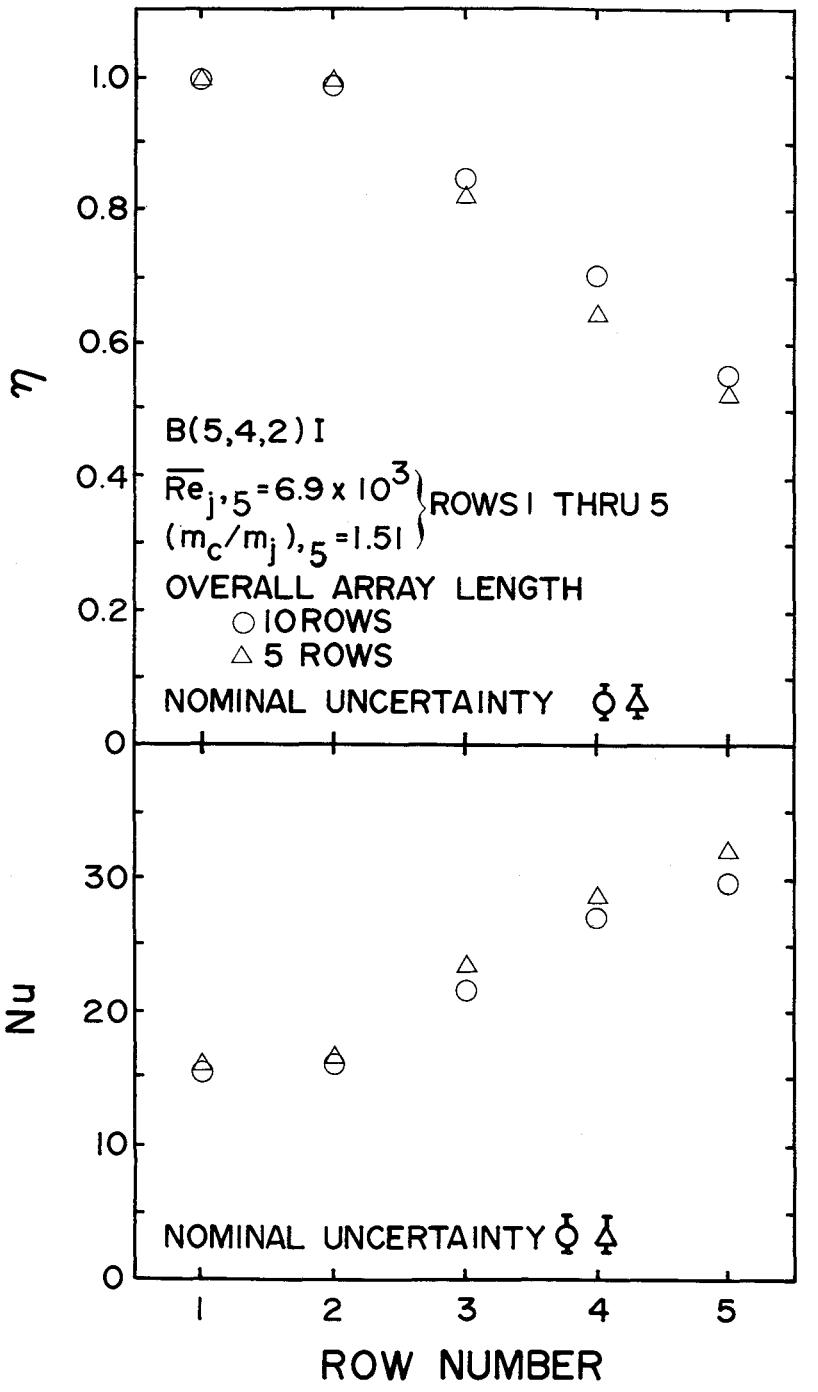

Fig. 7.17 Comparisons of η and Nu for different overall array lengths.

7.4 Array Mean Heat Transfer

In this section the average heat transfer coefficient over each of the standard 10 row arrays tested is examined relative to the total air flow rate utilized per unit heat transfer surface area. The quantity of interest therefore is $\bar{h}/[(m_c+m_j)/(WL)]$. For a given fluid (specific heat) this quantity is proportional to a Stanton number defined by

$$\overline{St}^* = \bar{h}/[c_p(m_c+m_j)/(WL)]$$

The quantity $(m_c+m_j)/(WL)$ is a superficial mass flux representing the total flow rate per unit of impingement heat transfer surface area.

$\overline{St}^*$ was calculated for each of the eleven geometries for which data was obtained at the impingement surface opposite 10 rows of the array (see Figs. 7.1 to 7.11). It was first calculated under the condition that the total jet flow to the array (m_j) was held constant while the initial crossflow rate (m_c) was increased from zero to a nominal value of m_c equal to the value of m_j (the total flow rate thus increases). The largest value of $\overline{St}^*$ obtained was for the (10,8,3)I geometry for $m_c = 0$. Values of $\overline{St}^*$ normalized by the largest value (relative $\overline{St}^*$) are plotted as a function of m_c/m_j in Fig. 7.18 for the eleven geometries.

$\overline{St}^*$ values were then also calculated under the condition that the total flow rate (m_c+m_j) remained constant; therefore, as the initial crossflow was increased the jet flow was correspondingly decreased. These values of relative $\overline{St}^*$ are shown as a function of m_c/m_j in Fig. 7.19 for the same eleven geometries.

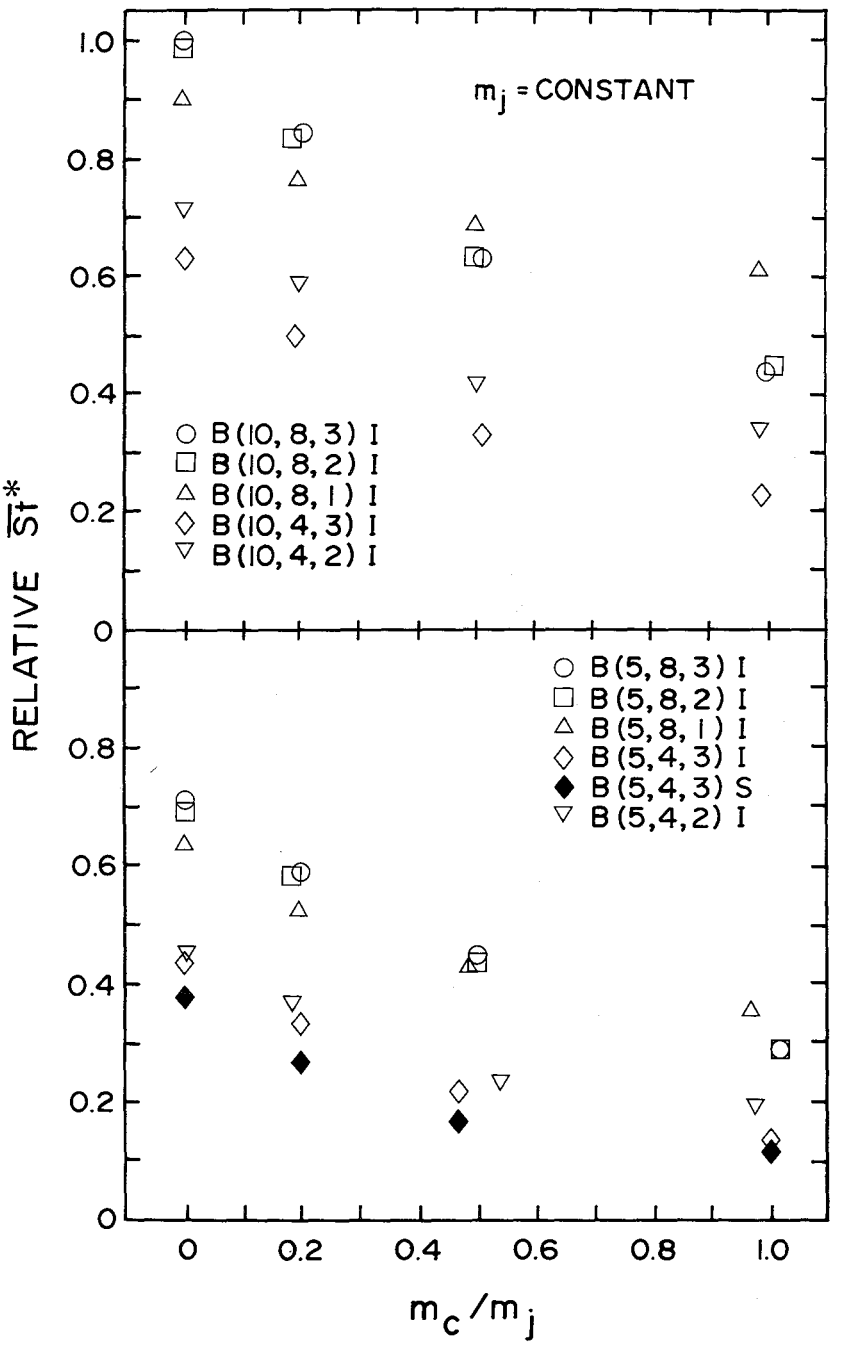

Fig. 7.18 Effect of initial crossflow rate on overall array heat rate per unit temperature difference per unit total flow rate (m_c+m_j) for constant total jet flow rate (m_j).

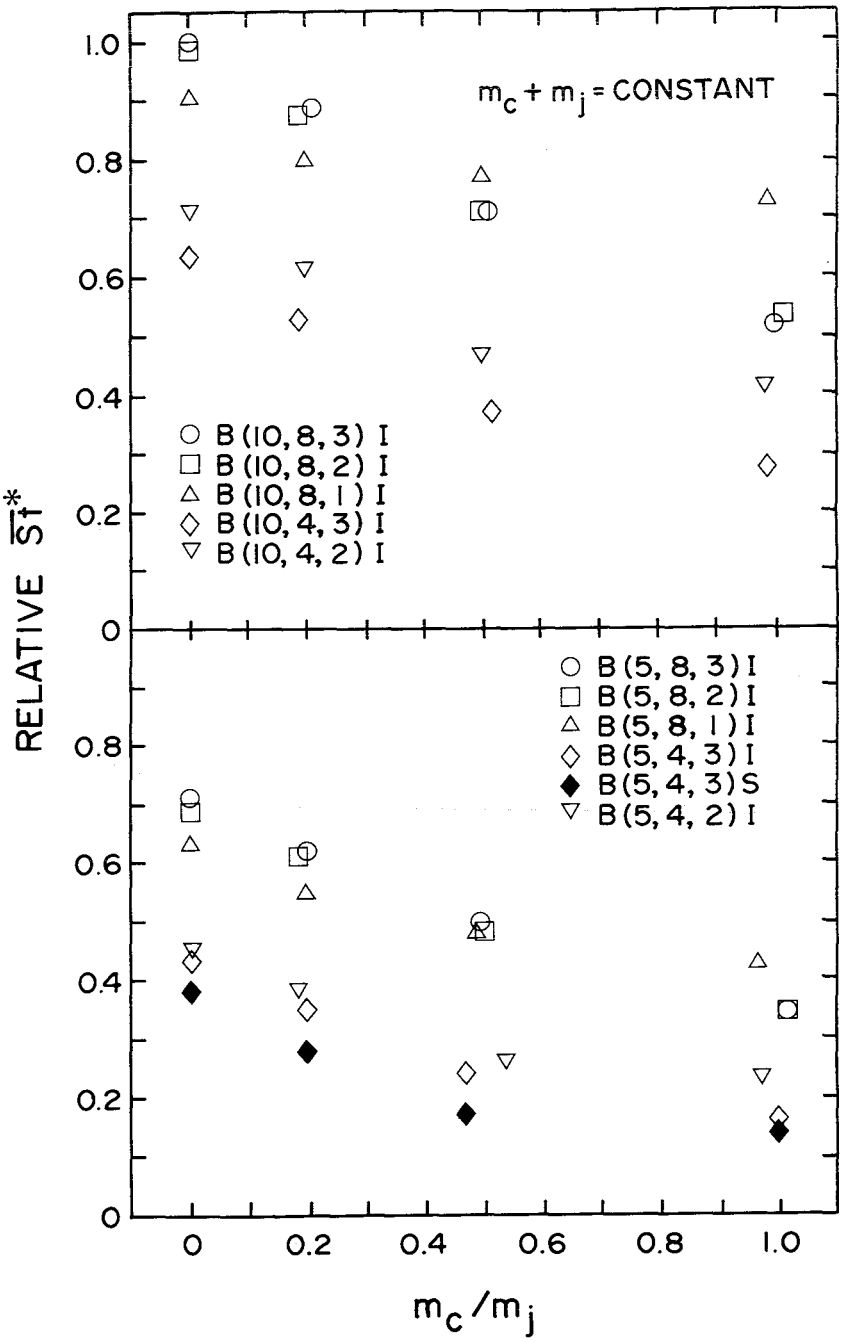

Fig. 7.19 Effect of ratio of initial crossflow rate-to-total jet flow rate (m_c/m_j) on overall array heat rate per unit temperature difference per unit total flow rate (m_c+m_j) for constant total flow rate.

8. RECOVERY EFFECTS

8.1 Recovery Effects in Data Reduction

The equal temperature heat flux, ε, appearing in Eq. (2.1) is associated with recovery effects. The effect of neglecting ε in the determination of η and Nu is larger for the (10,8,1)I geometry than for any other geometry tested. Because of the narrow channel height of one hole diameter for this geometry, the jet flow distribution is highly nonuniform (Fig. 6.2). Even for the smallest m_c/m_j of 0.2 the jet mass flux at the last (downstream) row is about twice the value at the first (upstream) row, while for the largest initial crossflow tested, m_c/m_j of unity, this factor is about seven. Even for this case with large downstream jet and crossflow velocities, the effect on Nu of including ε (open data symbols, denoted ω/ε in Fig. 8.1) versus neglecting ε (symbols with center point, denoted $\omega/o\ \varepsilon$) in the data reduction via Eq. (2.1) is within experimental uncertainty. The effect on η becomes increasingly noticeable downstream, the maximum difference being about 0.18. For a specified heat flux, jet temperature, and initial crossflow temperature the corresponding change in magnitude of the calculated surface temperature would be 18% of the initial crossflow-to-jet temperature difference. This may or may not be significant depending on the particular design application.

The same type of comparison is shown in Fig. 8.2 at the same mean jet Reynolds number for a jet array geometry, (5,8,3)I, for which the jet flow distribution remains approximately uniform even at the largest initial crossflow rate (Fig. 6.1). In this case the effect on both Nu and η of retaining versus neglecting ε is not significant. This was typical for most of the initial crossflow test cases.

Now consider the heat transfer parameters Nu_r and η_r defined for the domain of an individual spanwise row. These parameters are shown plotted as a function of G_c/G_j in Figs. 8.3 and 8.4 for the same two jet array geometries discussed above. The comparisons shown in Fig. 8.3 for the (10,8,1)I jet array show that the effect of neglecting ε_r in data reduction based on Eq. (2.5) has little effect on Nu_r, but the effect on η_r for this extreme case is

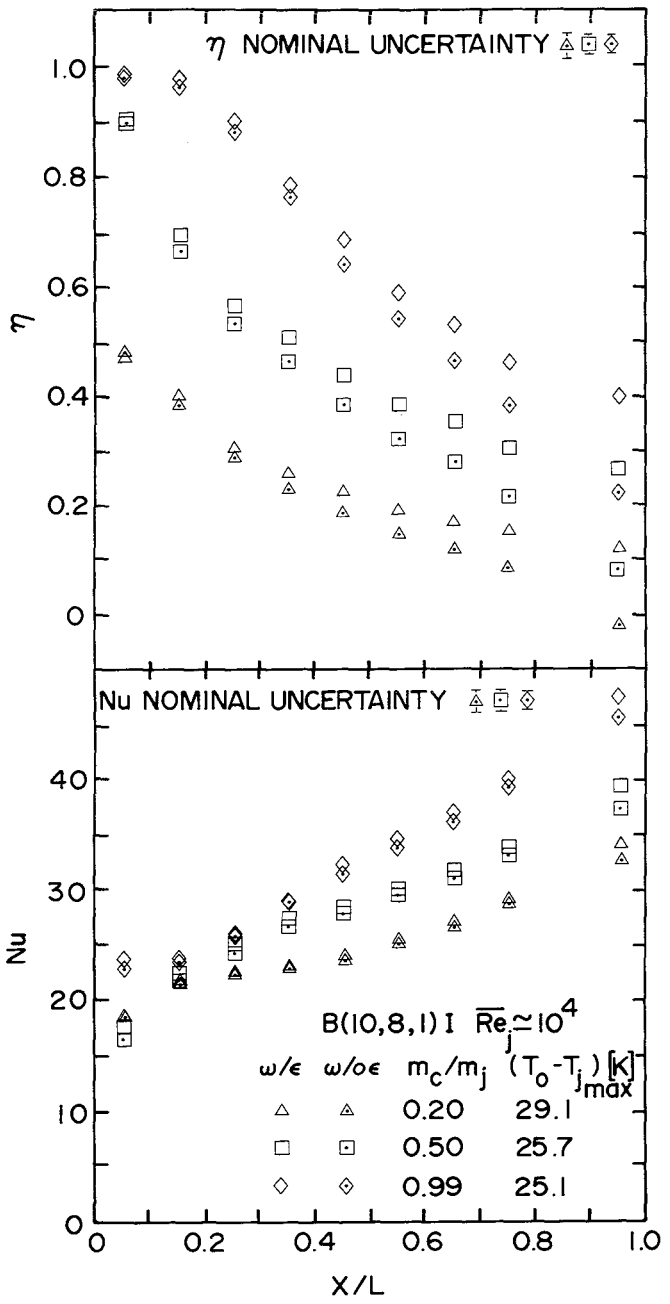

Fig. 8.1 Effect of the term ε associated with recovery effects on evaluation of η and Nu via Eq. (2.1) for B(10,8,1)I geometry.

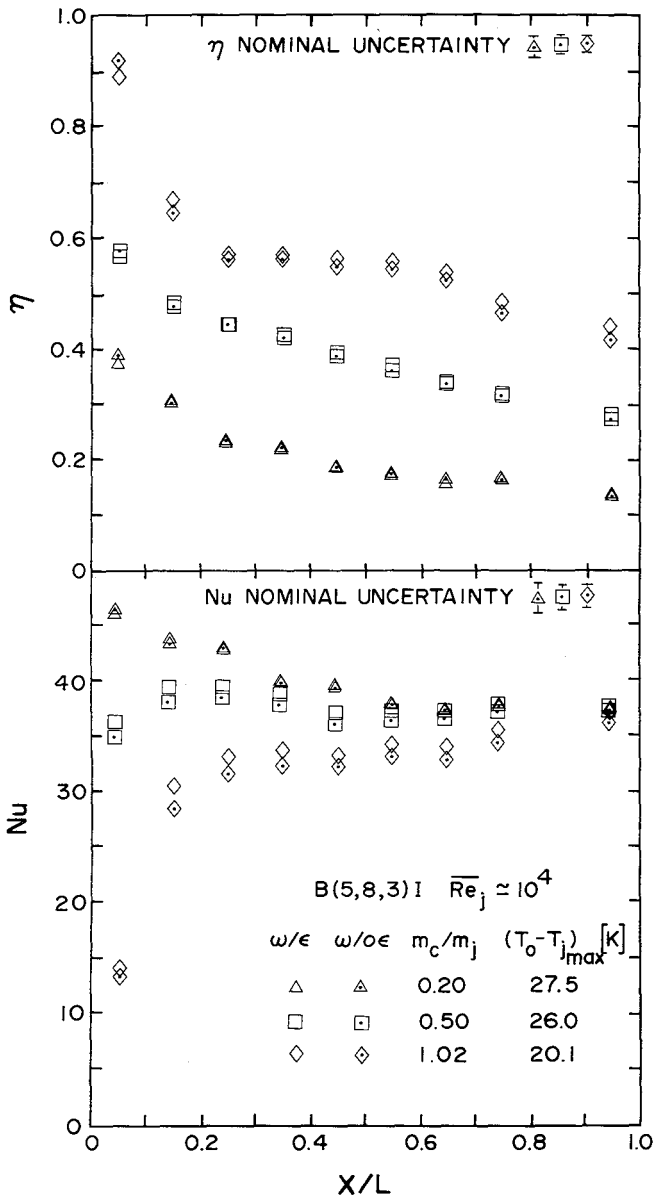

Fig. 8.2 Effect of the term ε associated with recovery effects on evaluation of η and Nu via Eq. (2.1) for B(5,8,3)I geometry.

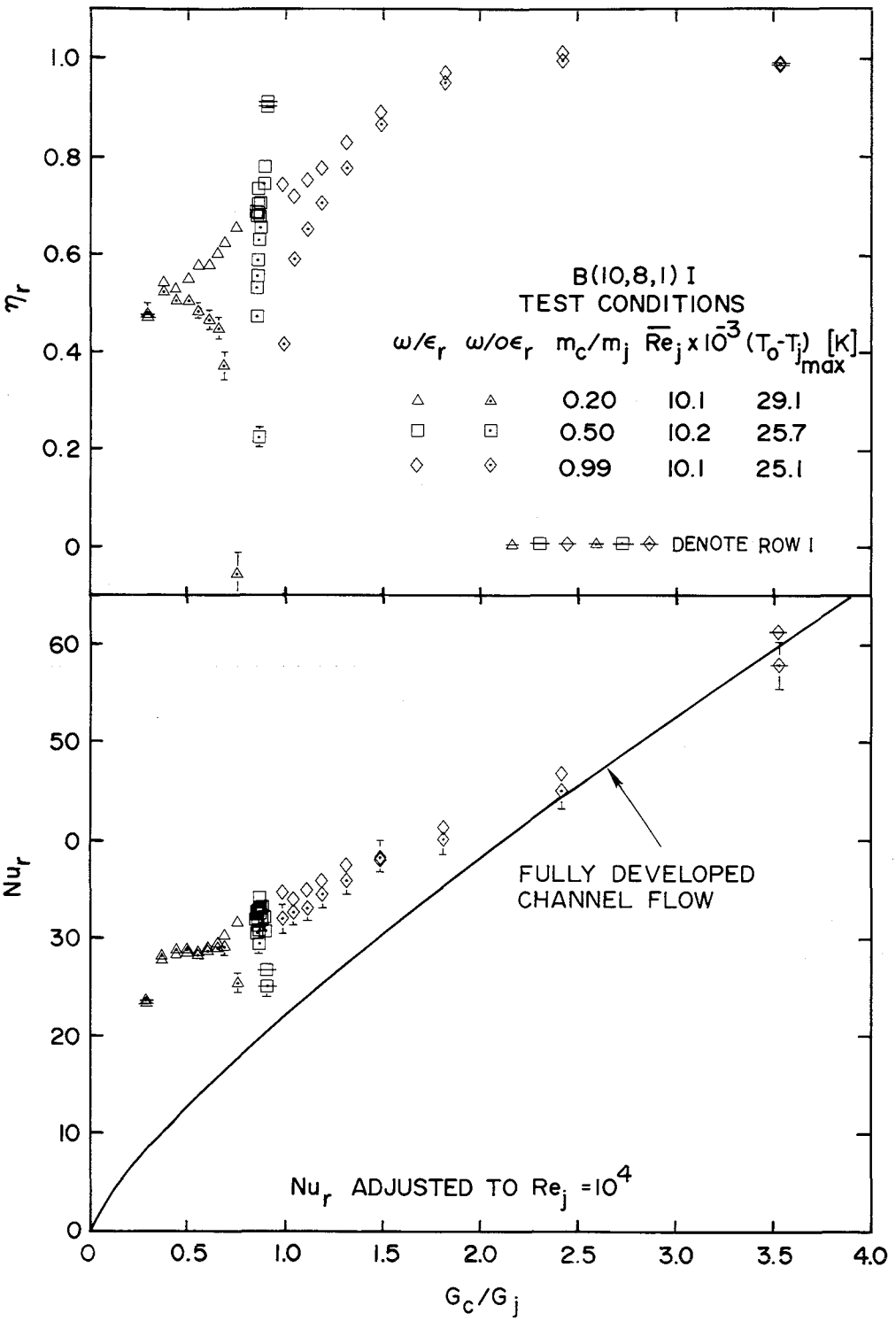

Fig. 8.3 Effect of the term ε_r associated with recovery effects on evaluation of η_r and Nu_r via Eq. (2.5) for B(10,8,1)I geometry.

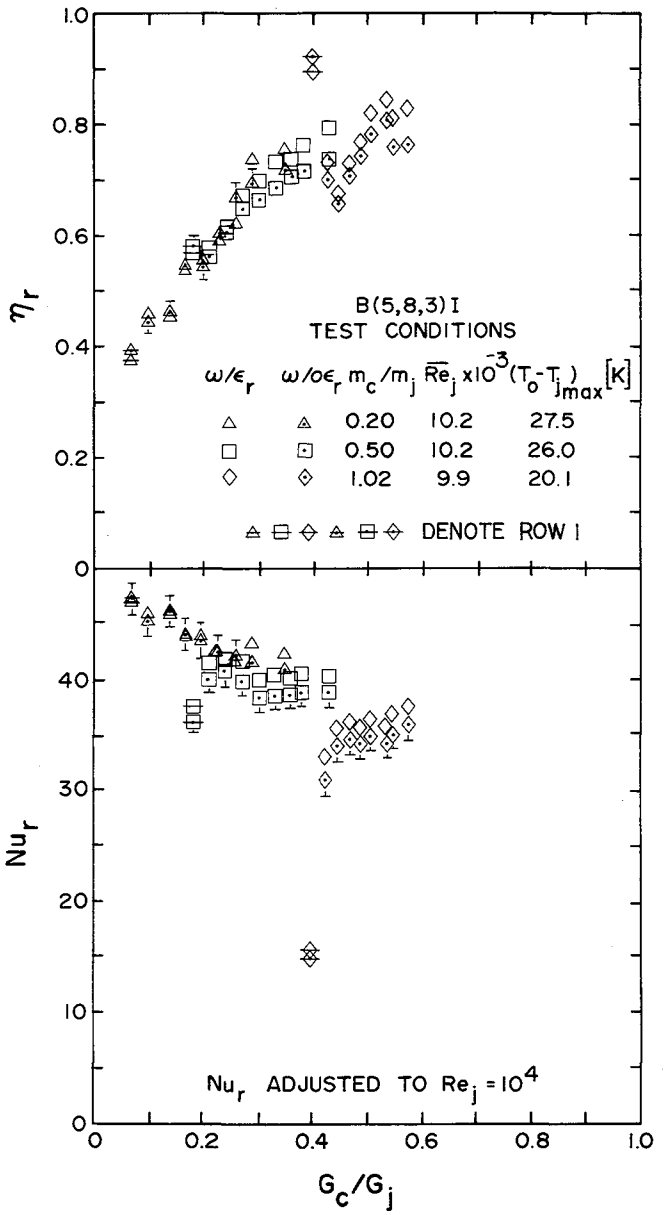

Fig. 8.4 Effect of the term ϵ_r associated with recovery effects on evaluation of η_r and Nu_r via Eq. (2.5) for B(5,8,3)I geometry.

quite significant. The η_r values reduced neglecting ε_r (those with center point shown) indicate a behavior as a function of G_c/G_j that appears quite irregular. However, when ε_r is retained the η_r values (the open points) form a pattern through which a monotonic curve could reasonably be drawn which could be extrapolated to zero as G_c/G_j goes to zero and asymptotically approaches one as G_c/G_j goes to infinity. An exception is the point from the $m_c/m_j = 0.50$ case (the square points) at the first row of the array. This exception may be attributed to the flow history effects already noted in Section 6.2 and discussed in Section 6.3. For the (5,8,3)I jet array the results in terms of individual row parameters shown in Fig. 8.4 show little effect on either η_r or Nu_r of the neglect of ε_r.

It is emphasized that even though under certain conditions neglecting to properly account for recovery effects does not significantly alter the evaluation of Nusselt numbers (Nu and Nu_r) there may still be significant effects in the evaluation of η and η_r. This is clearly the case for the (10,8,1)I jet array (Figs. 8.1 and 8.3). Also, as has already been pointed out, the effects on η and η_r increase in the downstream direction. These observations may be explained by examining Eq. (2.5) rewritten in the form

$$\bar{q} = (k/d)\, Nu_r[(T_s - T_j) - \eta_r(T_{m,n} - T_j) + \varepsilon_r/h_r]$$

If the third term in the square brackets, ε_r/h_r, is relatively small compared with the first term, $(T_s - T_j)$, but not small compared with the second term, $\eta_r (T_{m,n} - T_j)$, then the neglect of ε_r will not affect the evaluation of Nu_r but will affect the evaluation of η_r. For an isothermal impingement surface with jet air from a single plenum, as in the present tests, $(T_s - T_j)$ is essentially uniform along the array, while $(T_{m,n} - T_j)$ decreases (see Figs. 6.3 and 6.4) and velocities increase downstream. For the (10,8,1)I jet array and to a lesser extent some other geometries with small channel heights and/or small spanwise hole spacings, velocities became high enough and temperature differences $(T_{m,n} - T_j)$ small enough at downstream locations such that the above conditions were satisfied.

8.2 Recovery Factors

Results for the recovery factor r_r defined by Eq. (2.6) and calculated here via Eq. (2.7) are displayed as a function of individual row Reynolds number Re_j in Figs. 8.5 to 8.8. These results indicate that r_r is essentially independent of Re_j, except in some cases for row 1 at the smaller Re_j.

Based on the above conclusion, the effect of G_c/G_j on r_r could be examined without regard to Re_j. Values of r_r as a function of G_c/G_j are plotted in Figs. 8.9 to 8.20 for all of the array geometries tested. Consider the (5,8,3)I array results (Fig. 8.13) which are representative of those for the array geometries having the more nearly uniform flow distributions for which the maximum value reached by G_c/G_j was less than unity. The value of r_r, considering experimental uncertainties, appears to fall at or near unity, with the exception of row 1. For this geometry the value of G_c/G_j does not exceed 0.6. A regional average value of unity seems quite reasonable for a row of jets within an array subject to a relatively small crossflow velocity.

At row 1 values larger than unity are obtained, but it appears that a curve drawn through these points would extrapolate to unity as G_c/G_j goes to zero. Since the recovery factor is defined in terms of a recovery temperature for equal mixed-mean total temperatures of the two fluid streams, the static temperature of the crossflow will be larger than that of the jet flow for G_c/G_j less than unity. With these two fluid streams mixing as they interact with the surface it is possible that the recovery temperature could achieve a value greater than the total temperature of the jet flow. Local recovery factors greater than unity for a single jet in a crossflow were reported by Sparrow et al. (1975) who suggested a similar explanation.

A single jet in a crossflow or jets in the first row of an array with an initial crossflow both have spanwise uniform crossflow streams approaching. Rows within an array, i.e., rows downstream of the first row, even when subject to a crossflow at the same mixed-mean total temperature as the jet flow, tend to mix most directly with the crossflow originating from the immediately upstream jet rows. This may explain why the recovery factors for downstream rows within an array sometimes differ from the values at the first

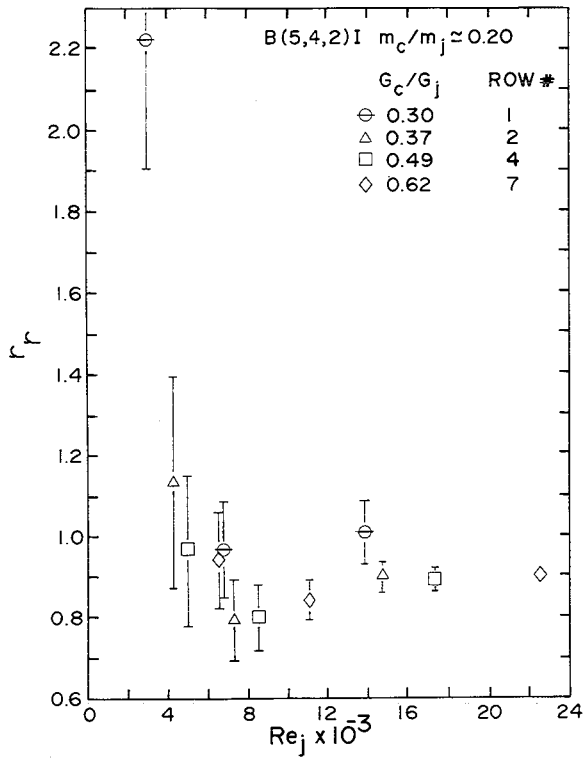

Fig. 8.5 Effect of jet Reynolds number on r_r for B(5,4,2)I geometry.

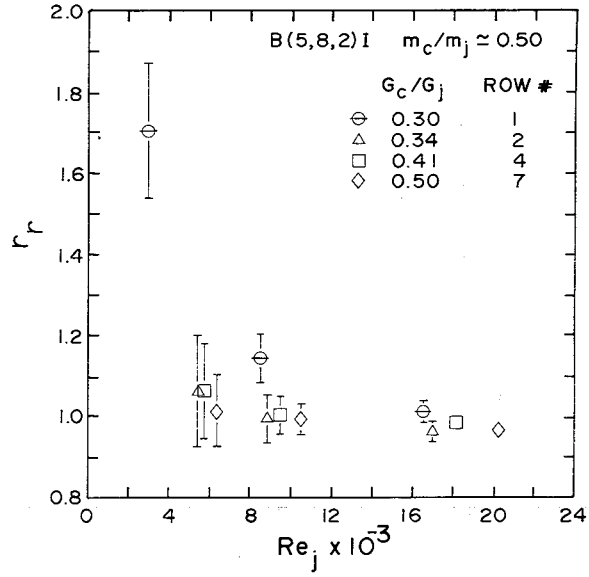

Fig. 8.6 Effect of jet Reynolds number on r_r for B(5,8,2)I geometry.

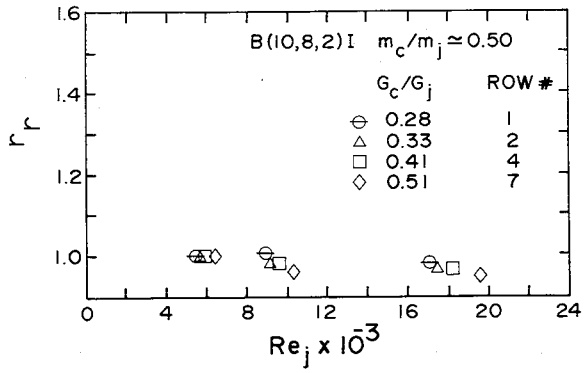

Fig. 8.7 Effect of jet Reynolds number on r_r for B(10,8,2)I geometry.

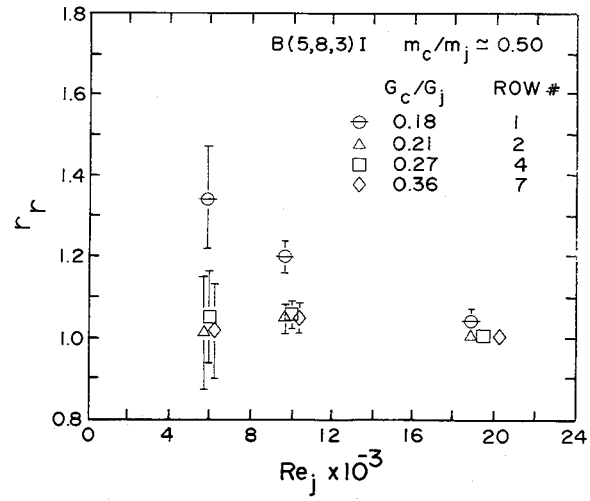

Fig. 8.8 Effect of jet Reynolds number on r_r for B(5,8,3)I geometry.

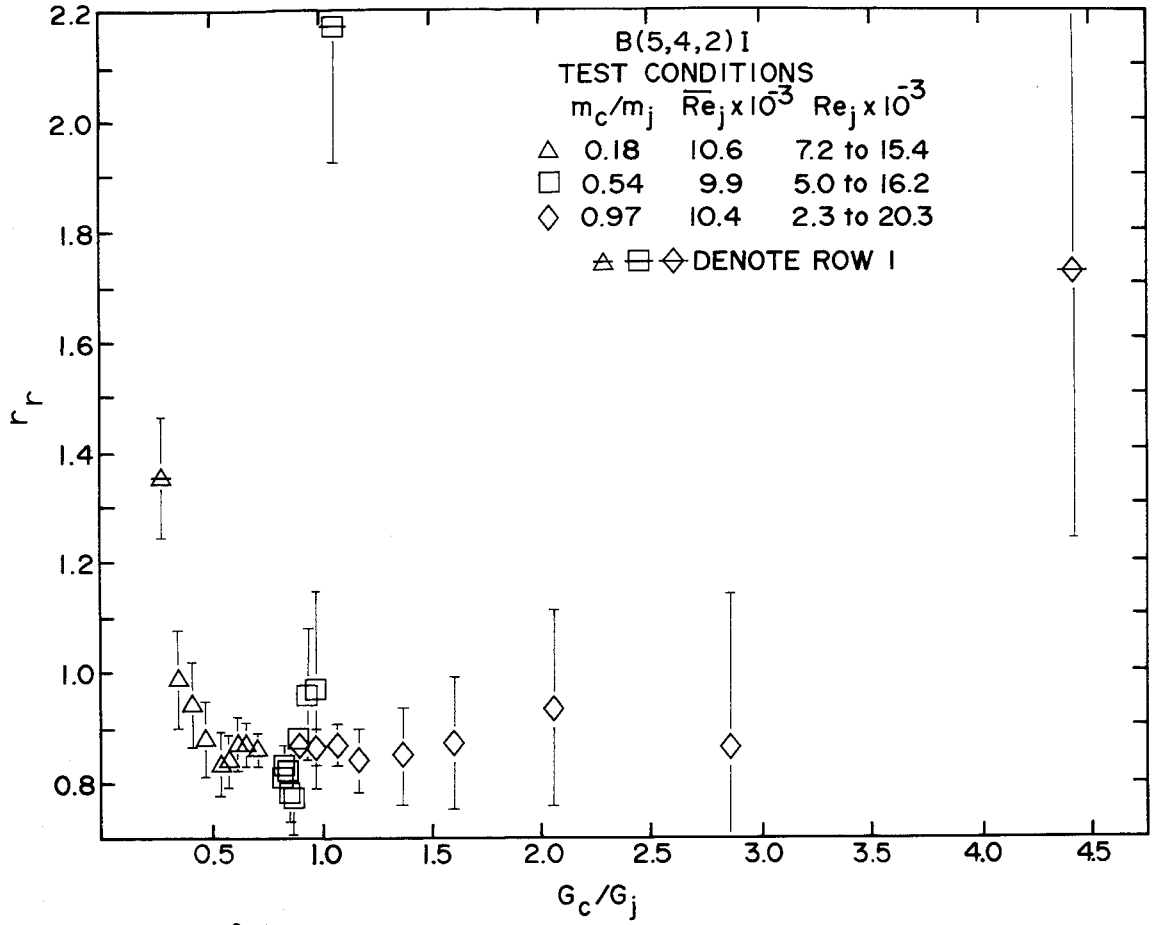

Fig. 8.9 Effect of crossflow-to-jet mass flux ratio on r_r for B(5,4,2)I geometry.

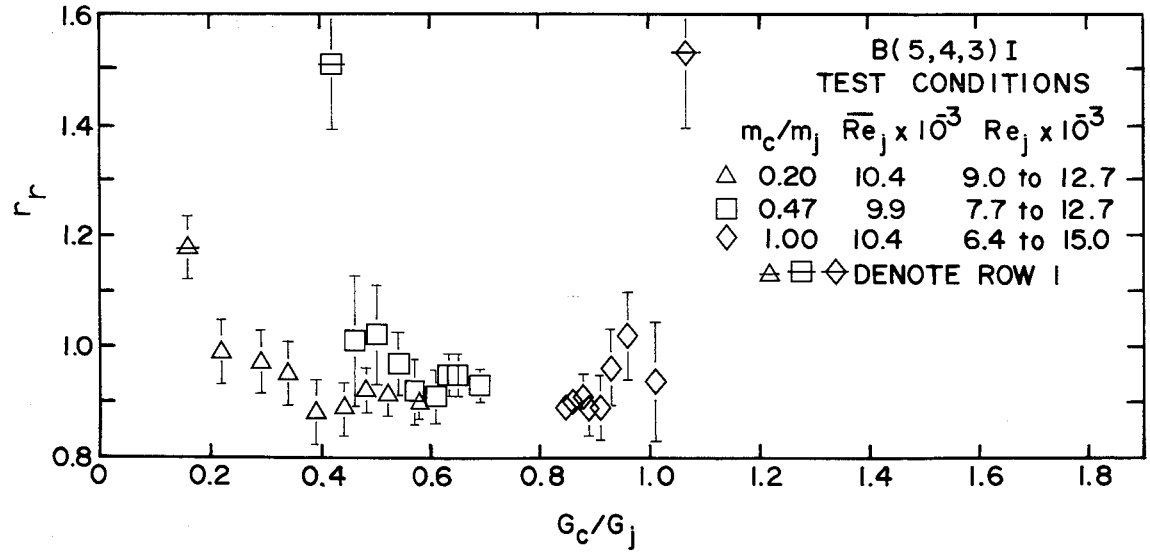

Fig. 8.10 Effect of crossflow-to-jet mass flux ratio on r_r for B(5,4,3)I geometry.

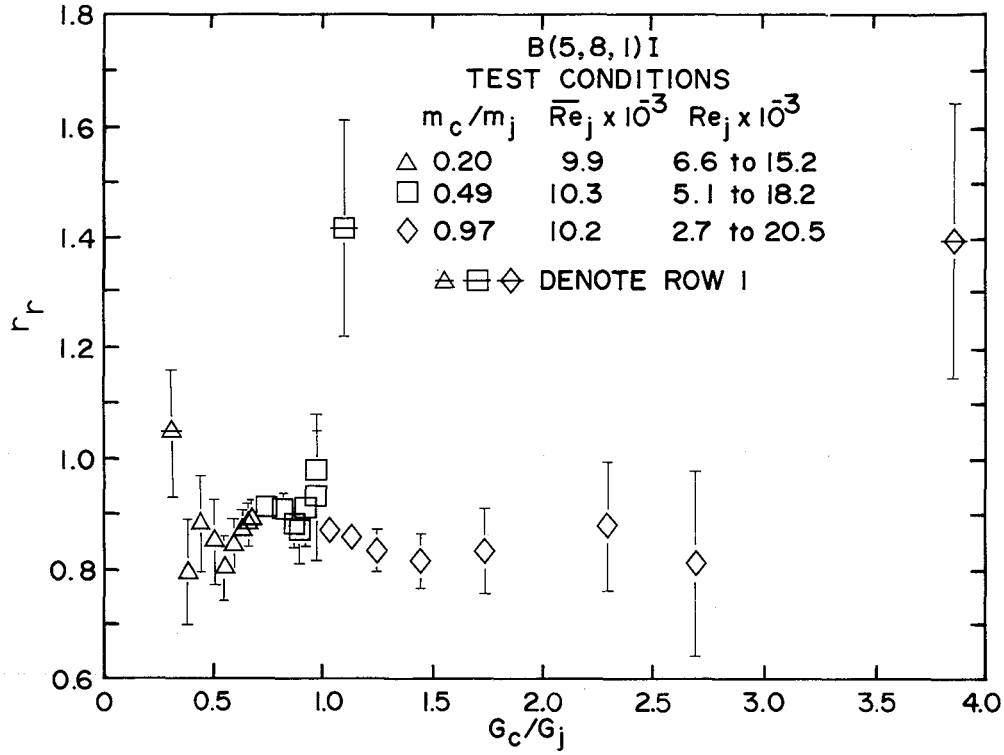

Fig. 8.11 Effect of crossflow-to-jet mass flux ratio on r_r for B(5,8,1)I geometry.

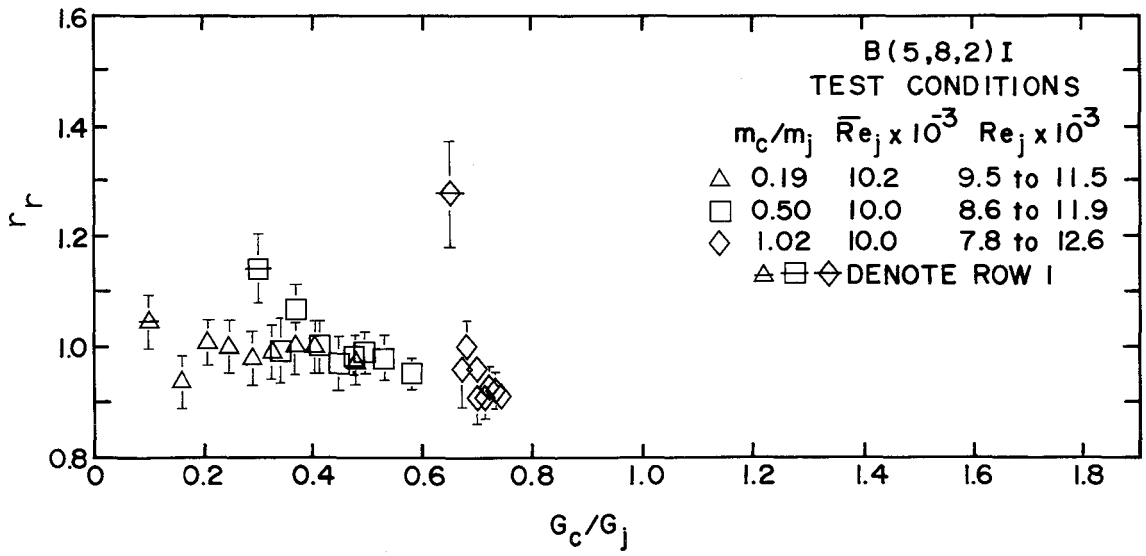

Fig. 8.12 Effect of crossflow-to-jet mass flux ratio on r_r for B(5,8,2)I geometry.

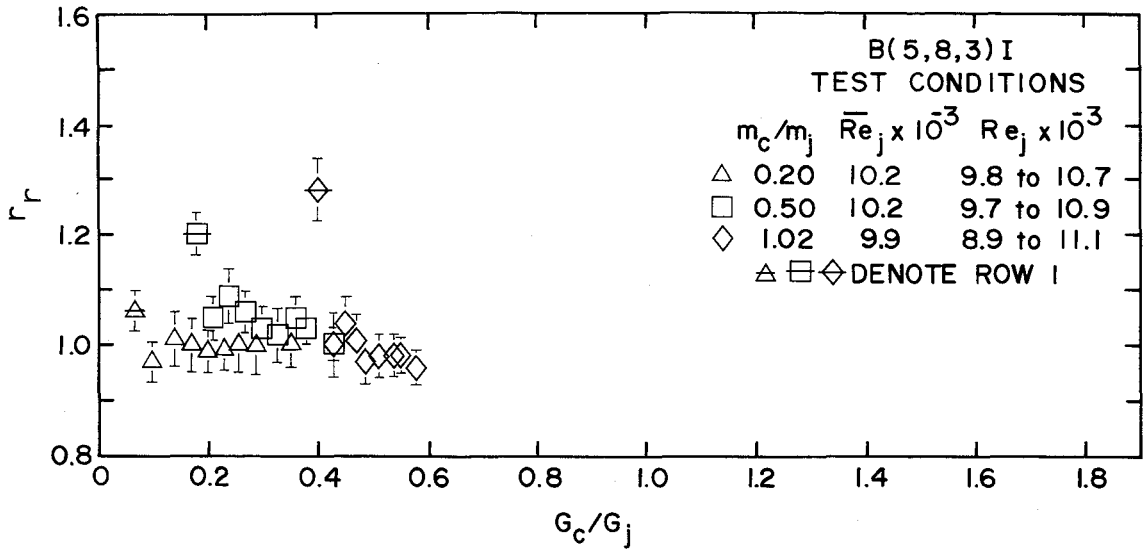

Fig. 8.13 Effect of crossflow-to-jet mass flux ratio on r_r for B(5,8,3)I geometry.

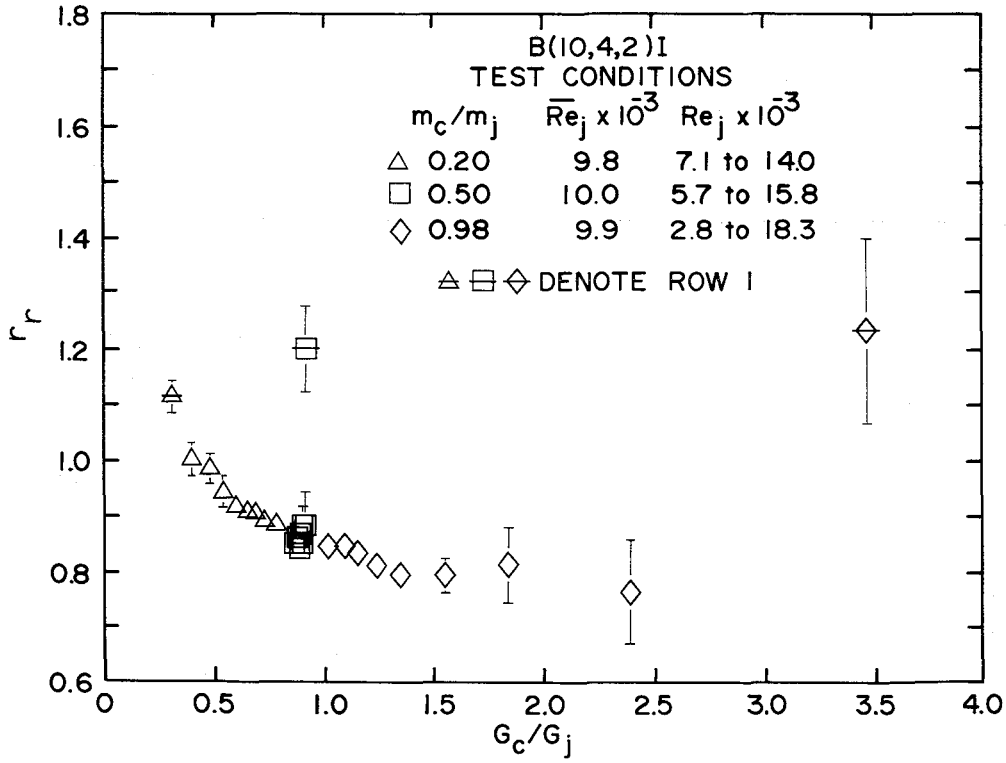

Fig. 8.14 Effect of crossflow-to-jet mass flux ratio on r_r for B(10,4,2)I geometry.

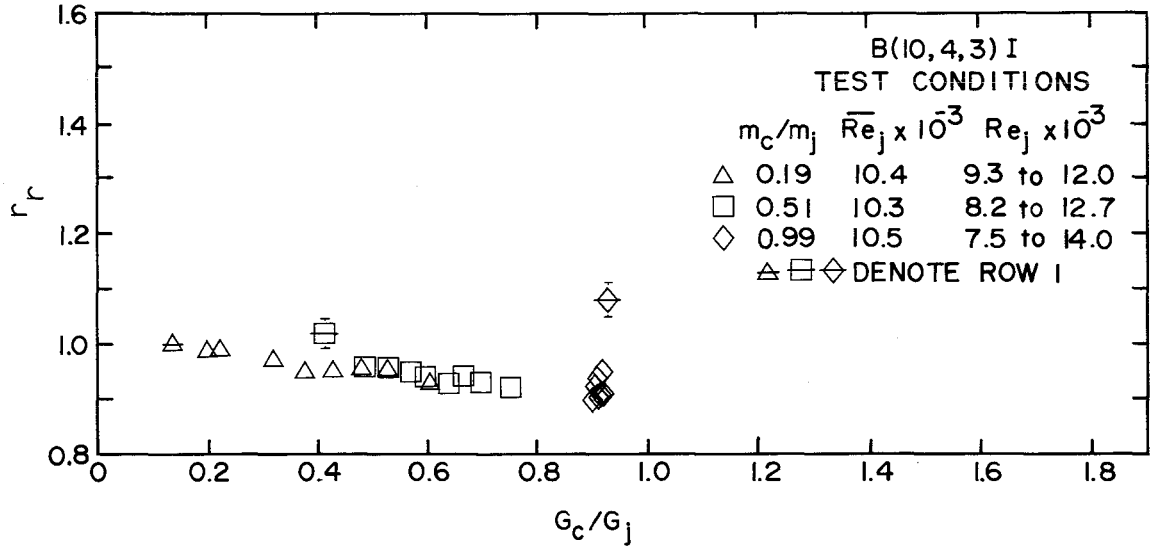

Fig. 8.15 Effect of crossflow-to-jet flux mass ratio on r_r for B(10,4,3)I geometry.

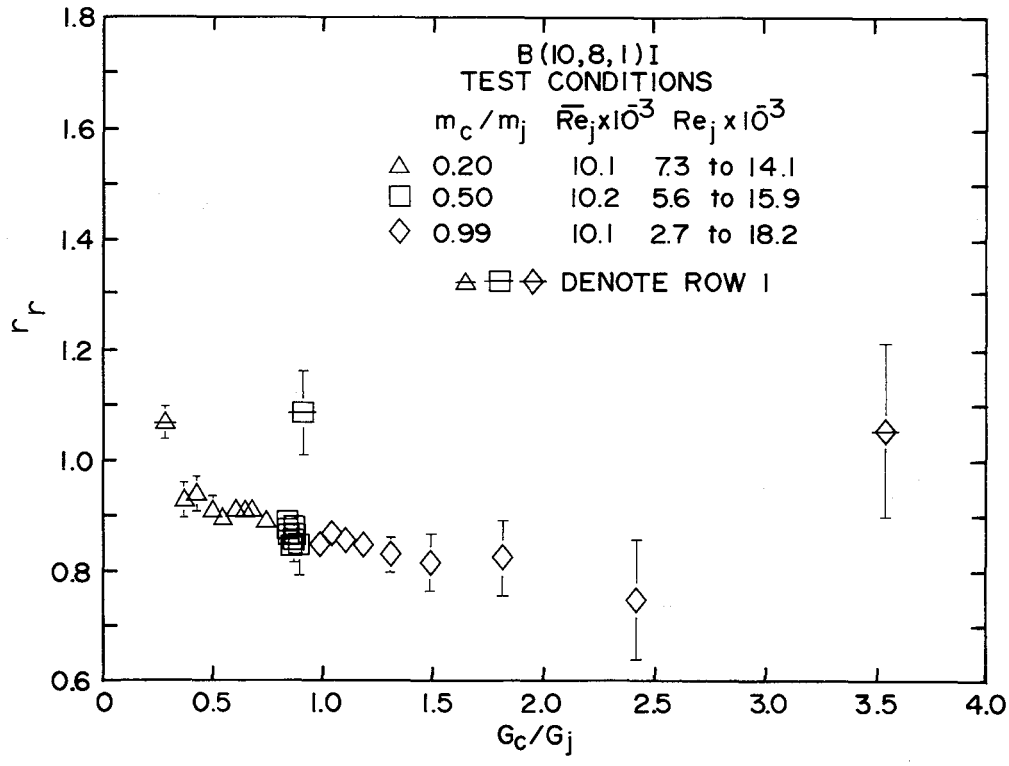

Fig. 8.16 Effect of crossflow-to-jet mass flux ratio on r_r for B(10,8,1)I geometry.

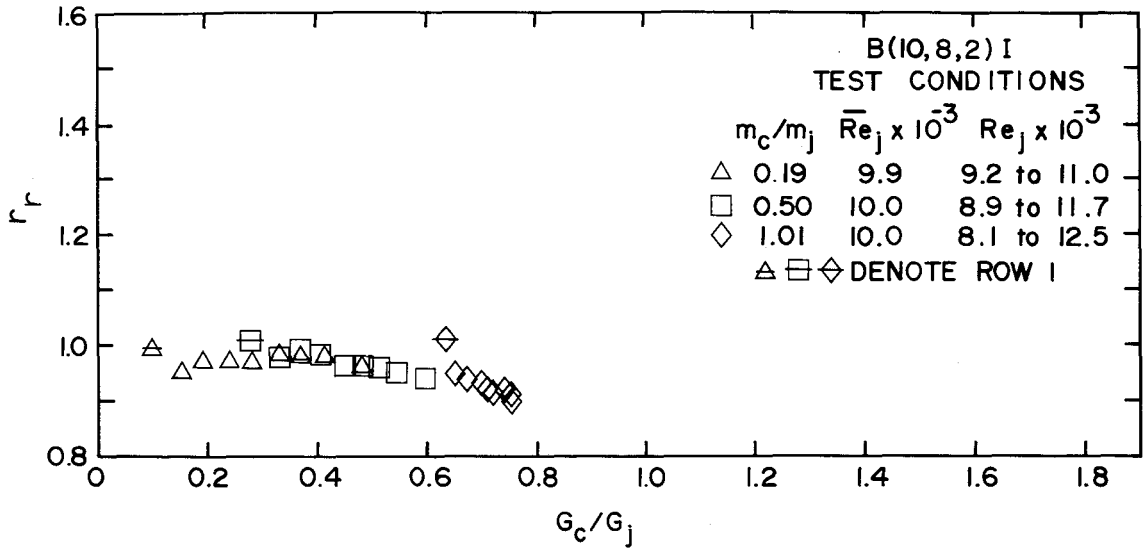

Fig. 8.17 Effect of crossflow-to-jet mass flux ratio on r_r for B(10,8,2)I geometry.

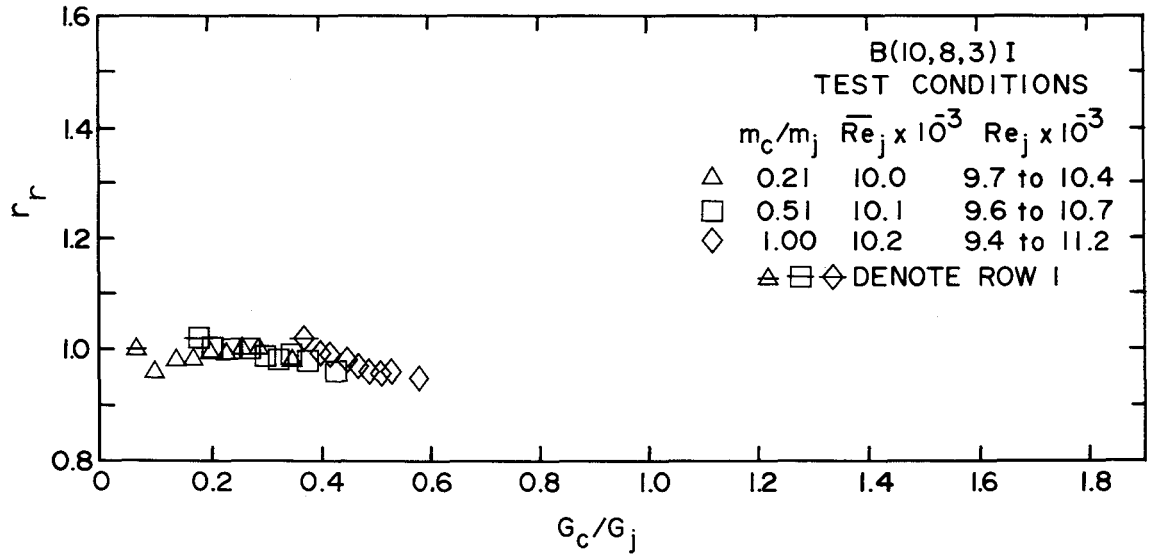

Fig. 8.18 Effect of crossflow-to-jet mass flux ratio on r_r for B(10,8,3)I geometry.

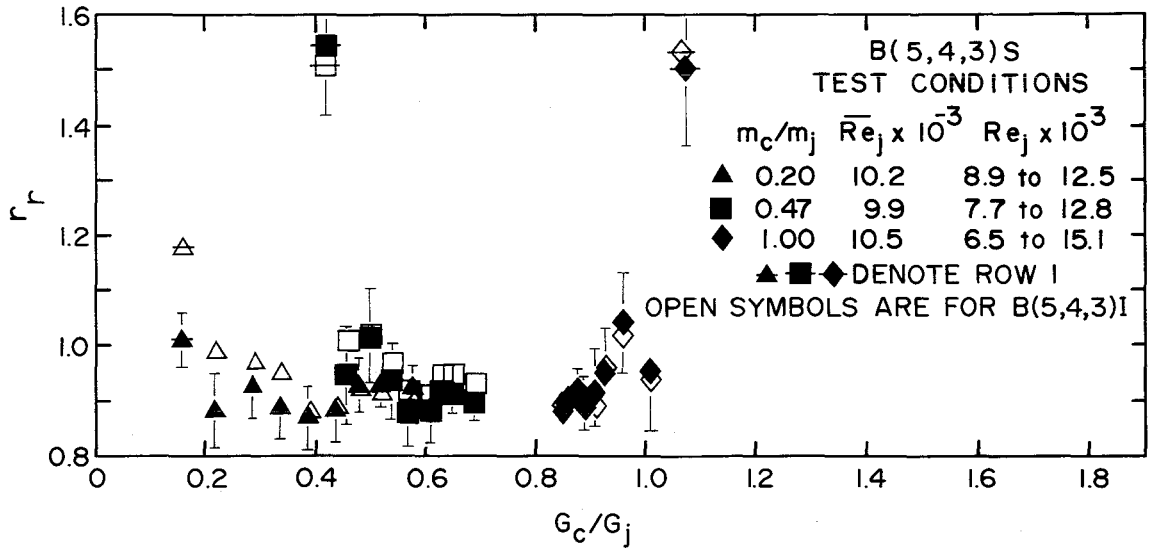

Fig. 8.19 Effect of crossflow-to-jet mass flux ratio on r_r for B(5,4,3)S geometry - comparison with inline case.

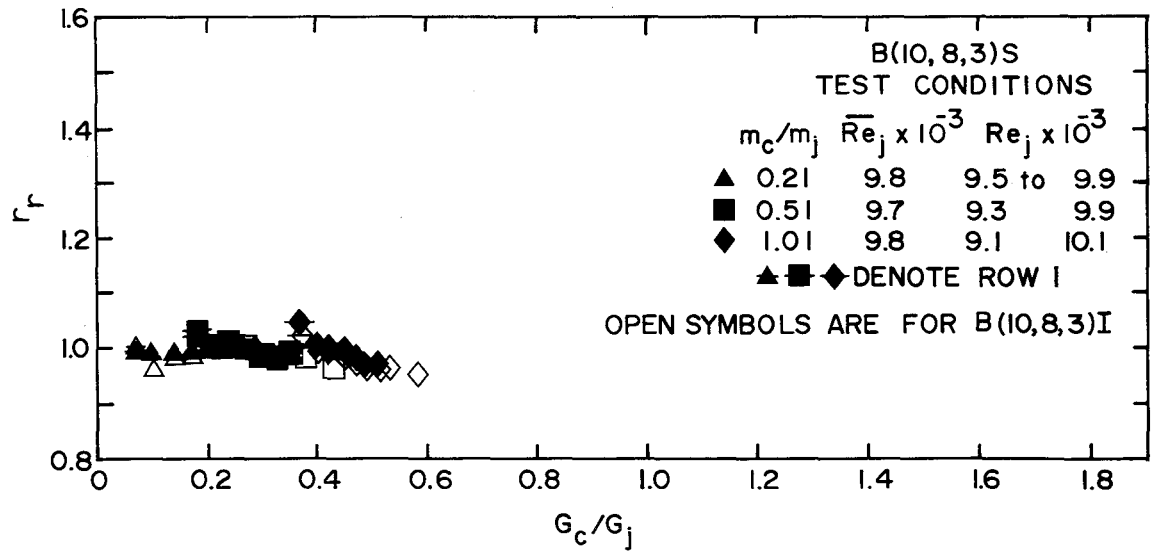

Fig. 8.20 Effect of crossflow-to-jet mass flux ratio on r_r for B(10,8,3)S geometry - comparison with inline case.

row. That is, the recovery factor values will, in general, depend on the normalized velocity and temperature profiles of the approaching crossflow. Similar flow hisory effects were discussed in Section 6.3 in connection with the results for η_r and Nu_r.

Now consider the (10,8,1)I array results (Fig. 8.16) as representative of those for the array geometries having the more highly nonuniform flow distributions with maximum values of G_c/G_j greater than unity. Recovery factors for this geometry are slightly below unity (row 1 excepted) for the smaller values of G_c/G_j and decrease slowly with increasing G_c/G_j. This decreasing r_r as the crossflow becomes more dominant is quite reasonable. The value of r_r of about 0.85 in the vicinity of $G_c/G_j = 1$ is reasonably consistent with results for boundary layer flows with free streams parallel to the surface and also with results for channel flows such as the circular duct results reported by McAdams et al. (1946). Note that a curve drawn through these points would again extrapolate to unity as G_c/G_j goes to zero and the jet flow dominates. The row 1 values are again greater than unity with the explanation for the values at G_c/G_j less than unity possibly being similar to that noted in the previous paragraph. However, it should be recognized that as G_c/G_j increases the definition of r_r in terms of jet flow parameters becomes inappropriate since the crossflow becomes dominant and the flow approaches the characteristics of a pure channel flow.

Recovery factor results for two staggered hole pattern arrays are compared with their inline counterparts in Figs. 8.19 and 8.20. (For clarity, uncertainty intervals for the inline data points are omitted, since they are indicated in Figs. 8.10 and 8.18. Note that for the (10,8,3) array results uncertainties did not exceed the size of the data point symbols.) To within experimental uncertainty, it appears that the effect of hole pattern on r_r is not significant in these cases.

Values of r as defined by Eq. (2.2) were also determined for each test condition utilizing Eq. (2.3). These values are not presented since they were essentially identical with the values for r_r presented above.

9. CONCLUDING REMARKS

For the baseline case of constant fluid properties, the regional average heat flux at the impingement surface opposite an individual spanwise row of an array of jets where the jets are subject to a unidirectional crossflow may be calculated as

$$\bar{q} = (k/d)Nu[(T_s-T_j) - \eta(T_o-T_j) + (1-r)(G_j/\rho)^2/2c_p]$$

where, based on dimensional analysis, the three regional average parameters, Nu, η, and r, may be shown to depend, in general, on the following independent parameters associated with the overall array:

Geometric parameters (x/L, x_n/d, y_n/d, z_n/d, L/x_n, hole pattern)

Flow and fluid parameters ($\overline{Re}_j$, m_c/m_j, Pr, normalized velocity and temperature profiles at array entrance)

Alternatively, $\bar{q}$ may be expressed in terms of heat transfer parameters which are functions of independent parameters associated with individual spanwise rows within the array. Thus,

$$\bar{q} = (k/d)Nu_r[(T_s-T_j) - \eta_r(T_{m,n}-T_j) + (1-r_r)(G_j/\rho)^2/2c_p]$$

where the regional average parameters Nu_r, η_r, and r_r may be considered as functions of the following independent parameters associated with an individual spanwise row (regional domain):

Geometric parameters (x_n/d, y_n/d, z_n/d)

Flow and fluid parameters (Re_j, G_c/G_j, Pr, normalized velocity and temperature profiles at entrance to regional domain)

For brevity the normalized velocity and temperature profiles at the domain entrance are referred to as the flow history since they depend on the conditions upstream of the domain entrance.

In the gas turbine application of the above formulations the temperature differences are typically large enough and the velocities small enough such that the term containing the recovery factor is negligible. Therefore, the primary information required is for Nusselt numbers and fluid temperature difference influence factors (η or η_r).

The advantage of the individual spanwise row formulation is that, to the extent that the flow history effect is not significant, results for Nu_r and η_r at specified (x_n/d, y_n/d, z_n/d, Re_j, G_c/G_j, Pr) can be applied at arbitrary rows of an array, whereas Nu and η can be applied only at a specified spanwise row location, x/L, within an array of a specified length, L/x_n, for specified (x_n/d, y_n/d, z_n/d, $\overline{Re}_j$, m_c/m_j, Pr).

Experimental results for both (Nu, η, and r) and for (Nu_r, η_r, and r_r) over ranges of the above specified independent parameters have been obtained using test model geometries operated at nominally ambient pressure and temperature levels. A major difference between the present results and prior results for heat transfer characteristics within a two-dimensional array of impinging jets is that the present results were obtained and formulated in such a way as to account independently for the effect of the crossflow temperature on the heat flux. Conclusions reached regarding these results and their relationship and sensitivity to the independent parameters are summarized below. The summary is rather lengthy because of the complexity of the problem induced by the large number of parameters involved.

Results in terms of row parameters:

(1) η_r is relatively insensitive to Re_j.

(2) As should be expected the η_r data appears to extrapolate to zero (jet flow dominates)as G_c/G_j goes to zero. As G_c/G_j increases, the η_r data, in its overall trend, asymptotically approaches unity (crossflow dominates) or in cases where the range of G_c/G_j was not large enough appears that it would extrapolate asymptotically to unity. Values of η_r greater than unity were

observed in some cases for G_c/G_j of order unity or greater. Possible explanations were discussed in Section 6.

(3) As z_n/d is increased η_r increases somewhat more rapidly with G_c/G_j. For the smallest channel heights, $z_n/d = 1$, η_r reaches unity as G_c/G_j reaches about 2. For $z_n/d = 2$ the η_r data reaches unity, or if extrapolated appears to reach unity, as G_c/G_j approaches unity, while for $z_n/d = 3$, it either reaches or would extrapolate to unity for G_c/G_j smaller than unity but never less than 0.5.

(4) η_r is relatively insensitive to x_n/d and y_n/d.

(5) Nu_r is proportional to Re_j^n where $n = 0.73$.

(6) The overall trend of Nu_r is decreasing as G_c/G_j increases from zero. However, Nu_r increases slightly in some cases for $G_c/G_j << 1$, before the decreasing trend begins. If G_c/G_j becomes large enough for the crossflow to dominate, Nu_r begins to increase again and approaches values equivalent to those for a parallel plate channel flow with one side heated. This behavior generally occurs as η_r is approaching unity.

(7) In contrast with η_r, Nu_r is relatively insensitive to z_n/d over the range covered, but sensitive to hole spacings. For fixed Re_j and G_c/G_j, Nu_r decreases as both x_n/d and y_n/d increase.

Flow history:

(1) Both Nu_r and η_r are insensitive to flow history for $G_c/G_j << 1$. For larger values of G_c/G_j both Nu_r and η_r for spanwise uniform crossflow (e.g. at row 1) may differ significantly from values for nonuniform crossflow (e.g. at downstream rows) for fixed geometric parameters. Therefore, results for a single jet in a crossflow or a single row of jets in a crossflow cannot, in general, be applied to individual rows beyond row 1 for a two-dimensional array.

(2) Values of Nu_r and η_r beyond row 2 are insensitive to flow history for fixed geometric parameters. Therefore, they can be applied to individual rows of an array of arbitrary length for rows beyond row 2.

(3) Based on points (1) and (2) above it is recommended that if measurements are to be made for application to a two-dimensional array, the minimum array length utilized for testing should be three rows.

(4) When the flow history develops from a staggered hole pattern with the smallest hole spacing, Nu_r is smaller and η_r is larger than when the flow history develops from the corresponding inline pattern. For the largest hole spacings the effect on Nu_r is much smaller and the effect on η_r is insignificant.

(5) When differing flow histories arise from differing combinations of initial crossflow and upstream jet flow, the effects on Nu_r are not very significant for any of the array geometries studied. The effects on η_r vary from insignificant to moderate depending on the magnitude of G_c/G_j and (x_n/d, y_n/d, z_n/d). It does appear, as would be expected, that increasing x_n/d tends to minimize the effect of flow history.

Results in terms of array parameters:

(1) η is insensitive to $\overline{Re}_j$.

(2) η decreases monotonically with x/L. At a fixed x/L (i.e., fixed spanwise row), η increases from zero as m_c/m_j increases from zero; i.e., η profiles for large m_c/m_j lie above those for small m_c/m_j. In some cases, η decreases from a maximum value of unity at upstream rows to as small as 0.3 at the last row of a 10 row array.

(3) η profiles are sensitive to the row-by-row jet flow distribution and therefore, like the jet flow distribution, are sensitive to y_n/d and z_n/d, but independent of x_n/d.

(4) Nu is proportional to $\overline{Re}_j^n$ where n = 0.73.

(5) Nu profiles take a variety of patterns from monotonically increasing with x/L for large m_c/m_j to monotonically decreasing in some cases for small to zero m_c/m_j to profiles with a local minimum and some with both a local minimum and maximum for intermediate m_c/m_j. The pattern depends on the flow distribution which in turn depends on m_c/m_j and the geometric parameters y_n/d and z_n/d. At a specified x/L, the magnitude of Nu always decreases with increasing x_n/d.

(6) Nu will depend on the flow history (in the case of array parameters this is just the initial crossflow history) only at upstream rows of the array

and then only if the crossflow dominates at the upstream rows, a condition which would not normally be used in an application.

(7) Values of Nu and η over the first N rows of an N_c row array, where $N < N_c$, can be applied to an N row array at the values of m_c/m_j and $\overline{Re}_j$ applicable to the first N rows of the N_c row array. Values of $(m_c/m_j)_{,N}$ and $\overline{Re}_{j,N}$ for $1 < N < N_c$ for each of the test cases of the present study (where $N_c = 10$) are included in the tables of Appendix B.

(8) The heat rate per unit surface-to-jet temperature difference per unit total flow rate (crossflow plus jet flow) considered for either constant jet flow rate or constant total flow rate decreases with increasing m_c/m_j, increases with increasing hole spacing, and is nearly independent of channel height over the ranges covered by the tests.

Recovery effects:

(1) The neglect of the recovery factor term in the regional heat flux equation did not significantly affect the evaluation of Nu from the present test results. Results for η were noticeably affected only for geometries with highly nonuniform flow distributions, and then only for downstream rows.

(2) The neglect of the recovery factor term was noticeable in the evaluation of Nu_r but did not exceed experimental uncertainties. Results for η_r were quite strongly affected for downstream rows of geometries with highly nonuniform flow distributions.

(3) The observations under (1) and (2) above lead to the conclusion that conditions may exist where neglect of the recovery factor term does not affect the evaluation of Nusselt numbers, but for the same conditions may significantly affect the evaluation of fluid temperature difference influence factors.

(4) For the present tests the defined recovery factors r_r ranged from 0.8 to 1.0 for rows beyond row 1, and from 1.0 to 2.2 for row 1. Values greater than one may occur because the recovery temperature is defined for equal total temperatures of the crossflow and jet flow. Thus, when the crossflow velocity is less than the jet velocity the static temperature of the crossflow is higher than that of the jet. Mixing of the two flow streams may cause the

recovery temperature to be higher than the jet total temperature. Values of r were found to be essentially identical to r_r.

REFERENCES

Behbahani, A. I., and Goldstein, R. J. (1983): "Local Heat Transfer to Staggered Arrays of Impinging Circular Air Jets," ASME Journal of Engineering for Power, Vol. 105, pp. 354-360.

Bouchez, J. P., and Goldstein, R. J. (1975): "Impingement Cooling from a Circular Jet in a Crossflow," International Journal of Heat and Mass Transfer, Vol. 18, pp. 719-730.

Florschuetz, L. W., Metzger, D. E., Takeuchi, D. I., and Berry, R. A. (1980a): Multiple Jet Impingement Heat Transfer Characteristics - Experimental Investigation of Inline and Staggered Arrays with Crossflow, NASA Contractor Report 3217, Department of Mechanical Engineering, Arizona State University, Tempe.

Florschuetz, L. W., Berry, R. A., and Metzger, D. E. (1980b): "Periodic Streamwise Variations of Heat Transfer Coefficients for Inline and Staggered Arrays of Circular Jets with Crossflow of Spent Air," ASME Journal of Heat Transfer, Vol. 102, pp. 132-137.

Florschuetz, L. W., Metzger, D. E., and Truman, C. R. (1981a): Jet Array Impingement with Crossflow--Correlation of Streamwise Resolved Flow and Heat Transfer Distributions, NASA Contractor Report 3373, Department of Mechanical Engineering, Arizona State University, Tempe.

Florschuetz, L. W., Truman C. R., and Metzger, D. E. (1981b): "Streamwise Flow and Heat Transfer Distributions for Jet Array Impingement with Crossflow," ASME Journal of Heat Transfer, Vol. 103, pp. 337-342.

Florschuetz, L. W., Metzger, D. E., Su, C. C., Isoda, Y., and Tseng, H. H. (1982): Jet Array Impingement Flow Distributions and Heat Transfer Characteristics - Effects of Initial Crossflow and Nonuniform Array Geometry, NASA Contractor Report 3630, Department of Mechanical and Aerospace Engineering, Arizona State University, Tempe, Arizona.

Florschuetz, L. W., and Isoda, Y. (1983): "Flow Distributions and Discharge Coefficient Effects for Jet Array Impingement with Initial Crossflow," ASME Journal of Engineering for Power, Vol. 105, pp. 296-304.

Florschuetz, L. W., Metzger, D. E. and Su, C. C. (1984): "Heat Transfer Characteristics for Jet Array Impingement with Initial Crossflow," ASME Journal of Heat Transfer, Vol. 106, pp. 34-41.

Florschuetz, L.W., and Tseng, H.H., (1985): "Effect of Nonuniform Geometries on Flow Distributions and Heat Transfer Characteristics for Arrays of Impinging Jets," ASME Journal of Engineering for Gas Turbines and Power, Vol. 107, pp. 68-75.

Goldstein, R. J., and Behbahani, A. I. (1982): "Impingement of Circular Jet with and without Crossflow," International Journal of Heat and Mass Transfer, Vol. 25, pp. 1377-1382.

Hippensteele, S. A., Russel, L. M., and Stepka, F. S. (1983): "Evaluation of a Method for Heat Transfer Measurements and Thermal Visualization Using a Composite of a Heater Element and Liquid Crystals," ASME Journal of Heat Transfer, Vol. 105, pp. 184-189.

Holdeman, J.D., and Walker, R.E., (1977): "Mixing of a Row of Jets with a Confined Crossflow," AIAA Journal, Vol. 15, pp. 243-249.

Kays, W. M., Crawford, M. E. (1980): Convective Heat and Mass Transfer, Second Edition, McGraw-Hill, New York.

Kercher, D. M., and Tabakoff, W. (1970): "Heat Transfer by a Square Array of Round Air Jets Impinging Perpendicular to a Flat Surface Including the Effect of Spent Air," ASME Journal of Engineering for Power, Vol. 92, pp. 73-82.

Kline, S. J. and McClintock, F. (1953): "Describing Uncertainties in Single Sample Experiments," Mechanical Engineering, Vol. 75, January pp. 3-8.

McAdams, W. H., Nocolai, A. L., and Keenan, J. H. (1946): "Measurements of Recovery Factors and Coefficients of Heat Transfer in a Tube for Subsonic Flow of Air," Transactions AIChE, Vol. 42, pp. 907-925.

Metzger, D. E., and Korstad, R. J. (1972): "Effects of Cross Flow in Impingement Heat Transfer," ASME Journal of Engineering for Power, Vol. 94, pp. 35-41.

Metzger, D. E., Florschuetz, L. W., Takeuchi, D. I., Behee, R. D., and Berry, R. A. (1979): "Heat Transfer Characteristics for Inline and Staggered Arrays of Circular Jets with Crossflow of Spent Air," ASME Journal of Heat Transfer, Vol. 101, pp. 526-531.

Saad, N. R., Mujumdar, A. S., Abdel Messeh, W., and Douglas, W. J. M. (1980): "Local Heat Transfer Characteristics for Staggered Arrays of Circular Impinging Jets with Crossflow of Spent Air," Paper No. 80-HT-23, American Society of Mechanical Engineers, New York.

Sparrow, E. M., Goldstein, R. J., and Rouf, M. A. (1975): "Effect of Nozzle-Surface Separation Distance on Impingement Heat Transfer for a Jet in a Crossflow," ASME Journal of Heat Transfer, Vol. 97, pp. 528-533.

Srinivasan, R., Berenfeld, A., and Mongia, H.C., (1982): Dilution Jet Mixing Program--Phase I Report, NASA Contractor Report 168031, Garrett Turbine Engine Company, Phoenix, Arizona.

Wittig, S.L.K., Elbahar, O.M.F., and Noll, B.E., (1983): "Temperature Profile Development in Turbulent Mixing of Coolant Jets with a Confined Hot Cross Flow," Paper No. 83-GT-220, American Society of Mechanical Engineers, New York.

APPENDIX A

Tabular Results in Terms of Individual Spanwise Row Parameters

The following is a presentation in tabular form of the experimental results for the heat transfer parameters Nu_r and η_r. The notations used in the tables are identified below in terms of the nomenclature used throughout the text of the report as defined in the NOMENCLATURE section.

Notation used in APPENDIX A	Corresponding NOMENCLATURE
ETAR	η_r
GC/GJ	G_c/G_j
MC/MJ	m_c/m_j
NUR	Nu_r
REJ(K)	$Re_j \times 10^{-3}$
$\overline{\text{REJ}}$(K)	$\overline{Re}_j \times 10^{-3}$
X/L	x/L

Jet array geometries are identified using B(x_n/d, y_n/d, z_n/d)I where B refers to array length (see Table 4.1) I = inline hole pattern, S = staggered pattern.

B(5,4,2)I

$\overline{REJ}$(K)	X/L	0.05	0.15	0.25	0.35	0.45	0.55	0.65	0.75	0.85	0.95
MC/MJ											
10.6	NUR	31.5	39.2	41.6	40.9	42.2	43.7	45.5	48.1	54.0	54.9
0.18	ETAR	0.41	0.52	0.62	0.68	0.73	0.73	0.77	0.77	0.74	0.86
	REJ(K)	7.2	7.6	8.3	8.9	9.6	10.5	11.5	12./	14.0	15.4
	GC/GJ	0.27	0.35	0.41	0.47	0.53	0.57	0.61	0.64	0.67	0.70
9.9	NUR	16.8	17.9	23.9	29.7	30.7	34.9	38.1	42.2	50.1	51.2
0.54	ETAR	0.97	1.08	1.03	0.97	0.85	0.84	0.82	0.83	0.82	0.87
	REJ(K)	5.0	5.9	6.8	7.8	8.9	10.0	11.3	12.7	14.3	16.2
	GC/GJ	1.07	0.97	0.93	0.89	0.87	0.85	0.84	0.83	0.82	0.83
10.4	NUR	26.3	26.1	27.6	28.8	32.5	36.1	40.4	46.3	52.2	56.4
0.97	ETAR	1.03	1.05	1.07	1.13	1.14	1.06	0.98	0.90	0.80	0.71
	REJ(K)	2.3	3.6	5.2	6.9	8.7	10.9	12.9	15.1	17.5	20.3
	GC/GJ	4.44	2.87	2.06	1.60	1.35	1.17	1.07	0.98	0.94	0.90

B(5,4,3)I

$\overline{REJ}$(K) MC/MJ	X/L	0.05	0.15	0.25	0.35	0.45	0.55	0.65	0.75	0.85	0.95
10.4	NUR	37.1	41.8	42.6	39.2	38.3	38.4	39.6	41.0	42.5	41.6
0.20	ETAR	0.48	0.56	0.71	0.76	0.82	0.84	0.91	0.92	0.88	0.87
	REJ(K)	9.0	9.1	9.2	9.4	9.9	10.3	10.8	11.3	12.1	12.7
	GC/GJ	0.16	0.22	0.29	0.34	0.39	0.44	0.48	0.51	0.54	0.58
9.9	NUR	11.2	22.4	32.3	33.5	32.8	32.9	33.4	35.2	37.1	37.3
0.47	ETAR	0.97	0.94	0.75	0.81	0.86	0.90	0.90	0.91	0.88	0.91
	REJ(K)	7.7	8.1	8.5	8.9	9.4	9.9	10.6	11.3	11.9	12.8
	GC/GJ	0.42	0.46	0.50	0.54	0.57	0.61	0.63	0.65	0.67	0.69
10.4	NUR	18.5	18.1	18.9	21.8	24.8	27.4	30.0	32.8	36.2	37.6
1.00	ETAR	0.96	1.03	1.08	1.14	1.14	1.13	1.11	1.10	1.06	1.06
	REJ(K)	6.4	7.3	8.1	8.9	9.8	10.7	11.6	12.6	13.8	14.9
	GC/GJ	1.07	1.00	0.96	0.93	0.91	0.89	0.88	0.86	0.86	0.85

B(5,8,1)I

$\overline{REJ}$(K)	X/L	0.05	0.15	0.25	0.35	0.45	0.55	0.65	0.75	0.85	0.95
MC/MJ											
9.9	NUR	23.3	29.3	31.3	33.7	36.0	38.5	41.9	45.4	50.4	54.5
0.20	ETAR	0.47	0.50	0.52	0.60	0.64	0.66	0.69	0.72	0.66	0.79
	REJ(K)	6.6	7.0	7.6	8.2	8.9	9.7	10.7	11.8	13.5	15.2
	GC/GJ	0.32	0.39	0.45	0.51	0.56	0.60	0.64	0.67	0.67	0.68
10.3	NUR	16.8	26.6	29.3	32.7	35.6	39.4	44.3	48.1	53.8	58.9
0.49	ETAR	0.96	0.72	0.60	0.59	0.57	0.57	0.60	0.58	0.52	0.63
	REJ(K)	5.1	6.2	6.8	7.8	8.9	10.1	11.6	13.3	15.3	18.2
	GC/GJ	1.10	0.97	0.97	0.93	0.90	0.88	0.85	0.83	0.81	0.76
10.2	NUR	24.0	25.0	28.8	32.7	37.0	41.8	46.7	52.4	60.2	64.5
0.97	ETAR	0.98	1.01	0.98	0.87	0.77	0.70	0.67	0.61	0.57	0.58
	REJ(K)	2.7	3.9	4.8	6.6	8.4	10.3	12.4	14.6	17.4	20.5
	GC/GJ	3.87	2.70	2.30	1.74	1.44	1.25	1.13	1.03	0.95	0.88

B(5,8,2)I

$\overline{REJ}$(K)	X/L	0.05	0.15	0.25	0.35	0.45	0.55	0.65	0.75	0.85	0.95
MC/MJ											
10.2	NUR	43.5	43.6	43.4	41.7	40.5	40.3	41.3	43.3	44.6	43.6
0.19	ETAR	0.33	0.43	0.45	0.49	0.50	0.50	0.58	0.68	0.58	0.62
	REJ(K)	9.5	9.4	9.5	9.7	9.9	10.2	10.5	10.8	11.1	11.5
	GC/GJ	0.10	0.15	0.20	0.24	0.29	0.33	0.37	0.41	0.44	0.48
10.0	NUR	28.6	36.4	37.3	38.2	39.3	38.2	40.5	42.4	44.8	45.9
0.50	ETAR	0.65	0.55	0.59	0.68	0.74	0.68	0.75	0.79	0.75	0.84
	REJ(K)	8.6	8.8	9.1	9.4	9.5	10.0	10.4	10.9	11.4	11.9
	GC/GJ	0.30	0.34	0.37	0.41	0.46	0.48	0.50	0.53	0.56	0.58
10.0	NUR	16.4	26.4	30.9	32.8	33.5	35.5	36.8	40.0	41.9	43.2
1.02	ETAR	0.99	0.88	0.69	0.69	0.70	0.72	0.73	0.79	0.74	0.76
	REJ(K)	7.8	8.2	8.6	9.0	9.6	10.1	10.7	11.3	12.0	12.6
	GC/GJ	0.65	0.67	0.68	0.70	0.70	0.71	0.72	0.73	0.73	0.74

B(5,8,3)I

$\overline{REJ}$(K)	X/L	0.05	0.15	0.25	0.35	0.45	0.55	0.65	0.75	0.85	0.95
MC/MJ											
10.2	NUR	46.2	45.9	45.8	43.8	43.8	42.6	42.4	44.3	44.6	44.3
0.20	ETAR	0.38	0.46	0.45	0.54	0.56	0.59	0.62	0.74	0.67	0.76
	REJ(K)	9.8	10.0	10.0	10.0	10.0	10.1	10.3	10.4	10.6	10.7
	GC/GJ	0.07	0.10	0.14	0.17	0.20	0.23	0.26	0.29	0.32	0.35
10.2	NUR	36.4	40.4	41.1	41.3	40.0	40.8	41.1	42.1	43.6	42.7
0.50	ETAR	0.57	0.58	0.62	0.67	0.70	0.73	0.74	0.76	0.75	0.79
	REJ(K)	9.7	9.7	9.8	10.0	10.1	10.2	10.4	10.6	10.7	10.9
	GC/GJ	0.18	0.21	0.24	0.27	0.30	0.33	0.36	0.38	0.41	0.43
9.9	NUR	14.1	30.5	33.6	34.6	34.7	36.0	36.2	38.0	39.8	40.4
1.02	ETAR	0.90	0.73	0.68	0.73	0.77	0.82	0.85	0.81	0.80	0.83
	REJ(K)	8.9	9.1	9.3	9.5	9.7	9.9	10.2	10.5	10.8	11.1
	GC/GJ	0.40	0.43	0.45	0.47	0.49	0.51	0.54	0.55	0.57	0.58

B(10,4,2)I

$\overline{REJ}$(K)	X/L	0.05	0.15	0.25	0.35	0.45	0.55	0.65	0.75	0.85	0.95
MC/MJ											
9.8	NUR	28.1	33.1	33.3	33.9	34.2	35.5	36.3	38.0	39.1	41.1
0.20	ETAR	0.50	0.62	0.69	0.75	0.76	0.79	0.82	0.80	0.70	0.78
	REJ(K)	7.1	7.4	7.9	8.4	9.0	9.7	10.6	11.5	12.7	14.0
	GC/GJ	0.32	0.40	0.48	0.54	0.60	0.65	0.69	0.73	0.76	0.78
10.0	NUR	15.0	23.0	26.5	28.6	29.5	31.9	33.9	37.1	40.2	42.3
0.50	ETAR	0.97	0.93	0.79	0.81	0.82	0.85	0.85	0.87	0.81	0.83
	REJ(K)	5.7	6.4	7.2	8.0	9.0	10.1	11.3	12.7	14.2	15.8
	GC/GJ	0.92	0.91	0.90	0.89	0.89	0.89	0.89	0.88	0.88	0.88
9.9	NUR	21.9	22.1	24.7	26.4	29.2	32.9	35.3	39.0	43.6	45.7
0.98	ETAR	0.95	0.98	1.01	1.02	1.01	0.99	0.95	0.92	0.87	0.83
	REJ(K)	2.8	4.2	5.7	7.2	8.7	10.4	12.1	14.0	16.1	18.3
	GC/GJ	3.47	2.40	1.84	1.55	1.36	1.24	1.15	1.09	1.04	1.01

B(10,4,3)I

$\overline{REJ}$(K) MC/MJ	X/L	0.05	0.15	0.25	0.35	0.45	0.55	0.65	0.75	0.85	0.95
10.4	NUR	33.6	36.6	34.5	31.5	29.7	28.8	28.6	29.1	29.2	28.6
0.19	ETAR	0.52	0.61	0.68	0.76	0.82	0.85	0.94	0.99	0.89	0.97
	REJ(K)	9.3	9.4	9.6	9.8	10.0	10.3	10.7	11.1	11.6	12.0
	GC/GJ	0.14	0.20	0.26	0.32	0.38	0.43	0.48	0.52	0.57	0.61
10.3	NUR	14.8	26.6	26.6	26.0	25.2	25.3	25.1	25.4	26.4	26.3
0.51	ETAR	0.88	0.84	0.83	0.88	0.89	0.91	0.94	0.98	0.98	1.05
	REJ(K)	8.2	8.6	9.0	9.4	9.8	10.4	10.9	11.4	12.0	12.7
	GC/GJ	0.44	0.49	0.53	0.57	0.60	0.64	0.67	0.70	0.73	0.75
10.5	NUR	15.7	16.4	20.1	21.8	22.4	23.1	24.2	25.1	27.3	27.8
0.99	ETAR	0.98	1.06	1.05	1.03	1.02	1.02	1.05	1.05	1.07	1.11
	REJ(K)	7.5	8.0	8.6	9.2	10.0	10.7	11.4	12.2	13.1	14.0
	GC/GJ	0.93	0.92	0.91	0.91	0.91	0.91	0.91	0.92	0.92	0.92

B(10,8,1)I

$\overline{REJ}$(K)	X/L	0.05	0.15	0.25	0.35	0.45	0.55	0.65	0.75	0.85	0.95
MC/MJ											
10.1	NUR	18.3	22.4	23.9	25.2	26.8	28.7	30.9	33.8	35.7	40.3
0.20	ETAR	0.47	0.54	0.52	0.54	0.57	0.57	0.59	0.62	0.44	0.65
	REJ(K)	7.3	7.6	8.0	8.6	9.3	10.0	10.8	11.9	13.0	14.1
	GC/GJ	0.28	0.37	0.43	0.50	0.55	0.60	0.65	0.68	0.72	0.75
10.2	NUR	17.2	22.8	26.0	29.2	30.7	33.1	35.5	38.1	43.1	45.8
0.50	ETAR	0.90	0.77	0.70	0.69	0.67	0.66	0.68	0.66	0.63	0.73
	REJ(K)	5.6	6.4	7.3	8.2	9.2	10.3	11.5	13.0	14.4	15.9
	GC/GJ	0.91	0.89	0.87	0.87	0.86	0.86	0.85	0.85	0.84	0.86
10.1	NUR	23.6	24.4	27.3	30.4	34.3	37.1	40.2	43.7	50.2	53.1
0.99	ETAR	0.98	1.01	0.96	0.88	0.82	0.77	0.74	0.71	0.68	0.74
	REJ(K)	2.7	4.1	5.7	7.4	9.0	10.7	12.4	14.4	16.4	18.2
	GC/GJ	3.54	2.43	1.82	1.49	1.31	1.19	1.11	1.04	1.00	0.99

B(10,8,2)I

$\overline{REJ}$(K) MC/MJ	X/L	0.05	0.15	0.25	0.35	0.45	0.55	0.65	0.75	0.85	0.95
9.9	NUR	30.4	34.2	33.5	32.5	30.8	30.3	30.5	31.1	31.9	33.0
0.19	ETAR	0.40	0.48	0.50	0.53	0.56	0.58	0.65	0.67	0.57	0.70
	REJ(K)	9.2	9.3	9.4	9.5	9.7	9.8	10.1	10.4	10.7	11.0
	GC/GJ	0.10	0.15	0.19	0.24	0.28	0.33	0.37	0.41	0.44	0.48
10.0	NUR	22.9	28.0	29.4	29.2	29.5	29.8	30.3	31.0	32.6	33.4
0.50	ETAR	0.60	0.61	0.65	0.69	0.75	0.75	0.77	0.78	0.71	0.80
	REJ(K)	8.9	9.1	9.2	9.5	9.7	10.0	10.3	10.7	11.1	11.6
	GC/GJ	0.28	0.33	0.37	0.41	0.45	0.48	0.51	0.54	0.57	0.59
10.0	NUR	14.8	22.6	25.2	26.0	27.0	28.0	29.3	30.5	32.9	33.3
1.01	ETAR	0.93	0.80	0.75	0.77	0.79	0.79	0.80	0.81	0.78	0.80
	REJ(K)	8.1	8.5	8.7	9.1	9.6	10.0	10.5	11.1	11.7	12.5
	GC/GJ	0.63	0.65	0.67	0.70	0.71	0.72	0.74	0.75	0.75	0.75

B(10,8,3)I

$\overline{REJ}$(K)	X/L	0.05	0.15	0.25	0.35	0.45	0.55	0.65	0.75	0.85	0.95
MC/MJ											
10.0	NUR	33.5	35.9	35.6	34.3	32.6	32.0	30.8	31.0	31.9	32.9
0.21	ETAR	0.47	0.49	0.52	0.55	0.61	0.65	0.66	0.69	0.65	0.79
	REJ(K)	9.7	9.7	9.8	9.8	9.9	10.0	10.1	10.2	10.3	10.4
	GC/GJ	0.07	0.10	0.14	0.17	0.20	0.23	0.26	0.29	0.32	0.35
10.1	NUR	26.5	30.6	31.8	30.1	29.6	29.5	29.5	30.1	31.3	31.0
0.51	ETAR	0.61	0.66	0.66	0.70	0.73	0.74	0.79	0.82	0.77	0.83
	REJ(K)	9.6	9.7	9.8	9.9	10.0	10.1	10.3	10.4	10.5	10.7
	GC/GJ	0.18	0.21	0.24	0.27	0.30	0.33	0.35	0.38	0.41	0.43
10.2	NUR	16.8	26.1	27.2	27.1	27.0	27.3	27.5	28.4	29.7	29.1
1.00	ETAR	0.85	0.75	0.77	0.83	0.83	0.83	0.85	0.85	0.81	0.82
	REJ(K)	9.4	9.6	9.7	9.9	10.0	10.2	10.5	10.7	10.9	11.2
	GC/GJ	0.36	0.40	0.42	0.45	0.47	0.49	0.51	0.53	0.56	0.58

B(5,4,3)S

$\overline{REJ}$(K) MC/MJ	X/L	0.05	0.15	0.25	0.35	0.45	0.55	0.65	0.75	0.85	0.95
10.2	NUR	38.5	40.6	34.8	32.5	30.0	28.2	27.0	26.6	27.6	26.9
0.20	ETAR	0.49	0.60	0.71	0.78	0.85	0.90	0.96	1.00	1.03	1.05
	REJ(K)	8.9	9.0	9.1	9.3	9.7	10.1	10.6	11.2	11.9	12.5
	GC/GJ	0.16	0.22	0.29	0.34	0.39	0.44	0.48	0.51	0.54	0.58
9.9	NUR	10.9	23.6	21.2	21.0	21.2	21.7	22.5	23.7	26.1	26.5
0.47	ETAR	0.94	0.93	0.99	1.05	1.10	1.17	1.21	1.25	1.28	1.31
	REJ(K)	7.7	8.0	8.4	8.9	9.4	9.9	10.5	11.2	11.9	12.8
	GC/GJ	0.42	0.46	0.50	0.54	0.57	0.61	0.63	0.65	0.67	0.69
10.5	NUR	18.0	17.4	18.1	19.3	21.2	23.7	26.1	28.2	32.0	32.6
1.00	ETAR	0.96	1.03	1.08	1.17	1.22	1.28	1.33	1.37	1.40	1.42
	REJ(K)	6.5	7.3	8.2	9.0	9.8	10.8	11.7	12.7	13.9	15.0
	GC/GJ	1.07	1.00	0.96	0.93	0.91	0.89	0.88	0.86	0.86	0.85

B(10,8,3)S

$\overline{REJ}$(K) MC/MJ	X/L	0.05	0.15	0.25	0.35	0.45	0.55	0.65
9.8	NUR	33.8	33.1	32.5	30.8	30.4	29.4	27.6
0.21	ETAR	0.45	0.52	0.49	0.52	0.54	0.55	0.57
	REJ(K)	9.5	9.5	9.6	9.6	9.7	9.8	9.9
	GC/GJ	0.07	0.10	0.14	0.17	0.20	0.23	0.26
9.7	NUR	25.7	28.3	26.8	25.7	24.8	24.5	23.9
0.51	ETAR	0.59	0.60	0.60	0.63	0.64	0.68	0.74
	REJ(K)	9.2	9.3	9.4	9.5	9.6	9.7	9.9
	GC/GJ	0.18	0.21	0.24	0.27	0.30	0.33	0.35
9.8	NUR	18.0	22.1	23.2	23.5	22.6	23.4	22.6
1.01	ETAR	0.85	0.81	0.84	0.86	0.87	0.88	0.89
	REJ(K)	9.1	9.3	9.4	9.5	9.6	9.8	10.1
	GC/GJ	0.36	0.40	0.42	0.45	0.47	0.49	0.51

B(5,4,2)I

$\overline{REJ}$(K) MC/MJ	X/L	0.05	0.15	0.25	0.35	0.45	0.55	0.65
6.0	NUR	23.7	28.9	29.4	29.3	29.5	30.8	31.1
0.19	ETAR	0.60	0.66	0.77	0.82	0.85	0.87	0.86
	REJ(K)	4.0	4.3	4.6	5.0	5.4	5.9	6.5
	GC/GJ	0.30	0.37	0.43	0.49	0.55	0.58	0.62
10.1	NUR	30.9	40.3	41.3	41.5	42.0	43.2	45.9
0.19	ETAR	0.52	0.61	0.70	0.76	0.80	0.81	0.88
	REJ(K)	6.8	7.2	7.8	8.5	9.2	10.0	11.1
	GC/GJ	0.30	0.37	0.43	0.49	0.54	0.58	0.62
20.6	NUR	52.3	67.2	69.8	67.2	69.3	72.3	73.1
0.20	ETAR	0.48	0.59	0.67	0.69	0.72	0.71	0.73
	REJ(K)	13.8	14.7	16.0	17.3	18.7	20.4	22.5
	GC/GJ	0.30	0.37	0.43	0.49	0.55	0.58	0.62

B(5,8,2)I

$\overline{REJ}$(K) MC/MJ	X/L	0.05	0.15	0.25	0.35	0.45	0.55	0.65
6.1	NUR	16.4	25.5	26.2	26.7	26.6	27.5	27.8
0.50	ETAR	0.59	0.55	0.60	0.66	0.66	0.66	0.68
	REJ(K)	5.2	5.3	5.5	5.7	5.8	6.1	6.3
	GC/GJ	0.30	0.34	0.37	0.41	0.46	0.48	0.50
10.0	NUR	28.6	36.4	37.3	38.2	39.3	38.2	40.5
0.50	ETAR	0.65	0.55	0.59	0.68	0.74	0.68	0.75
	REJ(K)	8.6	8.8	9.1	9.4	9.5	10.0	10.4
	GC/GJ	0.30	0.34	0.37	0.41	0.46	0.48	0.50
19.3	NUR	45.9	59.0	58.8	59.6	60.2	61.5	61.1
0.50	ETAR	0.56	0.49	0.53	0.64	0.68	0.67	0.70
	REJ(K)	16.6	17.0	17.6	18.1	18.3	19.3	20.1
	GC/GJ	0.30	0.34	0.37	0.41	0.46	0.48	0.50

B(5,8,3)I

$\overline{REJ}$(K) MC/MJ	X/L	0.05	0.15	0.25	0.35	0.45	0.55	0.65
6.1	NUR	23.4	27.0	27.7	27.5	27.5	27.2	27.5
0.50	ETAR	0.59	0.54	0.59	0.63	0.65	0.66	0.68
	REJ(K)	5.8	5.8	5.9	6.0	6.1	6.1	6.3
	GC/GJ	0.18	0.21	0.24	0.27	0.30	0.33	0.36
10.2	NUR	36.4	40.4	41.1	41.3	40.0	40.8	41.1
0.50	ETAR	0.57	0.58	0.62	0.67	0.70	0.73	0.74
	REJ(K)	9.7	9.7	9.8	10.0	10.1	10.2	10.4
	GC/GJ	0.18	0.21	0.24	0.27	0.30	0.33	0.36
19.9	NUR	60.1	64.1	65.6	65.1	63.1	64.1	62.7
0.50	ETAR	0.56	0.54	0.58	0.63	0.65	0.69	0.69
	REJ(K)	18.9	18.9	19.1	19.5	19.7	19.9	20.3
	GC/GJ	0.18	0.21	0.24	0.27	0.30	0.33	0.36

B(10,8,2)I

$\overline{REJ}$(K) MC/MJ	X/L	0.05	0.15	0.25	0.35	0.45	0.55	0.65
6.2	NUR	17.3	19.7	21.0	21.2	20.9	21.6	21.7
0.49	ETAR	0.68	0.65	0.68	0.72	0.74	0.76	0.77
	REJ(K)	5.5	5.7	5.7	5.9	6.0	6.2	6.4
	GC/GJ	0.28	0.33	0.37	0.41	0.45	0.48	0.51
10.0	NUR	22.9	28.0	29.4	29.2	29.5	29.8	30.3
0.50	ETAR	0.60	0.61	0.65	0.69	0.75	0.75	0.77
	REJ(K)	8.9	9.1	9.2	9.5	9.7	10.0	10.3
	GC/GJ	0.28	0.33	0.37	0.41	0.45	0.48	0.51
19.2	NUR	40.2	46.7	48.2	47.2	45.6	46.9	46.3
0.50	ETAR	0.56	0.57	0.62	0.66	0.71	0.72	0.75
	REJ(K)	17.1	17.5	17.6	18.2	18.6	19.2	19.7
	GC/GJ	0.28	0.33	0.37	0.41	0.45	0.48	0.51

APPENDIX B

Tabular Results in Terms of Overall Array Parameters

The following is a presentation in tabular form of the experimental results for the heat transfer parameters Nu and η. The notations used in the tables are identified below in terms of the nomenclature used throughout the text of the report as defined in the NOMENCLATURE section.

Notation used in APPENDIX A	Corresponding NOMENCLATURE
ETA	η
MC/MJ	m_c/m_j
(MC/MJ),N	$(m_c/m_j)_{,N}$
NU, $\overline{NU}$	Nu, $\overline{Nu}$
$\overline{REJ}$(K)	$\overline{Re}_j x10^3$
$\overline{REJ}$,N(K)	$\overline{Re}_{j,N} x10^3$
X/L	x/L

Jet array geometries are identified using $B(x_n/d, y_n/d, z_n/d)I$ where B refers to array length (see Table 4.1) I = inline hole pattern, S^n = staggered pattern.

B(5,4,2)I

$\overline{REJ}$(K)	$\overline{NU}$	X/L	-0.25	-0.15	-0.05	0.05	0.15	0.25	0.35	0.45	0.55	0.65	0.75	0.85	0.95	1.05
MC/MJ																
9.7	40.8	NU	**********			45.2	42.8	40.4	37.8	37.5	37.8	38.3	40.7	43.4	44.6	45.8
0.0		ETA	**********			**********	**********	**********	**********	**********	**********	**********	**********	**********	**********	**********
		$\overline{REJ}$,N(K)				7.8	7.9	8.1	8.1	8.2	8.4	8.7	9.0	9.3	9.7	
		(MC/MJ),N				0.0	0.0	0.0	0.0	0.0	0.0	0.0	0.0	0.0	0.0	
10.6	41.5	NU	8.5	8.1	7.2	31.5	38.4	39.9	38.7	39.4	40.7	42.1	44.5	50.0	50.2	53.0
0.18		ETA	1.00	1.00	1.00	0.41	0.38	0.35	0.31	0.28	0.23	0.21	0.18	0.15	0.15	0.14
		$\overline{REJ}$,N(K)				7.2	7.4	7.7	8.0	8.3	8.7	9.1	9.6	10.0	10.6	
		(MC/MJ),N				2.66	1.29	0.83	0.60	0.46	0.37	0.30	0.25	0.21	0.18	
9.9	32.6	NU	17.9	16.6	16.4	16.8	17.7	23.6	29.2	30.1	34.0	37.0	40.7	48.2	48.9	52.4
0.54		ETA	1.00	1.00	1.00	0.97	0.99	0.86	0.73	0.57	0.51	0.45	0.40	0.36	0.34	0.30
		$\overline{REJ}$,N(K)				5.0	5.5	5.9	6.4	6.9	7.4	8.0	8.6	9.2	9.9	
		(MC/MJ),N				10.68	4.92	3.02	2.10	1.56	1.21	0.96	0.78	0.65	0.54	
10.4	36.4	NU	25.4	23.5	23.2	26.3	25.9	27.1	28.1	31.6	34.9	39.2	44.9	50.7	54.9	59.5
0.97		ETA	1.00	1.00	1.00	1.03	1.02	1.01	1.02	0.97	0.84	0.71	0.60	0.48	0.39	0.30
		$\overline{REJ}$,N(K)				2.3	3.0	3.7	4.5	5.4	6.3	7.2	8.2	9.2	10.4	
		(MC/MJ),N				44.07	17.02	9.08	5.60	3.77	2.68	1.99	1.53	1.21	0.97	

B(5,4,3)I

$\overline{REJ}$(K) MC/MJ	$\overline{NU}$	X/L	-0.25	-0.15	-0.05	0.05	0.15	0.25	0.35	0.45	0.55	0.65	0.75	0.85	0.95	1.05
10.5	42.0	NU	**********			50.3	47.9	47.8	43.7	39.7	38.3	37.0	37.5	39.5	38.7	39.5
0.0		ETA	**********			**********	**********	**********	**********	**********	**********	**********	**********	**********	**********	**********
	$\overline{REJ}$,N(K)					9.5	9.6	9.6	9.8	9.8	9.9	10.0	10.1	10.3	10.5	
	(MC/MJ),N					0.0	0.0	0.0	0.0	0.0	0.0	0.0	0.0	0.0	0.0	
10.4	37.9	NU	6.6	6.1	5.2	37.1	40.9	40.7	37.0	35.7	35.6	36.4	37.6	39.2	38.3	39.6
0.20		ETA	1.00	1.00	1.00	0.48	0.39	0.38	0.32	0.30	0.26	0.24	0.22	0.18	0.16	0.15
	$\overline{REJ}$,N(K)					9.0	9.1	9.1	9.2	9.3	9.5	9.7	9.9	10.1	10.4	
	(MC/MJ),N					2.26	1.12	0.74	0.55	0.44	0.36	0.30	0.26	0.22	0.20	
9.9	29.8	NU	11.0	10.1	10.0	11.2	22.3	32.0	32.8	31.8	31.6	32.0	33.6	35.3	35.4	36.0
0.47		ETA	1.00	1.00	1.00	0.97	0.81	0.56	0.54	0.50	0.47	0.43	0.39	0.34	0.32	0.29
	$\overline{REJ}$,N(K)					7.7	7.9	8.1	8.3	8.5	8.7	9.0	9.3	9.6	9.9	
	(MC/MJ),N					6.08	2.97	1.93	1.41	1.10	0.89	0.74	0.63	0.54	0.47	
10.4	26.1	NU	19.1	17.9	17.8	18.5	18.0	18.8	21.5	24.3	26.8	29.3	31.9	35.3	36.5	38.8
1.00		ETA	1.00	1.00	1.00	0.96	0.98	0.95	0.94	0.88	0.81	0.75	0.68	0.61	0.57	0.50
	$\overline{REJ}$,N(K)					6.4	6.8	7.3	7.7	8.1	8.5	9.0	9.4	9.9	10.4	
	(MC/MJ),N					16.27	7.63	4.79	3.40	2.58	2.04	1.66	1.38	1.17	1.00	

B(5,8,1)I

$\overline{REJ}$(K)	$\overline{NU}$	X/L	-0.25	-0.15	-0.05	0.05	0.15	0.25	0.35	0.45	0.55	0.65	0.75	0.85	0.95	1.05
MC/MJ																
10.3	36.0	NU	**********			37.8	36.8	34.6	32.5	32.4	33.4	34.4	36.3	40.2	41.3	32.8
0.0		ETA	**********													
	$\overline{REJ}$,N(K)					8.1	8.2	8.3	8.4	8.6	8.8	9.1	9.5	9.9	10.3	
	(MC/MJ),N					0.0	0.0	0.0	0.0	0.0	0.0	0.0	0.0	0.0	0.0	
9.9	34.8	NU	8.6	8.1	7.3	23.3	28.4	29.7	31.2	32.7	34.6	37.1	39.9	44.7	46.8	40.5
0.20		ETA	1.00	1.00	1.00	0.47	0.38	0.31	0.29	0.26	0.22	0.20	0.18	0.14	0.15	0.15
	$\overline{REJ}$,N(K)					6.7	6.9	7.1	7.4	7.7	8.0	8.4	8.8	9.4	9.9	
	(MC/MJ),N					2.99	1.45	0.93	0.67	0.52	0.41	0.34	0.28	0.24	0.20	
10.3	36.6	NU	14.8	14.2	13.6	16.8	26.3	28.6	31.6	34.1	37.4	41.5	44.9	50.3	54.0	49.5
0.49		ETA	1.00	1.00	1.00	0.96	0.66	0.49	0.44	0.38	0.34	0.32	0.27	0.22	0.24	0.24
	$\overline{REJ}$,N(K)					5.1	5.7	6.1	6.5	7.0	7.5	8.1	8.7	9.5	10.3	
	(MC/MJ),N					9.88	4.47	2.79	1.96	1.46	1.13	0.90	0.73	0.60	0.49	
10.2	39.7	NU	23.9	22.8	23.2	24.0	24.6	28.0	31.6	35.7	40.1	44.6	50.0	57.2	60.9	59.0
0.97		ETA	1.00	1.00	1.00	0.98	0.99	0.92	0.78	0.65	0.56	0.49	0.41	0.35	0.32	0.34
	$\overline{REJ}$,N(K)					2.7	3.3	3.8	4.5	5.3	6.1	7.0	8.0	9.0	10.2	
	(MC/MJ),N					36.51	14.91	8.63	5.46	3.73	2.69	2.01	1.55	1.22	0.97	

B(5,8,2)I

$\overline{REJ}$(K)	$\overline{NU}$	X/L	-0.25	-0.15	-0.05	0.05	0.15	0.25	0.35	0.45	0.55	0.65	0.75	0.85	0.95	1.05
MC/MJ																
10.4	39.6	NU	**********			42.0	42.8	42.3	40.4	39.1	37.8	37.4	37.3	38.9	37.7	29.2
0.0		ETA	**********			**********	**********	**********	**********	**********	**********	**********	**********	**********	**********	**********
		$\overline{REJ}$,N(K)				9.8	9.8	9.9	9.9	9.9	10.0	10.1	10.2	10.3	10.4	
		(MC/MJ),N				0.0	0.0	0.0	0.0	0.0	0.0	0.0	0.0	0.0	0.0	
10.2	39.0	NU	6.4	5.5	8.9	43.5	41.8	40.7	38.4	36.9	36.5	36.6	37.6	39.5	38.1	32.9
0.19		ETA	1.00	1.00	1.00	0.33	0.29	0.23	0.20	0.17	0.14	0.15	0.15	0.12	0.11	0.13
		$\overline{REJ}$,N(K)				9.5	9.5	9.5	9.6	9.6	9.7	9.8	10.0	10.1	10.2	
		(MC/MJ),N				2.06	1.04	0.69	0.51	0.41	0.34	0.29	0.25	0.22	0.19	
10.0	36.4	NU	9.4	8.5	8.0	28.6	35.8	36.1	36.1	36.4	35.3	36.8	38.1	40.3	40.4	36.7
0.50		ETA	1.00	1.00	1.00	0.65	0.47	0.44	0.44	0.43	0.35	0.36	0.34	0.30	0.30	0.28
		$\overline{REJ}$,N(K)				8.6	8.7	8.8	9.0	9.1	9.2	9.4	9.6	9.8	10.0	
		(MC/MJ),N				5.79	2.86	1.88	1.39	1.10	0.90	0.76	0.65	0.57	0.50	
10.0	32.4	NU	15.4	14.6	14.2	16.4	26.2	30.5	32.1	32.5	34.1	35.0	37.6	39.4	40.3	39.6
1.02		ETA	1.00	1.00	1.00	0.99	0.81	0.60	0.56	0.53	0.51	0.48	0.49	0.42	0.41	0.40
		$\overline{REJ}$,N(K)				7.8	8.0	8.2	8.4	8.7	8.9	9.2	9.4	9.7	10.0	
		(MC/MJ),N				12.99	6.34	4.12	3.02	2.35	1.91	1.59	1.35	1.16	1.02	

B(5,8,3)I

$\overline{REJ}$(K) MC/MJ	$\overline{NU}$	X/L	-0.25	-0.15	-0.05	0.05	0.15	0.25	0.35	0.45	0.55	0.65	0.75	0.85	0.95	1.05
10.3	40.2	NU	**********			42.3	42.3	42.7	41.4	40.6	39.3	39.2	38.0	39.1	37.3	26.6
0.0		ETA	**********			**********	**********	**********	**********	**********	**********	**********	**********	**********	**********	**********
	$\overline{REJ}$,N(K)					10.0	10.1	10.1	10.1	10.2	10.2	10.2	10.3	10.3	10.3	
	(MC/MJ),N					0.0	0.0	0.0	0.0	0.0	0.0	0.0	0.0	0.0	0.0	
10.2	40.1	NU	5.4	4.7	16.5	46.2	43.9	43.0	40.0	39.5	37.9	37.2	37.8	38.6	37.4	30.3
0.20		ETA	1.00	1.00	1.00	0.38	0.31	0.23	0.22	0.19	0.17	0.16	0.17	0.14	0.14	0.17
	$\overline{REJ}$,N(K)					9.8	9.9	10.0	10.0	10.0	10.0	10.1	10.1	10.2	10.2	
	(MC/MJ),N					2.09	1.04	0.69	0.52	0.41	0.34	0.29	0.25	0.22	0.20	
10.2	38.0	NU	7.8	6.9	5.9	36.4	39.5	39.4	38.8	37.0	37.3	37.3	37.8	39.0	37.7	34.9
0.50		ETA	1.00	1.00	1.00	0.57	0.49	0.45	0.43	0.39	0.37	0.34	0.32	0.29	0.28	0.31
	$\overline{REJ}$,N(K)					9.7	9.7	9.7	9.8	9.9	9.9	10.0	10.1	10.2	10.2	
	(MC/MJ),N					5.25	2.63	1.74	1.30	1.03	0.86	0.73	0.63	0.56	0.50	
9.9	32.3	NU	12.0	10.9	11.2	14.1	30.4	33.1	33.6	33.3	34.2	34.0	35.5	37.1	37.3	37.1
1.02		ETA	1.00	1.00	1.00	0.90	0.67	0.57	0.57	0.57	0.56	0.54	0.49	0.45	0.44	0.44
	$\overline{REJ}$,N(K)					8.9	9.0	9.1	9.2	9.3	9.4	9.5	9.7	9.8	9.9	
	(MC/MJ),N					11.32	5.60	3.69	2.74	2.17	1.79	1.51	1.31	1.15	1.02	

B(10,4,2)I

$\overline{REJ}$(K) MC/MJ	$\overline{NU}$	X/L	-0.25	-0.15	-0.05	0.05	0.15	0.25	0.35	0.45	0.55	0.65	0.75	0.85	0.95	1.05
10.1	32.9	NU	**********			38.0	35.3	34.7	31.9	30.4	29.9	29.7	31.6	33.5	34.0	32.8
0.0		ETA	**********			**********										
		$\overline{REJ}$,N(K)				8.5	8.5	8.6	8.7	8.8	9.0	9.2	9.4	9.7	10.1	
		(MC/MJ),N				0.0	0.0	0.0	0.0	0.0	0.0	0.0	0.0	0.0	0.0	
9.8	32.0	NU	7.6	7.3	6.2	28.1	31.8	31.0	30.7	30.7	31.4	31.8	33.4	35.1	36.3	37.1
0.20		ETA	1.00	1.00	1.00	0.50	0.45	0.39	0.35	0.29	0.26	0.23	0.20	0.15	0.15	0.12
		$\overline{REJ}$,N(K)				7.1	7.3	7.5	7.7	8.0	8.3	8.6	9.0	9.4	9.8	
		(MC/MJ),N				2.76	1.35	0.88	0.64	0.49	0.40	0.33	0.27	0.23	0.20	
10.0	29.1	NU	13.6	13.2	13.5	15.0	22.7	25.8	27.5	27.9	29.9	31.5	34.2	37.2	38.9	42.0
0.50		ETA	1.00	1.00	1.00	0.97	0.83	0.63	0.58	0.53	0.49	0.44	0.40	0.33	0.30	0.26
		$\overline{REJ}$,N(K)				5.7	6.0	6.4	6.8	7.3	7.7	8.2	8.8	9.4	10.0	
		(MC/MJ),N				8.81	4.14	2.60	1.83	1.37	1.07	0.86	0.71	0.59	0.50	
9.9	30.8	NU	22.5	21.5	22.4	21.9	21.8	24.0	25.4	27.9	31.3	33.5	37.0	41.4	43.3	48.4
0.98		ETA	1.00	1.00	1.00	0.95	0.95	0.94	0.90	0.84	0.76	0.68	0.60	0.52	0.45	0.39
		$\overline{REJ}$,N(K)				2.8	3.5	4.2	5.0	5.7	6.5	7.3	8.1	9.0	9.9	
		(MC/MJ),N				34.76	13.91	7.65	4.88	3.39	2.49	1.90	1.49	1.19	0.97	

B(10,4,3)I

$\overline{REJ}$(K) MC/MJ	$\overline{NU}$	X/L	-0.25	-0.15	-0.05	0.05	0.15	0.25	0.35	0.45	0.55	0.65	0.75	0.85	0.95	1.05
10.6	30.4	NU	**********			40.3	37.5	35.7	32.6	29.9	27.6	25.2	25.0	25.8	24.6	23.8
0.0		ETA	**********			**********	**********	**********	**********	**********	**********	**********	**********	**********	**********	**********
	$\overline{REJ}$,N(K)					9.9	9.9	10.0	10.0	10.1	10.2	10.3	10.4	10.5	10.6	
	(MC/MJ),N					0.0	0.0	0.0	0.0	0.0	0.0	0.0	0.0	0.0	0.0	
10.4	28.2	NU	4.8	4.5	3.8	33.6	35.1	32.0	28.5	26.5	25.5	24.9	25.2	25.7	24.9	24.8
0.19		ETA	1.00	1.00	1.00	0.52	0.42	0.36	0.32	0.29	0.25	0.25	0.23	0.18	0.18	0.15
	$\overline{REJ}$,N(K)					9.3	9.3	9.4	9.5	9.6	9.7	9.9	10.0	10.2	10.4	
	(MC/MJ),N					2.17	1.08	0.71	0.53	0.42	0.35	0.29	0.25	0.22	0.19	
10.3	23.4	NU	9.4	8.8	8.5	14.8	26.3	25.9	24.9	23.9	23.7	23.3	23.4	24.3	24.0	24.7
0.51		ETA	1.00	1.00	1.00	0.88	0.73	0.63	0.59	0.53	0.49	0.46	0.43	0.40	0.39	0.35
	$\overline{REJ}$,N(K)					8.2	8.4	8.6	8.8	9.0	9.3	9.5	9.7	10.0	10.3	
	(MC/MJ),N					6.33	3.09	2.01	1.47	1.15	0.94	0.78	0.67	0.58	0.51	
10.5	21.6	NU	15.6	14.9	14.9	15.7	16.2	19.7	21.2	21.7	22.2	23.0	23.8	25.8	26.1	28.1
0.99		ETA	1.00	1.00	1.00	0.98	0.99	0.91	0.83	0.77	0.72	0.69	0.64	0.61	0.59	0.56
	$\overline{REJ}$,N(K)					7.5	7.7	8.0	8.3	8.6	9.0	9.3	9.7	10.1	10.5	
	(MC/MJ),N					13.85	6.69	4.30	3.11	2.39	1.92	1.58	1.33	1.14	0.99	

B(10,8,1)I

$\overline{REJ}$(K)	$\overline{NU}$	X/L	-0.25	-0.15	-0.05	0.05	0.15	0.25	0.35	0.45	0.55	0.65	0.75	0.85	0.95	1.05
MC/MJ																
10.3	25.6	NU	**********			27.4	25.0	25.0	23.9	22.8	23.2	23.7	26.3	28.6	29.7	23.8
0.0		ETA	**********													
	$\overline{REJ}$,N(K)					8.7	8.7	8.7	8.8	9.0	9.2	9.4	9.7	10.0	10.3	
	(MC/MJ),N					0.0	0.0	0.0	0.0	0.0	0.0	0.0	0.0	0.0	0.0	
10.1	25.6	NU	7.2	7.1	6.1	18.3	21.5	22.4	23.0	23.9	25.4	26.9	29.0	32.1	34.0	29.6
0.20		ETA	1.00	1.00	1.00	0.47	0.40	0.31	0.26	0.23	0.19	0.17	0.16	0.09	0.12	0.14
	$\overline{REJ}$,N(K)					7.3	7.4	7.6	7.9	8.2	8.5	8.8	9.2	9.6	10.1	
	(MC/MJ),N					2.76	1.36	0.88	0.64	0.49	0.40	0.33	0.27	0.23	0.20	
10.2	29.2	NU	12.1	11.8	11.5	17.2	22.3	24.9	27.3	28.2	29.9	31.6	33.7	38.1	39.3	36.1
0.50		ETA	1.00	1.00	1.00	0.90	0.69	0.56	0.50	0.44	0.39	0.35	0.31	0.26	0.27	0.27
	$\overline{REJ}$,N(K)					5.6	6.0	6.5	6.9	7.4	7.9	8.4	9.0	9.6	10.2	
	(MC/MJ),N					9.08	4.24	2.64	1.86	1.39	1.09	0.87	0.72	0.60	0.50	
10.1	33.9	NU	20.1	19.5	21.4	23.6	23.7	26.0	28.8	32.2	34.5	37.0	40.0	45.7	47.5	45.6
0.99		ETA	1.00	1.00	1.00	0.98	0.98	0.90	0.78	0.68	0.59	0.53	0.46	0.41	0.40	0.40
	$\overline{REJ}$,N(K)					2.7	3.4	4.2	5.0	5.8	6.6	7.4	8.3	9.2	10.1	
	(MC/MJ),N					36.58	14.54	7.92	4.99	3.44	2.52	1.92	1.50	1.21	0.99	

B(10,8,2)I

$\overline{REJ}$(K)	$\overline{NU}$	X/L	-0.25	-0.15	-0.05	0.05	0.15	0.25	0.35	0.45	0.55	0.65	0.75	0.85	0.95	1.05
MC/MJ																
10.3	28.1	NU	**********			31.5	30.9	30.9	29.8	27.8	26.9	25.7	25.3	26.7	25.8	17.1
0.0		ETA	**********													
	$\overline{REJ}$,N(K)					9.9	9.9	9.9	10.0	10.0	10.0	10.1	10.2	10.2	10.3	
	(MC/MJ),N					0.0	0.0	0.0	0.0	0.0	0.0	0.0	0.0	0.0	0.0	
10.0	27.6	NU	4.3	3.9	3.2	30.4	32.0	30.2	28.4	26.3	25.5	25.0	25.2	26.8	26.4	20.3
0.19		ETA	1.00	1.00	1.00	0.40	0.33	0.25	0.21	0.19	0.17	0.16	0.15	0.11	0.12	0.14
	$\overline{REJ}$,N(K)					9.3	9.3	9.4	9.4	9.5	9.5	9.6	9.7	9.9	10.0	
	(MC/MJ),N					2.04	1.02	0.67	0.50	0.40	0.33	0.28	0.24	0.21	0.19	
10.1	26.6	NU	7.1	6.9	6.3	22.9	27.2	27.6	26.7	26.2	26.2	26.2	26.5	28.2	28.0	24.1
0.50		ETA	1.00	1.00	1.00	0.60	0.51	0.48	0.45	0.44	0.39	0.36	0.33	0.28	0.29	0.29
	$\overline{REJ}$,N(K)					9.0	9.1	9.1	9.2	9.3	9.5	9.6	9.7	9.9	10.1	
	(MC/MJ),N					5.56	2.75	1.82	1.35	1.07	0.88	0.74	0.64	0.56	0.49	
10.0	25.1	NU	12.0	11.5	11.6	14.8	22.3	24.4	24.8	25.3	25.9	26.7	27.6	29.6	29.6	28.9
1.01		ETA	1.00	1.00	1.00	0.93	0.73	0.64	0.61	0.59	0.55	0.52	0.49	0.44	0.43	0.41
	$\overline{REJ}$,N(K)					8.1	8.3	8.4	8.6	8.8	9.0	9.2	9.5	9.7	10.0	
	(MC/MJ),N					12.43	6.07	3.97	2.92	2.28	1.86	1.56	1.33	1.15	1.01	

B(10,8,3)I

$\overline{REJ}$(K)	$\overline{NU}$	X/L	-0.25	-0.15	-0.05	0.05	0.15	0.25	0.35	0.45	0.55	0.65	0.75	0.85	0.95	1.05
MC/MJ																
10.4	28.6	NU	**********			31.9	31.2	31.3	30.7	29.1	27.9	26.5	25.6	26.5	25.4	14.9
0.0		ETA	**********			**********										
	$\overline{REJ}$,N(K)					10.2	10.2	10.2	10.2	10.2	10.3	10.3	10.3	10.3	10.4	
	(MC/MJ),N					0.0	0.0	0.0	0.0	0.0	0.0	0.0	0.0	0.0	0.0	
10.0	28.4	NU	3.2	3.0	2.4	33.5	33.7	32.0	29.8	27.4	26.3	25.1	25.0	26.0	25.4	17.4
0.21		ETA	1.00	1.00	1.00	0.47	0.33	0.27	0.23	0.22	0.20	0.18	0.16	0.14	0.15	0.16
	$\overline{REJ}$,N(K)					9.7	9.7	9.8	9.8	9.8	9.8	9.9	9.9	10.0	10.0	
	(MC/MJ),N					2.17	1.09	0.72	0.54	0.43	0.36	0.31	0.27	0.24	0.21	
10.1	26.8	NU	5.6	5.2	4.6	26.5	29.4	29.7	27.3	26.3	25.8	25.3	25.4	26.6	25.7	20.9
0.51		ETA	1.00	1.00	1.00	0.61	0.56	0.48	0.44	0.42	0.38	0.37	0.35	0.30	0.30	0.30
	$\overline{REJ}$,N(K)					9.6	9.7	9.7	9.8	9.8	9.9	9.9	10.0	10.0	10.1	
	(MC/MJ),N					5.34	2.65	1.76	1.31	1.05	0.87	0.74	0.64	0.57	0.51	
10.2	24.8	NU	9.2	8.7	8.7	16.8	25.8	26.4	25.6	25.2	25.3	25.0	25.6	26.8	25.9	24.7
1.00		ETA	1.00	1.00	1.00	0.85	0.69	0.65	0.65	0.61	0.56	0.54	0.51	0.45	0.44	0.41
	$\overline{REJ}$,N(K)					9.4	9.5	9.6	9.7	9.8	9.8	9.9	10.0	10.1	10.2	
	(MC/MJ),N					10.81	5.35	3.54	2.63	2.09	1.73	1.47	1.27	1.12	1.00	

B(5,4,3)S

$\overline{REJ}$(K) MC/MJ	$\overline{NU}$	X/L	-0.25	-0.15	-0.05	0.05	0.15	0.25	0.35	0.45	0.55	0.65	0.75	0.85	0.95	1.05
10.5	36.2	NU	**********			49.6	46.5	45.1	41.4	35.2	31.8	30.2	28.9	27.5	26.0	25.4
0.0		ETA	**********			**********										
		$\overline{REJ}$,N(K)				9.6	9.6	9.7	9.8	9.8	9.9	10.0	10.1	10.3	10.5	
		(MC/MJ),N				0.0	0.0	0.0	0.0	0.0	0.0	0.0	0.0	0.0	0.0	
10.2	29.6	NU	6.4	5.9	5.0	38.5	39.6	33.2	30.6	28.0	26.2	24.9	24.5	25.4	24.7	25.4
0.20		ETA	1.00	1.00	1.00	0.49	0.42	0.38	0.34	0.31	0.28	0.26	0.24	0.22	0.20	0.19
		$\overline{REJ}$,N(K)				8.9	8.9	9.0	9.1	9.2	9.4	9.5	9.7	10.0	10.2	
		(MC/MJ),N				2.33	1.16	0.77	0.57	0.45	0.37	0.31	0.27	0.23	0.20	
9.9	21.1	NU	10.5	9.7	9.5	10.9	23.4	20.9	20.4	20.5	20.8	21.6	22.6	24.8	25.1	26.6
0.47		ETA	1.00	1.00	1.00	0.94	0.80	0.74	0.69	0.64	0.61	0.57	0.53	0.49	0.46	0.41
		$\overline{REJ}$,N(K)				7.7	7.9	8.0	8.3	8.5	8.7	9.0	9.3	9.6	9.9	
		(MC/MJ),N				6.05	2.95	1.92	1.40	1.09	0.89	0.74	0.63	0.54	0.47	
10.5	23.1	NU	18.5	17.5	17.5	18.0	17.3	17.9	19.0	20.8	23.1	25.3	27.2	30.7	31.3	34.5
1.00		ETA	1.00	1.00	1.00	0.96	0.97	0.96	0.96	0.95	0.92	0.89	0.86	0.81	0.76	0.72
		$\overline{REJ}$,N(K)				6.5	6.9	7.3	7.7	8.2	8.6	9.0	9.5	10.0	10.5	
		(MC/MJ),N				16.25	7.63	4.79	3.40	2.58	2.04	1.66	1.38	1.17	1.00	

B(10,8,3)S

$\overline{REJ}$(K)	$\overline{NU}$	X/L	-0.25	-0.15	-0.05	0.05	0.15	0.25	0.35	0.45	0.55	0.65
MC/MJ												
10.1	27.8	NU	**********			30.9	29.6	28.7	27.5	26.6	26.3	25.1
0.0		ETA	**********			**********						
	$\overline{REJ}$,N(K)					9.9	9.9	9.9	9.9	9.9	10.0	10.0
	(MC/MJ),N					0.0	0.0	0.0	0.0	0.0	0.0	0.0
9.9	28.1	NU	1.5	2.2	1.8	33.8	30.8	29.5	27.3	26.5	25.4	23.5
0.21		ETA	1.00	1.00	1.00	0.45	0.36	0.26	0.22	0.19	0.17	0.15
	$\overline{REJ}$,N(K)					9.6	9.6	9.6	9.6	9.6	9.7	9.7
	(MC/MJ),N					2.20	1.10	0.73	0.55	0.44	0.36	0.31
9.8	23.9	NU	6.9	6.5	5.5	25.7	27.4	25.3	23.7	22.6	21.9	21.0
0.51		ETA	1.00	1.00	1.00	0.59	0.50	0.44	0.40	0.36	0.35	0.34
	$\overline{REJ}$,N(K)					9.3	9.3	9.4	9.4	9.5	9.5	9.6
	(MC/MJ),N					5.34	2.65	1.76	1.31	1.05	0.87	0.74
9.8	21.1	NU	10.0	9.4	9.2	18.0	21.7	22.4	22.3	21.2	21.7	20.8
1.01		ETA	1.00	1.00	1.00	0.85	0.75	0.71	0.67	0.63	0.60	0.57
	$\overline{REJ}$,N(K)					9.1	9.2	9.2	9.3	9.4	9.5	9.6
	(MC/MJ),N					10.90	5.40	3.57	2.66	2.11	1.74	1.48

B(5,4,2)I

$\overline{REJ}$(K)	$\overline{NU}$	X/L	-0.25	-0.15	-0.05	0.05	0.15	0.25	0.35	0.45	0.55	0.65
MC/MJ												
6.0	27.0	NU	7.3	7.5	5.3	23.7	27.9	27.4	27.0	26.8	27.9	28.1
0.19		ETA	1.00	1.00	1.00	0.60	0.49	0.45	0.38	0.33	0.29	0.24
		$\overline{REJ}$,N(K)				4.0	4.1	4.3	4.5	4.7	4.9	5.1
		(MC/MJ),N				2.92	1.41	0.91	0.65	0.50	0.40	0.33
10.1	38.7	NU	10.7	10.6	8.8	30.9	39.5	39.5	39.2	39.2	40.1	42.3
0.19		ETA	1.00	1.00	1.00	0.52	0.46	0.41	0.36	0.32	0.27	0.25
		$\overline{REJ}$,N(K)				6.8	7.0	7.3	7.6	7.9	8.3	8.7
		(MC/MJ),N				2.91	1.41	0.90	0.65	0.50	0.40	0.33
20.6	64.8	NU	15.6	14.8	13.3	52.3	66.1	67.4	64.3	65.8	68.5	69.1
0.20		ETA	1.00	1.00	1.00	0.48	0.44	0.39	0.33	0.28	0.24	0.21
		$\overline{REJ}$,N(K)				13.9	14.3	14.9	15.5	16.1	16.8	17.6
		(MC/MJ),N				2.91	1.41	0.91	0.65	0.50	0.40	0.33

B(5,8,2)I

$\overline{REJ}$(K) MC/MJ	$\overline{NU}$	X/L	-0.25	-0.15	-0.05	0.05	0.15	0.25	0.35	0.45	0.55	0.65
6.1	23.9	NU	8.3	8.5	6.7	16.4	25.1	25.2	25.1	24.7	25.3	25.4
0.50		ETA	1.00	1.00	1.00	0.59	0.47	0.44	0.43	0.38	0.34	0.32
	$\overline{REJ}$,N(K)					5.2	5.3	5.4	5.5	5.5	5.6	5.7
	(MC/MJ),N					5.77	2.85	1.87	1.38	1.09	0.90	0.75
10.0	35.0	NU	9.4	8.5	8.0	28.6	35.8	36.1	36.1	36.4	35.3	36.8
0.50		ETA	1.00	1.00	1.00	0.65	0.47	0.44	0.44	0.43	0.35	0.36
	$\overline{REJ}$,N(K)					8.6	8.7	8.8	9.0	9.1	9.2	9.4
	(MC/MJ),N					5.79	2.86	1.88	1.39	1.10	0.90	0.76
19.3	55.7	NU	17.4	16.4	14.7	45.9	58.3	57.3	57.0	56.8	57.7	56.9
0.50		ETA	1.00	1.00	1.00	0.56	0.42	0.40	0.42	0.40	0.35	0.33
	$\overline{REJ}$,N(K)					16.6	16.8	17.1	17.3	17.5	17.8	18.2
	(MC/MJ),N					5.82	2.88	1.89	1.39	1.10	0.90	0.76

B(5,8,3)I

$\overline{REJ}$(K) MC/MJ		$\overline{NU}$ X/L	-0.25	-0.15	-0.05	0.05	0.15	0.25	0.35	0.45	0.55	0.65
6.1	25.4	NU	5.9	6.0	4.4	23.4	26.4	26.6	25.8	25.6	25.0	25.0
0.50		ETA	1.00	1.00	1.00	0.59	0.45	0.43	0.40	0.37	0.33	0.31
	$\overline{REJ}$,N(K)					5.8	5.8	5.9	5.9	5.9	6.0	6.0
	(MC/MJ),N					5.21	2.61	1.73	1.29	1.02	0.85	0.72
10.2	37.9	NU	7.8	6.9	5.9	36.4	39.5	39.4	38.8	37.0	37.3	37.3
0.50		ETA	1.00	1.00	1.00	0.57	0.49	0.45	0.43	0.39	0.37	0.34
	$\overline{REJ}$,N(K)					9.7	9.7	9.7	9.8	9.9	9.9	10.0
	(MC/MJ),N					5.25	2.63	1.74	1.30	1.03	0.86	0.73
20.0	61.0	NU	13.4	12.4	10.7	60.1	63.1	63.6	62.2	59.6	60.0	58.4
0.50		ETA	1.00	1.00	1.00	0.56	0.45	0.42	0.40	0.37	0.35	0.32
	$\overline{REJ}$,N(K)					19.0	19.0	19.0	19.2	19.3	19.4	19.5
	(MC/MJ),N					5.32	2.66	1.77	1.32	1.05	0.87	0.74

B(10,8,2)I

$\overline{REJ}$(K)	$\overline{NU}$	X/L	-0.25	-0.15	-0.05	0.05	0.15	0.25	0.35	0.45	0.55	0.65
MC/MJ												
6.2	18.6	NU	8.4	7.8	6.3	17.3	18.9	19.5	19.1	18.4	18.7	18.5
0.49		ETA	1.00	1.00	1.00	0.68	0.55	0.50	0.46	0.42	0.39	0.36
		$\overline{REJ}$,N(K)				5.5	5.6	5.7	5.7	5.8	5.9	5.9
		(MC/MJ),N				5.53	2.74	1.81	1.34	1.06	0.87	0.74
10.1	26.1	NU	7.1	6.9	6.3	22.9	27.2	27.6	26.7	26.2	26.2	26.2
0.50		ETA	1.00	1.00	1.00	0.60	0.51	0.48	0.45	0.44	0.39	0.36
		$\overline{REJ}$,N(K)				9.0	9.1	9.1	9.2	9.3	9.5	9.6
		(MC/MJ),N				5.56	2.75	1.82	1.35	1.07	0.88	0.74
19.2	43.0	NU	5.3	8.7	11.2	40.2	45.6	45.9	44.0	41.6	42.4	41.4
0.50		ETA	1.00	1.00	1.00	0.56	0.49	0.46	0.43	0.41	0.38	0.35
		$\overline{REJ}$,N(K)				17.1	17.3	17.4	17.6	17.8	18.1	18.3
		(MC/MJ),N				5.65	2.79	1.85	1.37	1.08	0.89	0.75

1. Report No.	2. Government Accession No.	3. Recipient's Catalog No.
NASA CR-3936		

4. Title and Subtitle	5. Report Date
Heat Transfer Characteristics Within an Array of Impinging Jets - Effects of Crossflow Temperature Relative to Jet Temperature	October 1985
	6. Performing Organization Code
7. Author(s)	8. Performing Organization Report No.
L. W. Florschuetz and C. C. Su	CR-R-85020
	10. Work Unit No.
9. Performing Organization Name and Address	11. Contract or Grant No.
Arizona State University Department of Mechanical and Aerospace Engineering Tempe, Arizona 85287	NSG-3075
	13. Type of Report and Period Covered
12. Sponsoring Agency Name and Address	Contractor Report
National Aeronautics and Space Administration Washington, D.C. 20546	14. Sponsoring Agency Code
	533-04-12 (E-2696)

15. Supplementary Notes

Final report. Project Manager, Steven A. Hippensteele, Internal Fluid Mechanics Division, NASA Lewis Research Center, Cleveland, Ohio 44135.

16. Abstract

Spanwise average heat fluxes, resolved in the streamwise direction to one stream-wise hole spacing (regional average fluxes) were measured for two-dimensional arrays of circular air jets impinging on a heat transfer surface parallel to the jet orifice plate. The jet flow, after impingement, was constrained to exit in a single direction along the channel formed by the jet orifice plate and heat transfer surface. In addition to the crossflow that originated from the jets following impingement, an initial crossflow was present that approached the array through an upstream extension of the channel. Because of heat addition upstream of a given spanwise row within an array, the mixed-mean temperature of the crossflow approaching the row may be larger than the jet temperature. The regional average heat fluxes are considered as a function of parameters associated with corresponding individual spanwise rows within the array (the individual row domain). A linear superposition model was employed to formulate appropriate governing parameters for the individual row domain. The dependent parameters are a crossflow-to-jet fluid temperature difference influence factor, a Nusselt number, and a recovery factor. Independent parameters are the individual row jet Reynolds number and crossflow-to-jet mass flux ratio, and the geometric parameters. The effects of flow history upstream of an individual row domain (i.e., the normalized velocity and temperature distributions at the entrance to an individual row domain) are also considered. Results are presented and conclusions drawn based on data for twelve different array geometries. In addition to the results formulated in terms of individual spanwise row parameters, the report includes a corresponding set of streamwise resolved heat transfer characteristics formulated in terms of flow and geometric parameters characterizing the overall arrays.

17. Key Words (Suggested by Author(s))	18. Distribution Statement
Jet impingement; Jet array; Heat transfer; Gas turbine; Crossflow; Initial crossflow; Impingement cooling; Turbine cooling	Unclassified - unlimited STAR Category 34

19. Security Classif. (of this report)	20. Security Classif. (of this page)	21. No. of pages	22. Price*
Unclassified	Unclassified	173	A08

*For sale by the National Technical Information Service, Springfield, Virginia 22161 NASA-Langley, 1985

End of Document